AD-A163 990 A MODEL FOR OXYGEN ATOM RECOMBINATION ON A SILICON DIOXIDE SURFACE(U) AIR FORCE INST OF TECH WRIGHT-PATTERSON AFB OH SCHOOL OF ENGINEERING 1/2

UNCLASSIFIED W A SEWARD DEC 85 AFIT/DS/AA/85-1 F/G 7/4 NL

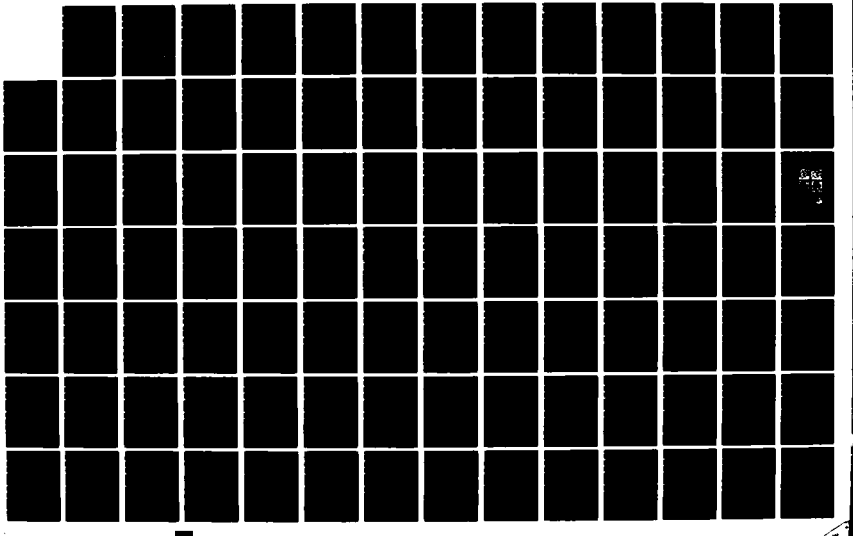

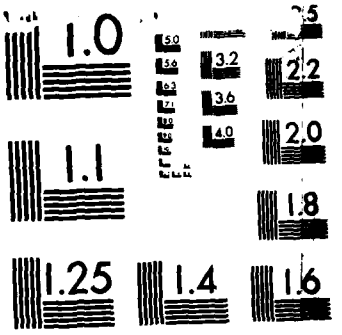

DEPARTMENT OF THE AIR FORCE
AIR UNIVERSITY

AIR FORCE INSTITUTE OF TECHNOLOGY

Wright-Patterson Air Force Base, Ohio

AFIT/DS/AA/85-1

A MODEL FOR OXYGEN ATOM RECOMBINATION ON A SILICON DIOXIDE SURFACE

DISSERTATION

William A. Seward
Major, USAF

AFIT/DS/AA/85-1

Approved for public release; distribution unlimited

AFIT/DS/AA/85-1

A MODEL FOR OXYGEN ATOM RECOMBINATION ON A SILICON DIOXIDE SURFACE

William A. Seward, B.S., M.S.
Major, USAF

Approved:

Chairman — 27 Nov 1985

James E. Hitchcock — Nov. 26, 1985

Ernest C. Page — Nov 9, 1985

James K. Hodge — Nov 27, 1985

Rodney E. Smith — 2 Dec 1985

Accepted:

Dean, School of Engineering — 2 Dec 85

AFIT/DS/AA/85-1

A MODEL FOR OXYGEN ATOM RECOMBINATION ON A SILICON DIOXIDE SURFACE

DISSERTATION

Presented to the Faculty of the School of Engineering
of the Air Force Institute of Technology
Air University
In Partial Fulfillment of the
Requirements for the Degree of
Doctor of Philosophy

William A. Seward, B. S., M.S.
Major, USAF

December 1985

Acknowledgments

I would like to express my appreciation to my advisor, Professor Lt Col Eric J. Jumper, for his patience, support, technical guidance, and encouragement during this study. My gratitude is extended to the other members of my research committee, Dr James Hitchcock, Dr Ernest Dorko, and Maj James Hodge for their patience and support.

My most sincere gratitude is extended to my wife Lynn and my children Heather and Nathan for their love and support. Without them I would never have undertaken this task nor have been able to complete it.

WILLIAM A. SEWARD

Table of Contents

List of Figures

List of Figures

List of Tables

List of Symbols

C_a	Surface sites per unit area
C_p	Specific heat at constant pressure
D_j	Diffusivity of species j into the mixture
D	Thermal desorption energy
h	Planck constant
h_j	Absolute enthalpy of species j
k	Thermal conductivity for the mixture
k_i	Thermal conductivity of species i
k_b	Backward rate constant
k_f	Forward rate constant
k_B	Boltzmann constant
m	Mass of particle
$\dot{N}$	Surface impingement rate
n	Number density
p	Pressure
R	Universal gas constant
S	Sticking coefficient
S_o	Clean surface sticking coefficient
P	Steric factor
T	Temperature
u	x-component of velocity
v	y-component of velocity
$\bar{c}$	Average velocity of the particles
$\dot{m}_j'''$	Rate of production of species j per unit volume
x	Cartesian coordinate in x direction

List of Symbols

y	Cartesian coordinate in y direction
x_j	Mole fraction of species j
w_j	Mass fraction of species j
M_j	Molecular weight of species j
M	Molecular weight of the mixture
E	Activation energy
K	Equilibrium constant
n_{s_j}	Number of chemisorbed particles of species j per unit area
f	Number of degrees of freedom
Z	Partition function
D_{ij}	Bimolecular diffusivity of species i into species j
Le_j	Lewis number of species j
γ	Recombination coefficient
δ	Thermal desorption rate per unit area
Θ	Fractional surface concentration
μ	Viscosity of the mixture
μ_i	Viscosity of species i
Ω	Reduced collision integral
ρ	Density of the mixture
ε_i	Lennard-Jones (6-12) characteristic energy of interaction
σ_i	Lennard-Jones (6-12) characteristic diameter
$(\Theta_j)_o$	Isolated fractional surface concentration of species j
ε	Emissivity
σ	Stefan-Boltzmann constant
ψ	Compressible stream function

Abstract

A steady state model for oxygen atom recombination for temperatures from 300°K to 2000°K on a silicon dioxide surface was developed based on the Langmuir-Rideal heterogeneous recombination mechanism. The bonding of atomic oxygen to the surface and the thermal desorption of atomic oxygen from the surface were also included in the model. The hypothesis was made that the gas-phase oxygen atoms combine directly with the oxygen atoms that constitute the silicon dioxide surface, with other gas-phase oxygen atoms replacing the lost atoms that were bonded on the silicon dioxide surface matrix. The model agrees with the experimental data that is available in the literature, and provides an insight into the processes that control the recombination as a function of temperature. A set of two-dimensional, steady-state, laminar boundary-layer calculations was made using explicit numerical methods to demonstrate the use of this model and to explore the rational limits which may be placed on the role of catalysis for oxygen recombination on a silicon dioxide surface like that of the Space Shuttle. The predicted catalycity of the silicon dioxide surface did reduce the overall heating below that which would be predicted by a fully catalytic surface.

A MODEL FOR OXYGEN ATOM RECOMBINATION ON A SILICON DIOXIDE SURFACE

I. Introduction

Discrepancies between wind tunnel and flight-test heating data for the reentry phase of the Space Shuttle flights have led to an interest in catalytic reactions for dissociated air species on silicon dioxide (Ref 1-3). In particular, detailed kinetic/physiochemical models for catalytic recombination of nitrogen and oxygen atoms on silicon dioxide do not exist. Models for these species are important because, depending on altitude/airspeed, relatively large concentrations of atomic oxygen and nitrogen are expected behind the strong portion (near-normal) of the bow shock. In nonequilibrium flow, these atomic species are swept (convected) along the heat-shield surface (Shuttle tiles) where they kinetically interact with the surface. Since the recombination process is exothermic, heating rate (and resulting surface temperature) predictions depend heavily on the extent to which the surface is catalytic. High catalycity leads to higher heating rates and higher surface temperatures and low catalycity to lower heating rates and lower surface temperatures (Ref 4-6). Therefore, surface catalycity provides an excellent scapegoat to blame discrepancies between expected heating (developed via wind tunnel testing) and experienced heating in flight testing.

Although such discrepancies may well be due to wall catalysis, they may also be due to other nonequilibrium effects. Scott (Ref 7) reviewed

the nonequilibrium calculation techniques developed by several authors and had to conclude that no method predicts the flight measurements of the heating over the entire windward centerline surface for the entire reentry. He noted that there are computational difficulties associated with properly characterizing the flow field. These difficulties arise from the complex flow and the gas-phase chemical reaction kinetics; in particular, the chemical composition of the flow has never been measured. There are disagreements as to the proper treatment of the boundary conditions at the surface due to recombination effects (Ref 8). Rosner (Ref 9) points out that the recombination data that has been inferred from arc jet experiments may not be reliable due to contaminants in the arc jet flow field (such as copper from the electrodes) and since flight conditions are not accurately simulated. In order to eliminate discrepancies, it is important to place rational limits on the relative role that catalysis can play in the overall heating problem. Such rational limits cannot come from comparisons between flight-test and wind tunnel data, as apparently has been done for the Space Shuttle (Ref 10). Such comparisons simply assign a catalycity which makes up for the discrepancy. That is, the flight-test data are due to thermal energy transfer (Fourier conduction) and chemical energy transfer due to recombination. The perfect gas wind tunnel data is assumed to be representative of equilibrium flow with a fully catalytic wall (Ref 7), and hence a catalycity is assigned to account for the flight-test heating data being significantly less than the wind tunnel data. Rational limits for catalysis cannot be made in this manner. However, rational limits for catalysis can be made by developing models which derive their confidence from controlled

experiments specifically tailored to provide data suitable to test the validity of models for catalysis.

Such modeling, verification of which is based on controlled experiments, is the object of the present research. Because of the extensive scope of the most general task, the work reported here deals with a subset of the most general problem, that of recombination of oxygen atoms (only) on silicon dioxide. Application of the results of this study, then, is possible for a limited portion of the Shuttle reentry profile when oxygen is dissociated and nitrogen is not. Because of the higher dissociation energy for nitrogen, such a portion of the reentry envelope does exist. Thus, a partial test of the rational limits of the role of catalytic recombination in heating predictions for the Shuttle is possible since the coating of Shuttle tiles is predominantly silicon dioxide (Ref 11). The objective of this research is to model oxygen recombination on silicon dioxide. Second, the use of the model will be demonstrated for the purpose of showing how rational limits for catalysis can be obtained.

II. Modeling of Heterogeneous Recombination

Kinetic studies of atom recombination on most surfaces show that the reactions are first order processes which become second order processes at higher temperatures (c.f., below) (Ref 12). Yet the most common method of collapsing catalytic data uses the following equation (Ref 13):

$$\gamma = \gamma_0 \exp(-\frac{E}{RT}) \qquad (1)$$

where γ_0 and E are constants. γ_0 is called the pre-exponential factor, and E is the activation energy. R is the universal gas constant that is used when energy is in molar units and often is replaced with the Boltzmann constant when energy is per molecule. Although this analytical form is sometimes useful for comparisons with other recombination coefficient data, the kinetic details are lost. The "lumped coefficient" γ_0 tells little about what it is composed of in terms of physical and/or chemical details. Furthermore, since, as will be shown, this form requires that the reaction be first order, it is unable to describe the recombination coefficient when the recombination kinetics are second order or when the recombination coefficient goes through a maximum.

A more detailed analytical form for the recombination coefficient is given by Jumper, et. al., (Ref 14). This model is semi-classical and describes the physical and chemical microscopic details of what may be occurring on the surface when atoms recombine and desorb as molecules. The Jumper model allows for the recombination kinetics to transition to second order at elevated temperatures and also allows the recombination

coefficient to pass through a maximum value with increasing temperature. As pointed out by Jumper, et. al., in Reference 14 for fluorine atom recombination on a nickel surface, each unknown constant in the recombination coefficient model led to a specific characteristic of the data. Although further studies are required to verify these results, Jumper's model provides much more insight into the phenomena possibly occurring on the surface where atom recombination is taking place. The present oxygen recombination study started with a detailed investigation of this model. In the following, a background for the conventional treatment of catalysis is addressed followed by a detailed treatment akin to the Jumper method.

Mechanisms for Heterogeneous Recombination of Atoms

Three mechanisms are most used either singularly or in combination to describe atom recombination on surfaces; a review of the derivation of the so-called Langmuir adsorption isotherm is first given since it is useful in understanding all three mechanisms. The Langmuir adsorption isotherm applies to the ideal case of adsorption where there are no interactions between adsorbed particles (either atoms or molecules). The isotherm relates to adsorption theory as the perfect gas law does to the study of real gases. The adsorption and desorption may be represented in the following manner:

$$A + -\overset{'}{S}- \underset{k_{-1}}{\overset{k_1}{\rightleftharpoons}} \overset{A}{\overset{'}{S}}-$$

where $-\overset{'}{S}-$ represents a vacant surface site and A is a particle, either

an atom or a molecule. If we let Θ be the fraction of the surface that is covered with adsorbed particles, $(1-\Theta)$ will be the fraction of the surface that is bare. The rate of adsorption will then be $k_1 p(1-\Theta)$, with k_1 being a rate constant and p the pressure of the particles that are being adsorbed, since p in effect represents the number of particle-surface collisions per unit area-time. The rate of desorption is then $k_{-1}\Theta$. At equilibrium, the adsorption and desorption rates are equal leading to the so-called Langmuir isotherm:

$$\Theta = \frac{Kp}{1 + Kp} \qquad (2)$$

where K is defined as k_1/k_{-1} (Ref 12).

Now that we have an expression for the fractional surface concentration Θ in terms of the equilibrium constant K and the pressure of the adsorbing species, we can look at the three mechanisms which are normally used to model the heterogeneous recombination of atoms.

Langmuir-Hinshelwood Mechanism. This mechanism is the recombination of two atoms adsorbed on neighboring surface sites and may be represented as:

$$A + A + \text{-S-S-} \underset{\text{desorption}}{\overset{\text{adsorption}}{\rightleftharpoons}} \begin{matrix} A\ A \\ \text{-S-S-} \end{matrix} \xrightarrow[\text{desorption}]{\text{recombination}} \text{-S-S-} + A_2$$

the recombination desorption rate R_{LH} is proportional to Θ times Θ since the two atoms must be adsorbed on neighboring sites. Using k as a proportionality constant:

$$R_{LH} = k\Theta\Theta \qquad (3)$$

Substituting the expression for Θ from the Langmuir adsorption isotherm we obtain:

$$R_{LH} = k\left(\frac{Kp}{1 + Kp}\right)^2 \qquad (4)$$

At low temperatures the surface is most likely fully covered, $\Theta \simeq 1$, which means that $Kp \gg 1$. Therefore, $R_{LH} = k$ and the recombination mechanism is zeroeth order in pressure, i.e., it does not depend on the pressure. At higher temperatures, the surface is sparsely covered, $Kp \ll 1$, and $R_{LH} = kK^2p^2$. The rate goes as pressure squared and thus the kinetics are second order at the elevated temperatures.

Slow Adsorption Followed by Rapid Migration and Recombination Mechanism. A second mechanism is considered by Laidler (Ref 15), and this is the surface migration of chemisorbed atoms. This mechanism could only be significant when the fractional surface concentration Θ is small, i.e., the surface is sparsely covered. The recombination rate would be proportional to the adsorption rate and given as:

$$R_{Migration} = kp(1 - \Theta) \qquad (5)$$

If Θ is small, the recombination rate would be first order with respect to the pressure of the recombining atomic species. However, this mechanism would remain first order even at higher temperatures.

Langmuir-Rideal Mechanism. The third mechanism is the recombination of an atom from the gas phase with an atom that is adsorbed to a surface site:

$$A + A + \text{-S-S-} \underset{\text{desorption}}{\overset{\text{adsorption}}{\rightleftharpoons}} A + \overset{A}{\text{-S-S-}} \xrightarrow[\text{desorption}]{\text{recombination}} \text{-S-S-} + A_2$$

The recombination desorption rate R_{LR} is now proportional to θ times p, the pressure of the atoms:

$$R_{LR} = kp\theta \tag{6}$$

Again substituting for θ:

$$R_{LR} = kp\left(\frac{Kp}{1 + Kp}\right) \tag{7}$$

At low temperatures $Kp \gg 1$, and the kinetics are first order. At elevated temperatures where $Kp \ll 1$, the recombination kinetics are second order with respect to the pressure of the atomic species.

Adopted Mechanism

In order to allow the recombination kinetics to transition from first to second order with respect to the atomic pressure as the temperature increases and also to keep the model from becoming unnecessarily complex, the Langmuir-Rideal recombination mechanism was adopted for the model for oxygen recombination and hydrogen recombination (see Appendix A) on silicon dioxide. Although this mechanism is acceptable and often used to explain the recombination process (Ref 12, 16-18), it is not the

only second order recombination mechanism at elevated temperatures. Wood and Wise (Ref 19) modeled the recombination of hydrogen on silicon dioxide using a Langmuir-Rideal mechanism from 300°K to 500°K and a Langmuir-Hinshelwood mechanism above 500°K. Hardy and Linnett (Ref 18) point out that both the Langmuir-Rideal and the Langmuir-Hinshelwood mechanisms require the thermal desorption of atoms to be large at the elevated temperatures where the kinetics are second order, and therefore, that the order of the recombination process will not exclude one of these two mechanisms from the other.

Components of the Rate Equation

Let us now look at the microscopic processes which are possibly occurring at the surface upon which heterogeneous reactions are taking place.

Physical and Chemical Adsorption. At a surface, a molecule or atom may experience a weak interaction due to Van der Waals forces. This weak interaction is physical adsorption and is associated with liquefaction and with condensation. If a molecule or atom experiences a strong interaction at the surface, the particle will undergo chemical adsorption (chemisorption) and a strong bond will be formed with the surface. In general, the heat of adsorption for physical adsorption is in the range 2-15 kcal/mole, whereas for chemisorption, the heat of adsorption is in the range 15-200 kcal/mole (Ref 20). Physical adsorption tends to occur only at temperatures near or below the boiling point of the adsorbed particles at the pressure considered (Ref 21). Jumper, et. al., (Ref 14), show that physical adsorption is negligible at temperatures above

100°K for their model for fluorine recombination on a nickel surface. Their soft cube model provides an explanation of the gas particle-surface interaction. For oxygen atom recombination on oxide surfaces at temperatures greater than 300°K, the only significant form of adsorption is chemisorption (Ref 13). Since the recombination of oxygen atoms on silicon dioxide from 300°K to 2000°K is modeled, only chemisorption was considered.

Chemisorption Rate. The rate of chemisorption of particles (atoms or molecules) to silicon dioxide can be expressed as follows:

$$\text{chemisorption rate} = \dot{N}S \tag{8}$$

where $\dot{N}$ is the surface impingement rate per unit area and S is the sticking coefficient. The surface impingement rate is assumed to be gas kinetic and is given by (Ref 22):

$$\dot{N} = n\,\frac{\bar{c}}{4} \tag{9}$$

where n is the number density of particles in the gas and $\bar{c}$ is the average velocity of the particles. The average velocity is derived in kinetic theory as:

$$\bar{c} = \left(\frac{8k_B T}{\pi m}\right)^{\frac{1}{2}} \tag{10}$$

where k_B is the Boltzmann constant, T is the absolute temperature, and m is the mass of the particles. The sticking coefficient may be expressed as:

$$S = S_o(1 - \Theta) \tag{11}$$

where S_o is the initial or clean surface sticking coefficient and Θ is the fractional surface concentration. This functional dependence upon S_o and Θ assumes (1) that any particle striking an occupied site is reflected back into the gas phase, (2) each site can be occupied by only a single particle, and (3) surface mobility of chemisorbed particles is negligible.

Thermal Desorption Rate. The rate of thermal desorption of the particles is given by (Ref 23)

$$\text{thermal desorption rate} = \delta\,\Theta \tag{12}$$

where δ is the thermal desorption rate per unit area of covered surface. According to the theory of absolute reaction rates and assuming the ratio of the activated complex partition function to the adsorbed particle partition function is unity:

$$\delta = C_a \frac{k_B T}{h} \exp\left(-\frac{D}{k_B T}\right) \tag{13}$$

where C_a is the number of adsorption surface sites per unit area, h is the Planck constant, and D is the thermal desorption energy.

Recombination Desorption Rate. The rate at which the chemisorbed atoms recombine with atoms from the gas phase and desorb from the surface as molecules is given by

$$\text{Recombination Desorption Rate} = \left[\text{Surface impingement rate}\right]\left[\begin{array}{l}\text{Impact probability on a site occupied by an atom}\end{array}\right]\left[\begin{array}{l}\text{Fraction of collisions that have sufficient energy to react}\end{array}\right]\left[\begin{array}{l}\text{Fraction of sufficiently energetic collisions that actually react}\end{array}\right] \tag{14}$$

which is analogous to the collision theory results for homogeneous

reactions (Ref 22). The four factors in equation (14) may be written as:

$$\begin{matrix}\text{Recombination} \\ \text{Desorption Rate}\end{matrix} = \dot{N}\Theta\,[\exp\,(-\frac{E}{k_B T})]P \qquad (15)$$

where E is the apparent activation energy and P is the steric factor which must be empirically determined.

Surface Catalyzed Formation Desorption Rate. If a molecule is formed as a result of a gas phase particle (atom or molecule) striking a chemisorbed particle (atom or molecule), the Langmuir-Rideal mechanism can again be used to describe the formation of product molecules and desorption:

$$\begin{matrix}\text{Surface Catalyzed} \\ \text{Formation} \\ \text{Desorption Rate}\end{matrix} = \dot{N}\Theta\,[\exp(-\frac{E}{k_B T})]P \qquad (16)$$

Rate Equation

As mentioned in the previous chapter, air consists predominantly of five species at temperatures below 8000°K (Ref 22): N, N_2, O, O_2, and NO. The time rate of change of the number of chemisorbed nitrogen atoms per unit area assuming atoms are chemisorbing, thermally desorbing, recombining via the Langmuir-Rideal mechanism and subsequently desorbing as molecules, and forming NO via a Langmuir-Rideal mechanism and then desorbing can now be expressed as:

$$\frac{dn_{s_N}}{dt} = S_{o_N}\,\dot{N}_N\,(1-\Theta_T) - \delta_N\Theta_N - P_{NN}\,\dot{N}_N\,\Theta_N\,\exp(-\frac{E_{NN}}{k_B T}) - P_{ON}\,\dot{N}_O\,\Theta_N\,\exp(-\frac{E_{ON}}{k_B T}) \qquad (17)$$

where n_{s_N} is the number of chemisorbed nitrogen atoms per unit area. The subscript N on the parameters signifies that the variable is for atomic nitrogen. The double subscript NN and ON mean that the variable is for the nitrogen recombination and NO, nitric oxide, formation, respectively. A similar equation may be written for the time rate of change of the number of chemisorbed oxygen atoms per unit area when oxygen atoms are undergoing the same processes:

$$\frac{dn_{s_O}}{dt} = S_{o_O} \dot{N}_O (1-\Theta_T) - \delta_O \Theta_O - P_{OO} \dot{N}_O \Theta_O \exp(-\frac{E_{OO}}{k_B T}) - P_{NO} \dot{N}_N \Theta_O \exp(-\frac{E_{NO}}{k_B T}) \quad (18)$$

The double subscript NO signifies the surface catalyzed NO formation via the collision of a gas phase nitrogen atom with a chemisorbed oxygen atom, while the ON subscript in equation (17) is for the formation of nitric oxide via the collision of a gas phase oxygen atom with a chemisorbed nitrogen atom.

If nitrogen, oxygen, and nitric oxide molecules are assumed to be able to chemisorb to and thermally desorb from the surface, then rate equations may be written for the time rate of change of the number of chemisorbed molecules of each of these species in the following way:

$$\frac{dn_{s_{N_2}}}{dt} = S_{o_{N_2}} \dot{N}_{N_2} (1 - \Theta_T) - \delta_{N_2} \Theta_{N_2} \quad (19)$$

$$\frac{dn_{s_{O_2}}}{dt} = S_{o_{O_2}} \dot{N}_{O_2} (1 - \Theta_T) - \delta_{O_2} \Theta_{O_2} \quad (20)$$

$$\frac{dn_{s_{NO}}}{dt} = S_{o_{NO}} \dot{N}_{NO} (1 - \Theta_T) - \delta_{NO} \Theta_{NO} \quad (21)$$

Note that these equations (19) - (21) have only one means whereby the molecules leave the surface —— via thermal desorption. Θ_T is the total fractional surface concentration and is bounded by $0 \leq \Theta_T \leq 1$.

$$\Theta_T = \Theta_N + \Theta_{N_2} + \Theta_O + \Theta_{O_2} + \Theta_{NO} \tag{22}$$

This expression for Θ_T may be substituted into equations (17) - (21). In steady state, these equations are each equal to zero, and therefore may be solved for the fraction of the surface that is covered by each species:

$$\Theta_N = \frac{1 - \Theta_{N_2} - \Theta_O - \Theta_{O_2} - \Theta_{NO}}{1 + \frac{\delta_N}{S_{o_N} \dot{N}_N} + \frac{P_{NN} \exp(-\frac{E_{NN}}{k_B T})}{S_{o_N}} + \frac{P_{ON} \dot{N}_O \exp(-\frac{E_{ON}}{k_B T})}{S_{o_N} \dot{N}_N}} \tag{23}$$

$$\Theta_{N_2} = \frac{1 - \Theta_N - \Theta_O - \Theta_{O_2} - \Theta_{NO}}{1 + \frac{\delta_{N_2}}{S_{o_{N_2}} \dot{N}_{N_2}}} \tag{24}$$

$$\Theta_O = \frac{1 - \Theta_N - \Theta_{N_2} - \Theta_{O_2} - \Theta_{NO}}{1 + \frac{\delta_O}{S_{o_O} \dot{N}_O} + \frac{P_{OO} \exp(-\frac{E_{OO}}{k_B T})}{S_{o_O}} + \frac{P_{NO} \dot{N}_N \exp(-\frac{E_{NO}}{k_B T})}{S_{o_O} \dot{N}_O}} \tag{25}$$

$$\Theta_{O_2} = \frac{1 - \Theta_N - \Theta_{N_2} - \Theta_O - \Theta_{NO}}{1 + \frac{\delta_{O_2}}{S_{o_{O_2}} \dot{N}_{O_2}}} \tag{26}$$

$$\Theta_{NO} = \frac{1 - \Theta_N - \Theta_{N_2} - \Theta_O - \Theta_{O_2}}{1 + \frac{\delta_{NO}}{S_{o_{NO}} \dot{N}_{NO}}} \tag{27}$$

Let us now make the following definitions for isolated fractional surface concentrations in a manner similar to Jumper's, et. al., (Ref 14):

$$(\Theta_N)_o \equiv \frac{1}{1 + \frac{\delta_N}{S_{o_N} \dot{N}_N} + \frac{P_{NN} \exp(-\frac{E_{NN}}{k_B T})}{S_{o_N}} + \frac{P_{ON} \dot{N}_O \exp(-\frac{E_{ON}}{k_B T})}{S_{o_N} \dot{N}_N}} \tag{28}$$

$$(\Theta_{N_2})_o \equiv \frac{1}{1 + \frac{\delta_{N_2}}{S_{o_{N_2}} \dot{N}_{N_2}}} \tag{29}$$

$$(\Theta_O)_o \equiv \frac{1}{1 + \frac{\delta_O}{S_{o_O} \dot{N}_O} + \frac{P_{OO} \exp(-\frac{E_{OO}}{k_B T})}{S_{o_O}} + \frac{P_{NO} \dot{N}_N \exp(-\frac{E_{NO}}{k_B T})}{S_{o_O} \dot{N}_O}} \tag{30}$$

$$(\Theta_{O_2})_o \equiv \frac{1}{1 + \frac{\delta_{O_2}}{S_{o_{O_2}} \dot{N}_{O_2}}} \tag{31}$$

$$(\Theta_{NO})_o \equiv \frac{1}{1 + \frac{\delta_{NO}}{S_{o_{NO}} \dot{N}_{NO}}} \tag{32}$$

These isolated fractional surface concentrations correspond to the actual surface coverages when the other species are not present. By substituting these definitions for the isolated fractional surface concentrations, equations (28) - (32), into equations (23) - (27), we obtain the following system of five equations in terms of the five fractional surface concentrations for the five species:

$$\begin{bmatrix} \frac{1}{(\Theta_N)_o} & 1 & 1 & 1 & 1 \\ 1 & \frac{1}{(\Theta_{N_2})_o} & 1 & 1 & 1 \\ 1 & 1 & \frac{1}{(\Theta_O)_o} & 1 & 1 \\ 1 & 1 & 1 & \frac{1}{(\Theta_{O_2})_o} & 1 \\ 1 & 1 & 1 & 1 & \frac{1}{(\Theta_{NO})_o} \end{bmatrix} \begin{bmatrix} \Theta_N \\ \Theta_{N_2} \\ \Theta_O \\ \Theta_{O_2} \\ \Theta_{NO} \end{bmatrix} = \begin{bmatrix} 1 \\ 1 \\ 1 \\ 1 \\ 1 \end{bmatrix} \tag{33}$$

This system of equations may now be solved in a straight forward manner for the fractional surface concentrations using Cramer's Rule.

Rather than give the details of this solution, it is sufficient here to comment on the complexity of the resulting expressions. The resulting expressions for the fractional surface concentrations are in terms of five initial sticking coefficients, five thermal desorption energies, four activation energies, and four steric factors. Some of

these parameters are not constants, and we have a very complex system to deal with. Considerable further simplifying must be accomplished before this system of equations can be handled since many of these parameters are unknown and must be experimentally determined. The next chapter discusses the simplifications that were made to reduce the complexity of the solution of equation (33).

III. Initial Approach to Modeling Oxygen Recombination on Silicon Dioxide

In order to limit the number of physical processes taking place on the catalytic silicon dioxide surface, it would be nice to consider only the O to O_2 reaction. Fortunately, this case has some practical significance. During the latter portion of the reentry, a vehicle like the Space Shuttle has decelerated sufficiently so that the nitrogen atom concentration in the flow over the vehicle surface is negligible (Ref 24). Under these conditions, air consists primarily of only four species: N_2, O, O_2, and NO. Therefore, the equations derived in Chapter II may be simplified to a case which can both be handled and have utility. If we further assume that the nitrogen and nitric oxide molecules act only as diluents and as such do not chemisorb to the surface sites on the silicon dioxide surface, we are left with only oxygen atoms and molecules actively participating on the surface.

In that which follows, a development is given which adapts wholesale the approach of Jumper, et. al., (Ref 14), for recombination of fluorine on nickel. As will be discussed in Chapter V, this approach leads to results which are unphysical; it does, however, provide a starting point. Using the approach, then, of Jumper, et. al., (Ref 14), and the above simplifications, equation (18) reduces to the following:

$$\frac{dn_{s_O}}{dt} = S_{o_O} \dot{N}_O (1 - \Theta_T) - \delta_O \Theta_O - P\dot{N}_O\Theta_O \exp(-\frac{E}{k_B T}) \qquad (34)$$

and equation (20) is still valid:

$$\frac{dn_{s_{O_2}}}{dt} = S_{o_{O_2}} \dot{N}_{O_2} (1 - \Theta_T) - \delta_{O_2} \Theta_{O_2} \tag{20}$$

(The subscripts on P_{00} and E_{00} are dropped due to there now being no confusion.)

$$\Theta_T = \Theta_0 + \Theta_{O_2} \tag{35}$$

At steady state conditions:

$$\Theta_0 = \frac{1 - \Theta_{O_2}}{1 + \frac{\delta_0}{S_{o_0} \dot{N}_0} + \frac{P \exp(-\frac{E}{k_B T})}{S_{o_0}}} \tag{36}$$

$$\Theta_{O_2} = \frac{1 - \Theta_0}{1 + \frac{\delta_{O_2}}{S_{o_{O_2}} \dot{N}_{O_2}}} \tag{37}$$

If we now define the isolated fractional surface concentrations as follows:

$$(\Theta_0)_o \equiv \frac{1}{1 + \frac{\delta_0}{S_{o_0} \dot{N}_0} + \frac{P \exp(-\frac{E}{k_B T})}{S_{o_0}}} \tag{38}$$

$$(\Theta_{O_2})_o \equiv \frac{1}{1 + \frac{\delta_{O_2}}{S_{o_{O_2}} \dot{N}_{O_2}}} \tag{39}$$

We can solve for the fractional surface concentrations:

$$\Theta_0 = \frac{(\Theta_0)_o \left[1 - (\Theta_{0_2})_o\right]}{1 - (\Theta_0)_o (\Theta_{0_2})_o} \tag{40}$$

$$\Theta_{0_2} = \frac{(\Theta_{0_2})_o \left[1 - (\Theta_0)_o\right]}{1 - (\Theta_0)_o (\Theta_{0_2})_o} \tag{41}$$

Recombination Coefficient

The recombination coefficient, γ, is defined as the fraction of collisions with the surface leading to recombination (Ref 25). Therefore, the recombination coefficient is equal to two times the recombination desorption rate divided by the atom impingement rate. The factor of two accounts for the fact that two atoms must collide with the surface for each recombination with the first atom chemisorbing to the surface. The recombination coefficient is then given by:

$$\gamma = 2 P \Theta_0 \exp(-\frac{E}{k_B T}) \tag{42}$$

If we substitute equation (40) for Θ,

$$\gamma = \frac{2 P (\Theta_0)_o \left[1 - (\Theta_{0_2})_o\right] \exp(-\frac{E}{k_B T})}{1 - (\Theta_0)_o (\Theta_{0_2})_o} \tag{43}$$

Alternatively, in terms of the basic parameters, equation (43) is:

$$\gamma = \frac{2 S_{o_0} \dot{N}_0 \delta_{0_2} P \exp(-\frac{E}{k_B T})}{S_{o_0} \dot{N}_0 \delta_{0_2} + \delta_0 S_{o_{0_2}} \dot{N}_{0_2} + \delta_0 \delta_{0_2} + \dot{N}_0 S_{o_{0_2}} \dot{N}_{0_2} P \exp(-\frac{E}{k_B T}) + \dot{N}_0 \delta_{0_2} P \exp(-\frac{E}{k_B T})} \tag{44}$$

In either form, we see that a number of physical parameters are needed to proceed further. These parameters are the initial sticking coefficients for atomic oxygen and molecular oxygen, S_{o_0} and $S_{o_{0_2}}$, respectively; the thermal desorption energies for atomic oxygen and molecular oxygen, D_0 and D_{0_2}, respectively; and also the steric factor and the activation energy for the recombination process.

Equation (44) is for the oxygen atom recombination coefficient when both the oxygen atoms and the oxygen molecules are assumed to chemisorb to the silicon dioxide surface. It is important to again note that we are assuming that both oxygen atoms and molecules chemisorb to the silicon dioxide surface, and that the sticking coefficient is given be equation (12), where S_o may be a function of temperature, consistent with the model for fluorine recombination on nickel suggested by Jumper, et. al. Although I will attempt in Chapter V to argue that this is not the case, it is of interest to explore the ramifications of these assumptions in light of interpretations of the effect on the character of the data each influencing parameter has.

Jumper, et. al., (Ref 14), made the observation that, while there was an interrelationship between the parameters, each had a distinct effect on the character of the data. Equation (43) is similar to that of Jumper's model for fluorine atom recombination when the temperature is sufficiently high so that physical adsorption is negligible, with the exception that Jumper, et. al., assumed that the activation energy is negligible for fluorine atom recombination on nickel and thus their equation-like equation (43) does not contain the exp $(-\frac{E}{k_B T})$ factor. In this form, it is clear that a competition for surface sites between the

atoms and molecules is indicated, and this competitive role formed the key mechanism to interpret the fluorine recombination data by providing the ability for the recombination coefficient to first increase with temperature but then decrease as the temperature continues to increase.

According to the explanation of Jumper, et. al., at temperatures where only chemisorption is significant, the recombination coefficient increases with increasing temperature to a maximum and then decreases as the temperature is further increased. The recombination coefficient is able to increase as the temperature increases because the chemisorbed molecules are thermally desorbing, thereby allowing more atoms to chemisorb to the surface and subsequently recombine. At still higher temperatures, however, the chemisorbed atoms begin to thermally desorb, thus allowing for the recombination coefficient to go through a maximum, i.e., the thermal desorption increases with increasing temperature causing a decrease in the fractional surface concentration of the atomic species and a decrease in the recombination rate.

Jumper, et. al., (Ref 14) modeled the initial sticking coefficients for both atomic and molecular fluorine on nickel and as a result only the steric factor and the two thermal desorption energies were unknown. They found that the remaining three variables affected the recombination data in distinctly different ways, and consequently could be determined from the data. There is, of course, no assurance that the same model that worked for the recombination of fluorine on nickel should work for the recombination of oxygen on silicon dioxide, but both the model and the method for obtaining the missing parameters at least formed a starting point. Indeed, this is what has been done. Rather than describing that

work immediately, however, the description is held until Chapter V. This has been done so that we may discuss the available data in order to have a metric against which to compare the model results.

IV. Data for Oxygen Recombination on Silicon Dioxide

Recombination Data

In principle, the heterogeneous recombination of atomic oxygen is an elementary surface reaction. However, the recombination coefficient results for oxygen recombination on silicon dioxide often vary by a factor of five within a single laboratory, and by up to two orders of magnitude between different laboratories (Ref 25). Linnett's work (Ref 17, 26-28) provides the recombination coefficient for oxygen recombination on silicon dioxide by two different methods. These results are considered the best data to date and have even been used for calibration purposes (Ref 9). Figure 1 shows the recombination coefficient data points as a function of the reciprocal of the absolute temperature as taken from Reference 17. The data points shown are for one series of experiments, but the flattening of the curve drawn through the data by the experimentalists at the elevated temperatures was confirmed in further tests. Rosner's work as reported by Breen, et. al., in Reference 9 also supports the results of Linnett. The flattening of the curve in Figure 1 appears to be due to a maximum value for the recombination coefficient. It is known that as the temperature is further increased, the recombination coefficient decreases (Ref 9).

As shown in Figure 1, Linnett's data increases in value nonlinearly as the temperature increases. Greaves and Linnett (Ref 17) proposed that the activation energy increases from 1 kcal/mole at room temperature to 13 kcal/mole at 300°C.

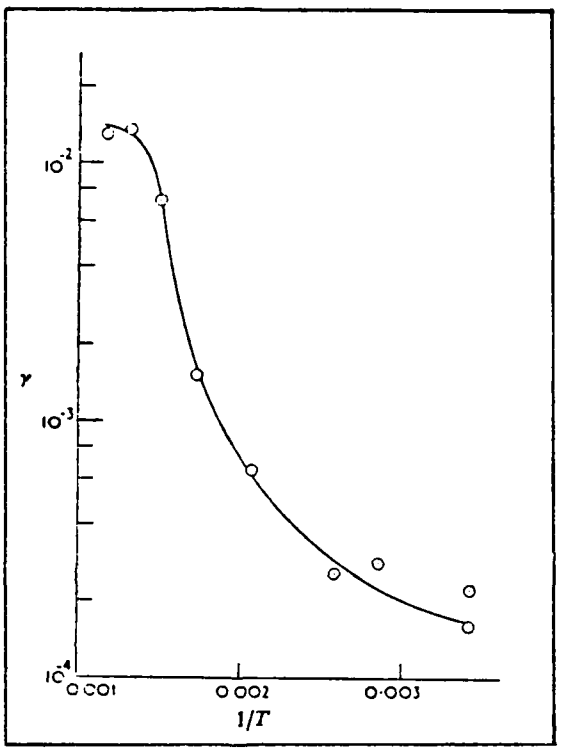

Figure 1. Graph Showing Variation of log γ with 1/T for Silica (Ref 17).

The order of the recombination process is also an extremely important piece of data. The recombination process is first order with respect to the oxygen atom pressure from room temperature to 350°K (Ref 26). The recombination process has been experimentally verified to remain first order from room temperature to above 1100°K (Ref 9). As was described in Chapter II, the recombination kinetics on most surfaces are in general first order processes which transition to second order at higher temperatures (Ref 12). While no empirical evidence exists for the recombination mechanism transitioning to second order for oxygen recombination on silicon dioxide, in view of the above, a satisfactory model should allow for such a transition.

Silicon Dioxide Surface Structure

In each of the various forms of silicon dioxide the silicon atom is bonded in a covalent manner (Ref 29) at the center of a regular tetrahedron (Ref 30). The tetrahedra link together corner to corner and the different structures formed determine the different forms of silicon dioxide---cristobalite, quartz, or tridymite. Figure 2 is a reproduction of Wells' Figure 288 and shows the different silicon dioxide structures.

The surface structure of silicon dioxide must satisfy the stoichiometric relationship SiO_2 in addition to the substructure matrix such that each silicon atom is bonded to four oxygen atoms via half bonds: $Si(\frac{1}{2}O)_4$. That is, each oxygen atom in the substructure is shared by two silicon atoms. Heterogeneous recombination is very dependent upon the surface structure and this may be the reason for such large differences in experimental results (Ref 31). Greaves and Linnett (Ref 17) discuss

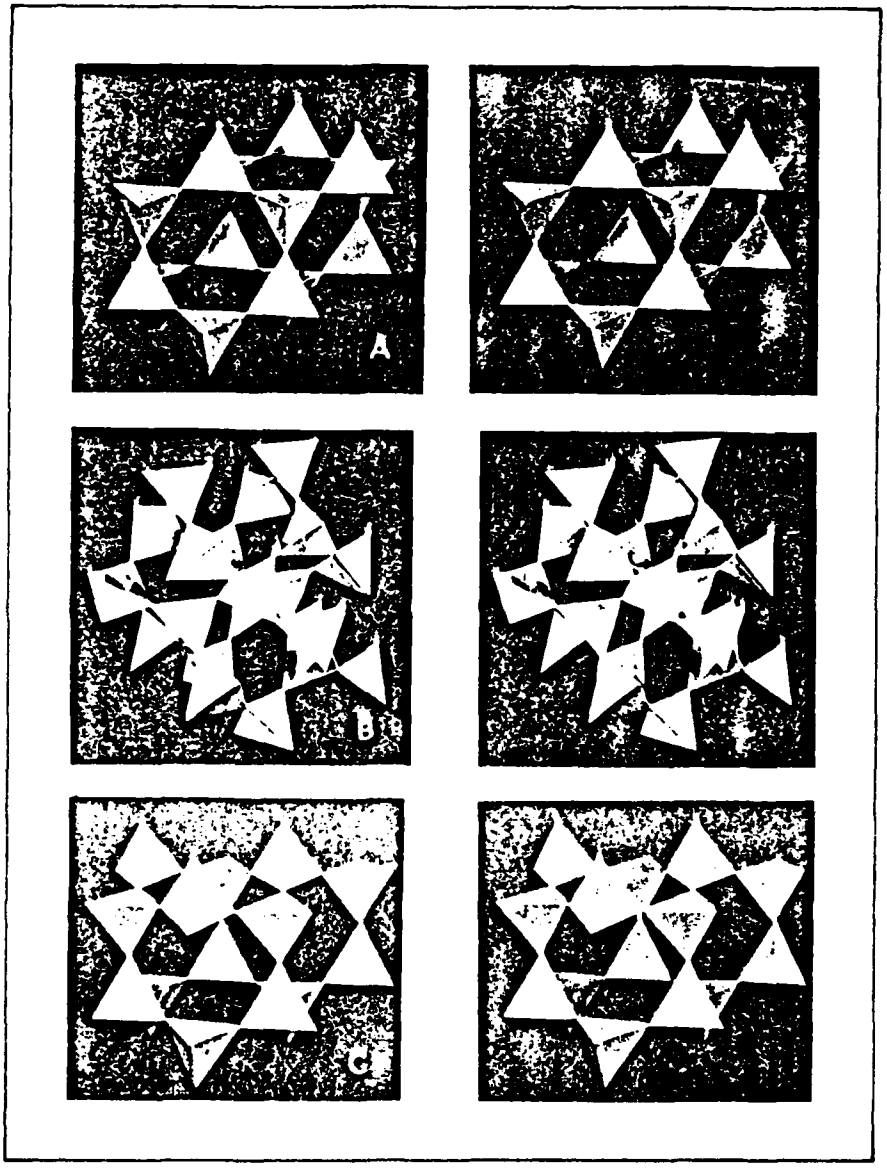

Figure 2. Stereoscopic Photographs Showing the Structures of the Three Forms of Silica, (A) Cristobalite, (B) Quartz, and (C) Tridymite, as Systems of Linked SiO_4 Tetrahedra (Ref 30).

the possible surface structure when hydrogen atoms are present in the form of water with the result that hydroxyl groups are attached to the silicon dioxide surface. They mention that when no OH groups are present, the surface structure might look like the following:

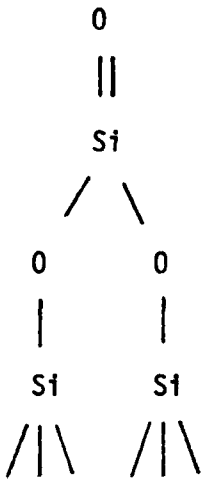

where the oxygen atom that has the double bond forms the surface layer with other oxygen atoms that have double bonds to silicon atoms below them.

Removal of Surface Oxygen Atoms

Experimental evidence that is independent of oxygen recombination data shows that oxygen atoms can be removed from a silicon dioxide surface. Hickmott (Ref 32) studied the interaction of atomic hydrogen with glass and found that the glass provided the oxygen atoms which were in the product molecules.

Campbell and Thrush (Ref 33) observed BN gas downstream of their

Pyrex flow tube following nitrogen recombination studies. Rahman and Linnett (Ref 34) state that nitrogen atoms evidently bond to boron, and therefore, the active sites may be the boron and silicon atoms in the glass.

Evenson and Burch (Ref 35) found that the recombination coefficient for nitrogen atom recombination on quartz decreased as the oxygen impurity of their nitrogen source gas increased. That is, the oxygen atoms act as a poison for nitrogen recombination on these quartz surfaces.

Rosner (Ref 9) used X-Ray Photoelectron Spectroscopy (XPS) to analyze silica and silicon carbide samples exposed to an oxygen atom plus nitrogen atom mixture. Silica samples exposed to this mixture at 1490°K showed that nitrogen atoms reacted with the silica forming either silicon nitride or silicon oxynitride or possibly just were absorbed. When silicon carbide samples were exposed to the same mixture of oxygen and nitrogen atoms at temperatures up to 1620°K, a surface of only silica was produced. Oxidation is evidently favored over nitridation at temperatures up to 1620°K. At higher temperatures following quenching in argon, the silicon carbide samples consisted of silicon carbide, silicon nitrides, or silicon oxynitrides. (This surface activity will be referred back to in Chapter V where the details of the modified model are given.) An atom that is chemisorbed to a surface is essentially the same as the one that has formed a covalent bond with a surface (Ref 12 and 36). For this reason bonding and chemisorption are hereafter used interchangeably. Wells (Ref 30) gives the Si-O bond energy in the SiO_2 molecule as 108 kcal.

Chemisorption Data

In Chapter II, the sticking coefficient was expressed as

$$S = S_0 (1 - \theta) \tag{11}$$

This form of S has been experimentally verified by Antonini (Ref 37) for CO_2 up to 180°C and for O_2 on "fresh" silica, and by Christmann, et. al., (Ref 38) for H_2 on nickel. However, oxygen atoms have not been observed to chemisorb to natural silicon dioxide surfaces (Ref 27). Further attempts to see oxygen atoms chemisorbed to natural silicon dioxide surfaces have failed (Ref 39).

Antonini (Ref 37) observed adsorption sites on freshly created glass and silica surfaces. These sites do not exist on glass and silica surfaces in their natural form. As a result, he was able to empirically determine the initial sticking coefficient for oxygen molecules on fresh silica as a function of temperature from 300°K to 800°K. His results may be expressed as

$$S_0 = 0.0375 \exp (-0.0021 T) \tag{45}$$

Hochstrasser and Antonini (Ref 40) found that there are 5×10^{14} bonds/cm^2 in the bulk of silicon dioxide. This value will be used later as the estimate of the number of adsorption sites on the silicon dioxide surface.

V. Evaluation of Initial Model and Proposal of a New Oxygen Recombination Model

In Chapter III the approach of Jumper, et. al., (Ref 14) was followed to derive an expression, equation (44), for the recombination coefficient when both oxygen atoms and oxygen molecules are assumed to chemisorb to the silicon dioxide surface. This model may be investigated to determine the influence of changing the values of the interrelated parameters in terms of attempting to match the character of the data described in the previous chapter.

Sensitivity Analysis

Following Jumper's approach, the activation energy for the oxygen recombination on silicon dioxide was assumed negligible which eliminated the exp $(-\frac{E}{k_B T})$ factors from equation (44). The recombination coefficient was then calculated as a function of temperature from 300°K to 2000°K using realistic values for the initial sticking coefficients for the oxygen atoms and oxygen molecules, number of surface sites, steric factor, and the thermal desorption energies for the oxygen atoms and oxygen molecules. The values for these six parameters were assumed to be independent of temperature. Further, the initial sticking coefficient for the atoms was first assumed equal to the initial sticking coefficient for the molecules. A study of the influence of changing the values of the parameters was made in an attempt to match the data from Greaves and Linnett (Ref 17) and also to keep the recombination kinetics first order

with respect to the atom pressure at low temperatures and transition to second order only at some elevated temperature.

This study led to a recombination coefficient of 4.6×10^{-4} at 300°K if the values of the parameters given in Table I were used. Further, the recombination coefficient experienced a maximum value of 9.7×10^{-2} at 940°K and then decreased to 1.4×10^{-2} at 2000°K, leading to a recombination process which was first order with respect to the pressure of the oxygen atoms at 300°K, transitioning to second order at a temperature of approximately 1300°K.

Using the values for parameters as given in Table I, one is also able to infer the physical processes at work in this model as a function of temperature. At 300°K, the fourth term in the denominator of equation (44), $\dot{N}_0 S_{O_2} \dot{N}_{O_2} P \exp(-\frac{E}{k_B T})$, is much larger than the other terms in the denominator. Since the initial sticking coefficients for atomic and molecular oxygen are assumed equal, the recombination coefficient may be expressed as

$$\gamma \simeq \frac{2 \delta_{O_2}}{\dot{N}_{O_2}} \tag{46}$$

The recombination coefficient thus increases as the thermal desorption of the molecules increases. The model thus predicts that the fractional surface concentration of the oxygen molecules is essentially unity at 300°K and decreases as the fractional surface concentration of the atoms increases. Note that this model with the values of the parameters as given in Table I has the recombination process first order with respect to the atomic species but inversely proportional to the pressure of the oxygen molecules.

Above 800°K the first term dominates the denominator of equation (44) so that

$$\gamma \simeq 2P \tag{47}$$

Thus, at this temperature, the recombination kinetics remain first order with respect to the atomic pressure but become independent of the molecular oxygen pressure.

TABLE I. Computational Parameters for Oxygen Atom Recombination on Silicon Dioxide Assuming Atomic and Molecular Oxygen Chemisorption.

PARAMETER	VALUE
P, STERIC FACTOR	0.1
E, ACTIVATION ENERGY	0
S_{o_O}, INITIAL STICKING COEFFICIENT FOR ATOMIC OXYGEN	0.3
$S_{o_{O_2}}$, INITIAL STICKING COEFFICIENT FOR MOLECULAR OXYGEN	0.3
C_a, SURFACE SITES	3.0×10^6
D_O, THERMAL DESORPTION ENERGY FOR ATOMIC OXYGEN	0.8×10^{-19} J/atom = 11.5 kcal/mole
D_{O_2}, THERMAL DESORPTION ENERGY FOR MOLECULAR OXYGEN	0.32×10^{-19} J/atom = 4.6 kcal/mole

As the temperature continues to increase, the recombination coefficient experiences a maximum at 940°K, and at 1300°K the third term

in the denominator begins to dominate. As a result,

$$\gamma \simeq \frac{2 P S_{o_0} \dot{N}_0}{\delta_0} \tag{48}$$

and the recombination process becomes second order with respect to the atomic species.

Thus, the model, adapted wholesale from Reference 14, is capable of matching the character of the available catalytic-oxygen-recombination data if the values of the parameters in Table I are used. These values are almost reasonable <u>except</u> for the extremely low value for the number of adsorption sites. There are approximately 10^{14} potential surface sites per square centimeter of surface (c.f., Chapter IV). To have only 10^6 sites active seems too low! Further, the thermal desorption values for atomic and molecular oxygen appear somewhat low since usual values of the chemisorption bond energy tend to be between 15-200 kcal/mole (Ref 20).

Finally, the assumption that oxygen molecules chemisorb to the silicon dioxide surface is both unlikely from the data (c.f., Chapter IV), and not in keeping with the usual assumptions concerning molecular adsorption. Laidler (Ref 41), for example, gives a convincing argument which concludes that molecular chemisorption in general is negligible except at very low temperatures. Ehrlich (Ref 42) also explains that molecular chemisorption is not observed for either hydrogen or nitrogen on many metals.

New Model

As a result of the arguments against molecular chemisorption, the lack of experimental evidence that molecular oxygen chemisorbs to natural silicon dioxide surfaces, the extremely low number of surface sites required for this model, and the functional dependence of the recombination coefficient upon the molecular impingement rate, the original model was set aside. A new model was developed which no longer required chemisorption of oxygen molecules. The role played by chemisorbed oxygen molecules was replaced by hypothesizing that the gas phase oxygen atoms combine directly with the oxygen atoms that constitute the silicon dioxide surface. Although a rather radical departure from previous approaches, it is really only a slight modification of thinking in terms of the Langmuir-Rideal recombination mechanism where the surface atoms now become the active surface-atom participants. In this new scheme then, gas phase oxygen atoms replace the oxygen atoms as they are removed from the surface-Si-O lattice by recombination reactions. In fact, this idea, although not used extensively, is not without precedent; Linnett and Marsden (Ref 27) proposed the same idea in 1956 and, as we will see, the experimental evidence seems to support the hypothesis.

If one now adapts this new model, a pattern begins to emerge from the data which at least qualitatively supports the notion. The results of Rosner's work (Ref 9), for example, can be interpreted as support for the idea that the surface sites are the silicon atoms rather than the oxygen atoms. For nitrogen atom recombination on silicon dioxide, Rosner found nitrogen atoms incorporated into the SiO_2 surface as silicon nitrides or silicon oxynitrides. This experimental data support the hypothesis

that the silicon atoms on a silicon dioxide surface are the active surface sites. Oxygen atoms bond to these silicon atoms forming the silicon-dioxide-matrix surface in a manner not unlike chemisorption of oxygen on a silicon surface. Gas phase oxygen atoms could then be colliding and combining with the oxygen atoms which form the surface of the silicon dioxide itself, with atoms from the gas phase then replacing the atoms lost from the surface.

In the new model the oxygen atom that is on the surface and possibly doubly bonded to the silicon atom (c.f., Chapter IV) is the oxygen atom that combines via the Langmuir-Rideal mechanism with a gas phase oxygen atom. The silicon atom is the surface site to which another gas phase oxygen atom readily attaches as follows:

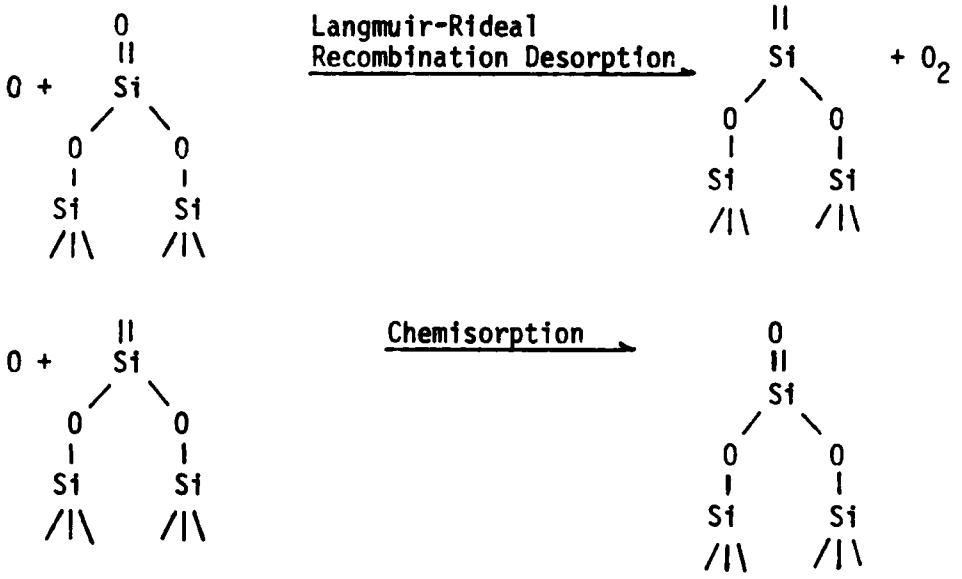

Rate Equation

The time rate of change of the number of surface-matrix-bonded oxygen atoms per unit area when atoms are chemisorbing, thermally desorbing, and recombining via the Langmuir-Rideal mechanism and subsequently desorbing

as molecules, can now be expresses as:

$$\frac{dn}{dt} = \dot{N} S_o(1 - \theta) - \delta\theta - P \dot{N} \theta \exp(-\frac{E}{k_B T}) \tag{49}$$

In a steady state, this equation can be solved for the fraction of the surface that is covered by oxygen atoms in the form:

$$\theta = \frac{S_o \dot{N}}{S_o \dot{N} + \delta + P\dot{N} \exp(-\frac{E}{k_B T})} \tag{50}$$

Recombination Coefficient

The recombination coefficient is then given by:

$$\gamma = 2P\theta \exp(-\frac{E}{k_B T}) \tag{51}$$

If we substitute equation (50) for θ,

$$\gamma = \frac{2 P S_o \dot{N} \exp(-\frac{E}{k_B T})}{S_o \dot{N} + \delta + P \dot{N} \exp(-\frac{E}{k_B T})} \tag{52}$$

A quick check of equation (50) for the fractional surface concentration shows that under steady state conditions the fractional surface concentration would be equal to ½ if both the initial sticking coefficient and the steric factor are equal to unity and if thermal desorption of the atoms is negligible. This means that under the conditions for maximum recombination only half the sites are filled at any instant in time. A steady state value of ½ for θ gives a maximum value of unity for gamma, i.e., a fully catalytic surface.

A qualitative look at the terms in the denominator of equation (52)

for the recombination coefficient is very instructive (Ref 18). If the term $S_o\dot{N}$ is large in comparison to the other two terms, then equation (50) reveals that $\Theta \simeq 1$ and that:

$$\gamma \simeq 2\ P \exp(-\frac{E}{k_B T}) \tag{53}$$

Since the recombination coefficient is independent of the impingement rate, the recombination process would be first order with respect to the atom pressure. Also note that the recombination process is controlled by the recombination desorption rate. If $P\ \dot{N} \exp(-\frac{E}{k_B T})$ is large, then Θ will be small and:

$$\gamma \simeq 2\ S_o \tag{54}$$

Then the recombination process would again be first order, but now the recombination process is controlled by the chemisorption rate. If δ is large, then Θ will be small and:

$$\gamma \simeq \frac{2\ P\ S_o\ \dot{N} \exp(-\frac{E}{k_B T})}{\delta} \tag{55}$$

The recombination process is now second order.

In order for the fractional surface coverage, Θ, to be large at low temperatures, this model requires $S_o\ \dot{N}$ to be large at these low temperatures; no other option is possible. However, at elevated temperatures where Θ may be smaller, the order of the recombination process must be determined empirically in order to know which term will dominate the denominator of equations (50) and (52). If the order is first at elevated

temperatures, then $P \dot{N} \exp(-\frac{E}{k_B T})$ must dominate. For second order recombination at the higher temperatures, this model requires high thermal desorption rate for the atoms.

Equation (52) for the recombination coefficient as a function of temperature requires data for the steric factor, sticking coefficient, number density, apparent activation energy, number of adsorption sites, and the chemisorption energy. The significance of the model is that the recombination coefficient is not dependent upon all of these variables at all temperatures. For a specific species of gas and surface at low temperatures where $\Theta \simeq 1$ and the recombination process is first order, an Arrhenius plot of the log of γ versus the reciprocal of absolute temperature will provide sufficient data so that the steric factor and the apparent activation energy can be determined. If the recombination process remains first order at elevated temperatures where Θ is small, the initial sticking coefficient is the only dependent variable in the expression for the recombination coefficient. On the other hand, if the recombination process goes second order at elevated temperatures, reasonable estimates can be obtained for the sticking coefficient and chemisorption energy when recombination coefficient data are available. Independent experiments like chemisorption and thermal atom desorption studies would confirm the values obtained for the dependent variables from the recombination coefficient results. Since all of the necessary data are not available to date to completely determine all the physio-chemical parameters, it is only possible to show how the Langmuir-Rideal mechanism satisfactorily models the recombination of oxygen or silicon dioxide, and to give the most reasonable estimate of the parameters.

Details of Model for Oxygen Recombination on Silicon Dioxide

Since in this model the surface concentration is that of the Si-O surface, Θ is going to be large at lower temperatures ($\Theta \simeq 1$). At the low temperatures, then, the recombination coefficient is given by:

$$\gamma \simeq 2\ P \exp(-\frac{E}{k_B T}) \qquad (53)$$

If both the steric factor and the activation energy are independent of temperature, a plot of the log of the recombination coefficient versus the reciprocal of the absolute temperature would give a straight line. However, as given in the previous chapter, Linnett's data increases in value nonlinearly as the temperature increases. Greaves and Linnett (Ref 17) proposed that the activation energy increases from 1 kcal/mole at room temperature to 13 kcal/mole at 300°C. If 13 kcal/mole is inserted into equation (53) along with a value of 1.6×10^{-3} for the recombination coefficient at 300°C, the steric factor must equal 73! This is not acceptable since by definition P must be ≤ 1.0. If, however, the steric factor is assumed to increase with temperature, and the activation energy is taken to be constant at its room temperature value of 1 kcal/mole (6.949×10^{-21} J/atom), a very satisfactory match of Linnett's data is obtained for an exponentially increasing steric factor with temperature of the following form:

$$P = 0.0000224 \exp(0.00908\ T) \qquad (56)$$

This value increases from 0.0003414 at 300°K to 0.1 at 925°K. At higher temperatures the steric factor is held equal to 0.1.

Assessing the Reasonableness of the Functional Dependence of the Steric Factor on Temperature

The steric factor is often explained as the fraction of the sufficiently energetic collisions that have the proper orientation for reaction to occur (Ref 43-44). Adamson states that the orientation explanation is probably valid for steric factors between 1.0 and 0.1 but would not likely be valid for very small values.

The term $\exp\left(-\frac{E}{k_B T}\right)$ represents the fraction of collisions that have sufficient energy E to react. This assumes that E comes only from the kinetic energy of relative motion of the colliding particles. However, if the internal energy of the particles could provide the activation energy E (Ref 44 and 22), or if the relative translational motion perpendicular to the line of centers could provide E, then we must modify $\exp\left(-\frac{E}{k_B T}\right)$ as follows:

$$\begin{array}{l}\text{Probability that f degrees of freedom have sufficient energy E}\end{array} = \frac{\left[\frac{E}{k_B T}\right]^{\left(\frac{f}{2}-1\right)}}{\left(\frac{f}{2}-1\right)!} \exp\left(-\frac{E}{k_B T}\right) \qquad (57)$$

The steric factor P could then be defined to include this pre-exponential factor:

$$\frac{\left[\frac{E}{k_B T}\right]^{\left(\frac{f}{2}-1\right)}}{\left(\frac{f}{2}-1\right)!}$$

which is a function of both temperature and the number of degrees of freedom available to supply E (Ref 45). Vincenti and Kruger explain that only a rough estimate can be made of f, due to the doubt as to

whether the vibration of the catalytic molecule can be effective and whether the relative translational motion normal to the line of centers should be considered. Although doubts exist, the steric factor could be temperature dependent.

Another explanation of the steric factor is given by Clarke and McChesney in terms of partition functions of the reactants:

TWO ATOMS		$P = 1$
Atom + Diatomic molecule	Nonlinear complex	$P = (Z_{vib})(Z_{rot})^{-1}$
	Linear complex	$P = (Z_{vib})^2(Z_{rot})^{-2}$
Two diatomic molecules	Nonlinear complex	$P = (Z_{vib})^3(Z_{rot})^{-3}$
	Linear complex	$P = (Z_{vib})^4(Z_{rot})^{-4}$

They explain that at ordinary temperatures $Z_{vib} \simeq 1$ and $Z_{rot} < 10$ so that for reactions between two atoms or an atom and a diatomic molecule, the steric factor is between 0.1 and 1. As the reacting molecules become more and more complicated, the steric factor decreases in value.

Even though these explanations give a functional dependence of the steric factor on temperature, the actual relationship depends on the assumptions made and can only be verified by further detailed experiments. Therefore, with the data that is available, the explanation given by Greaves and Linnett (Ref 17) is still probably the best. They state that the nonlinear increase in the recombination coefficient with temperature (therefore, nonlinear increase in the steric factor for a constant activation energy) could be explained in terms of changing the number of active surface sites. Dickens and Sutcliffe (Ref 13) found that the

recombination coefficient increased nonlinearly with temperature for Mn_2O_3, Fe_2O_3, NiO, CuO, CdO, and Co_3O_4. They explained this behavior as being due to a change in state of the surface. The relationship among the crystalline forms of silicon dioxide is as follows (Ref 46):

$$\underset{\text{quartz}}{\alpha} \overset{573^\circ C}{\rightleftharpoons} \underset{\text{quartz}}{\beta} \overset{870^\circ C}{\rightleftharpoons} \underset{\text{tridymite}}{\beta} \overset{1470^\circ C}{\rightleftharpoons} \underset{\text{cristobalite}}{\beta} \overset{1710^\circ C}{\rightleftharpoons} \text{liquid}$$

$$\underset{\text{tridymite}}{\alpha} \overset{160 \text{ to } 120^\circ C}{\rightleftharpoons} \underset{\text{tridymite}}{\beta} \qquad \underset{\text{cristobalite}}{\alpha} \overset{200 \text{ to } 275^\circ C}{\rightleftharpoons} \underset{\text{cristobalite}}{\beta}$$

Since silicon dioxide changes its surface structure with temperature, it appears that the best explanation for the steric factor increasing with increasing temperature is that the number of active surface sites increases with temperature as the surface structure changes causing the steric factor to also increase.

In the present model the surface sites are taken to be constant with temperature. Thus, if the explanation of Greaves and Linnett is correct, one must interpret the steric factor to include the surface site change as well as its normal meaning. It must be recognized, then, that the definition used here is at slight variance with the classical interpretation. What has not changed, however, is the real fact that the steric factor has always been and continues to be here a catch-all factor which includes the uncertainties in the model, the point being made that it is not unreasonable that it has a temperature dependence.

Further Details of Model

Since the recombination process remains first order to at least 1100°K which is above the temperature where gamma is a maximum, the

recombination coefficient is approximated by the following:

$$\gamma \simeq 2\ S_o \tag{54}$$

Figures 3 and 4 show how the initial sticking coefficient is only of significance at elevated temperatures. The influence of the quantitative changes in the initial sticking coefficient on the recombination coefficient is also shown. The same functional form as Antonini's results (c.f., Chapter IV) for O_2 chemisorption on "fresh" silicon dioxide is adapted here and is as follows:

$$S_o = 0.05 \exp(-0.002\ T) \tag{58}$$

for the initial sticking coefficient of oxygen atoms onto silicon dioxide. The initial sticking coefficient decreases from 0.02744 at 300°K to 0.0009158 at 2000°K.

At a temperature somewhere above 1100°K, the thermal desorption of atomic oxygen becomes significant. Equation (13) gives the thermal desorption rate per unit area of covered surface as:

$$\delta = \frac{C_a\ k_B T}{h}\ \exp(-\frac{D}{k_B T}) \tag{13}$$

C_a is the number of adsorption surface sites per unit area, and Hochstrasser and Antonini (Ref 40) found that there are 5×10^{14} bonds/cm^2 in the bulk of silicon dioxide. Therefore, I will use this value as the number of adsorption sites on the surface of silica.

Wells (Ref 30) gives the Si-O bond energy in the SiO_2 molecule as 108 kcal. Therefore, each half-bond strength would be 54 kcal. As a reasonable estimate, 150% of the half-bond strength is used as the energy

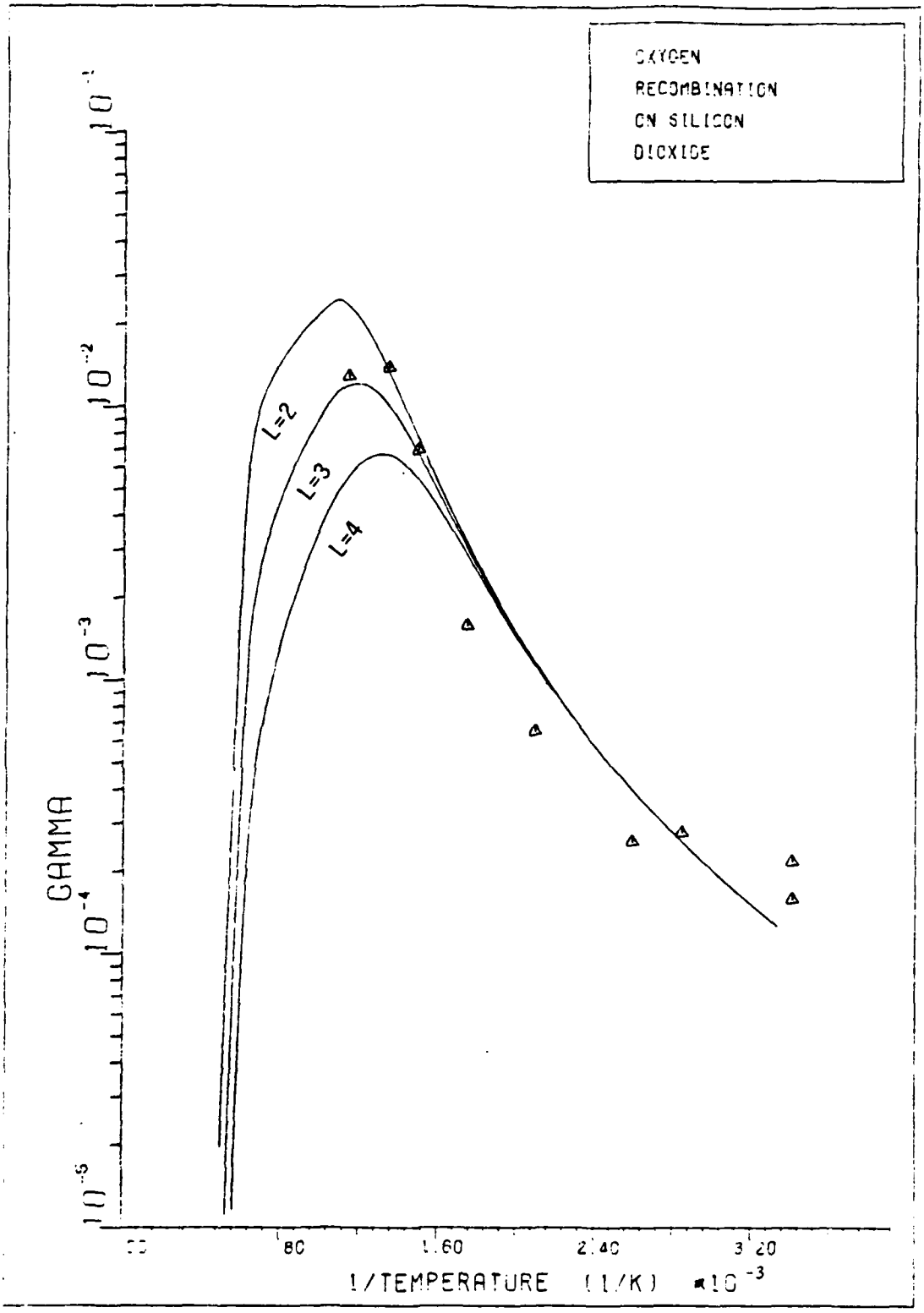

Figure 3. Recombination Coefficient vs. 1/Temperature for S_o = 0.1 exp(-0.001 T L), L = 2, 3, 4.

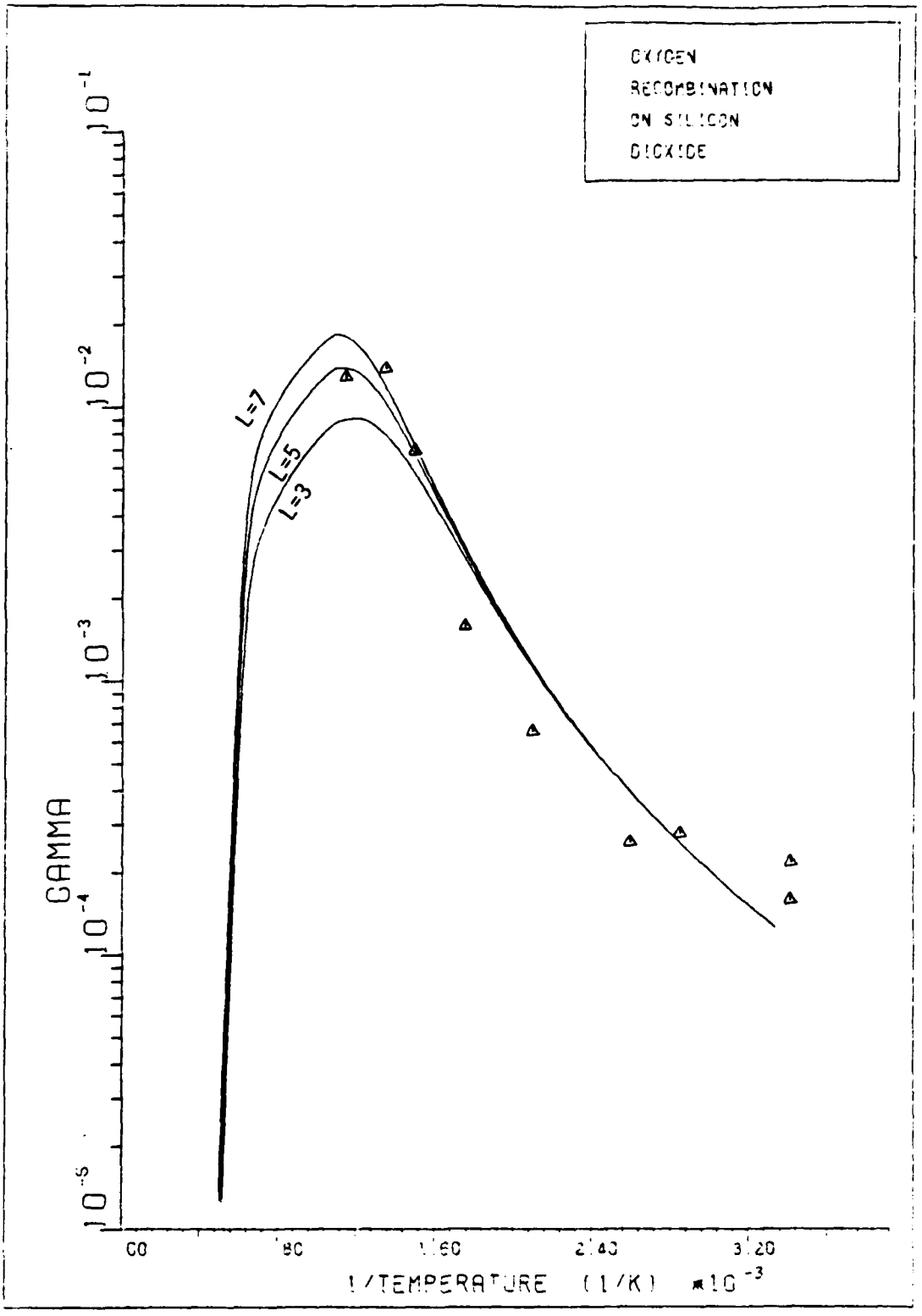

Figure 4. Recombination Coefficient vs. 1/Temperature for S_0 = 0.01 L exp(-0.002 T), L = 3, 5, 7.

required to extract from the surface the oxygen atom that has the double bond to the silicon atom. This 81 kcal (5.629×10^{-19} J/atom) is the value used for the chemisorption well depth. Therefore, all variables are quantified in equation (52) for the recombination coefficient as a function of temperature. Figure 5 demonstrates the influence of the thermal desorption energy on the recombination coefficient. The desorption energy was decreased in 5 kcal/mole increments from 85 to 45 kcal/mole. For negligible second order recombination at 1100°K the thermal desorption energy must be at least 60 kcal/mole (4.169×10^{-19} J/atom). An experimental investigation as to the temperature where the recombination process turns to second order would be very useful.

Figure 6 gives the results of the model for the recombination of oxygen atoms on silicon dioxide using the values for the parameters summarized in Table II. A close look at the calculations performed in 20°K increments from 300°K to 2000°K is very informative. The physical and chemical microscopic details are readily available from this model. As was discussed earlier, the $S_o\dot{N}$ term in the denominator of equation (52) for the recombination coefficient must be the dominant term at room temperature in order for the recombination process to be first order and for the fractional surface concentration to be approximately unity. From the details of the model this term dominates from 300°K to 740°K. With the $S_o\dot{N}$ dominating in this temperature range, the recombination process is controlled by the recombination desorption rate through the steric factor and the activation energy. From 740°K to 1600°K, the recombination process remains first order, and the recombination coefficient has a maximum value of 1.4×10^{-2} at 900°K. The $P\dot{N} \exp\left(-\frac{E}{k_B T}\right)$

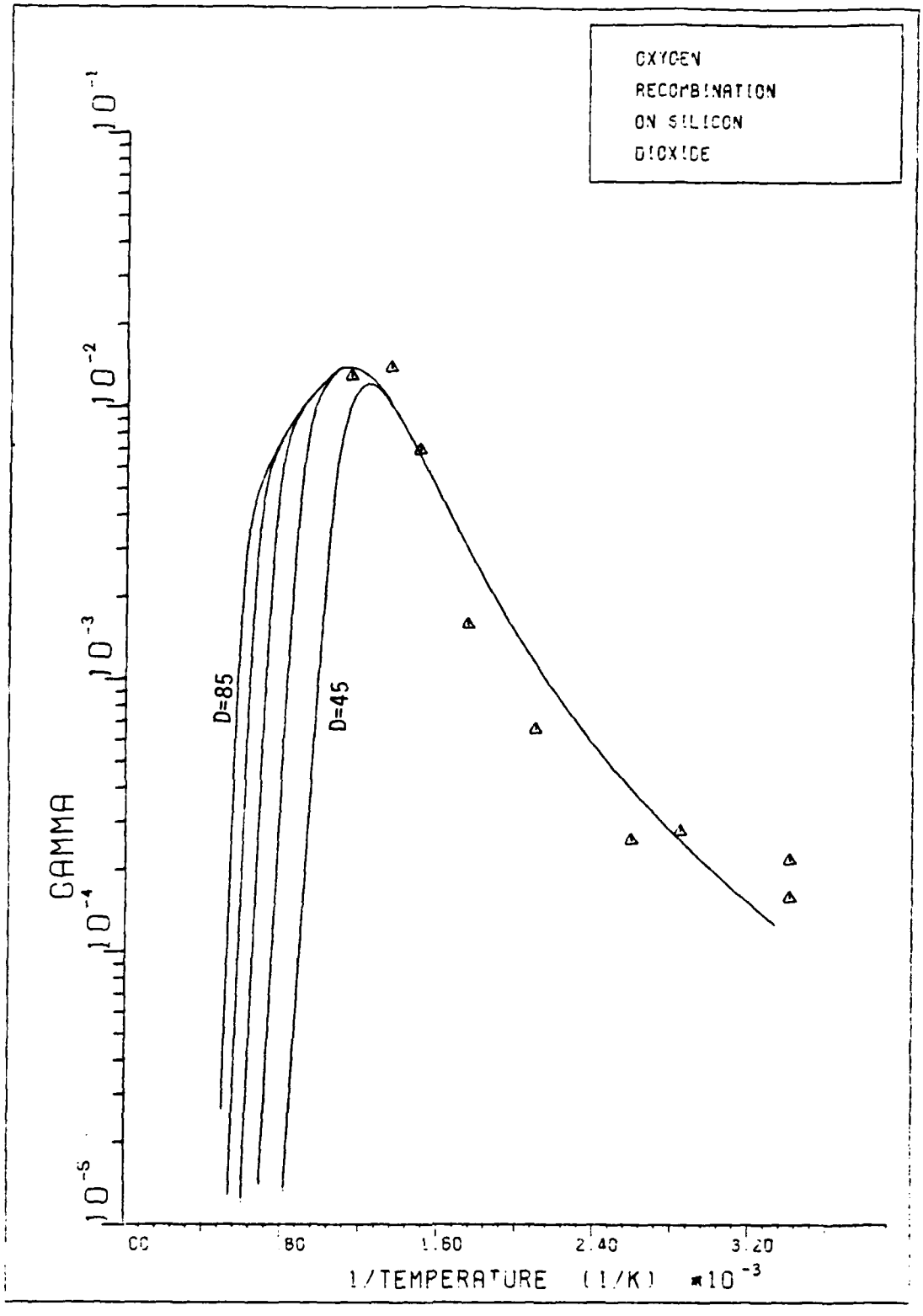

Figure 5. Recombination Coefficient vs. 1/Temperature for Bond Energy D = 45, 55, 65, 75, 85 kcal/mole.

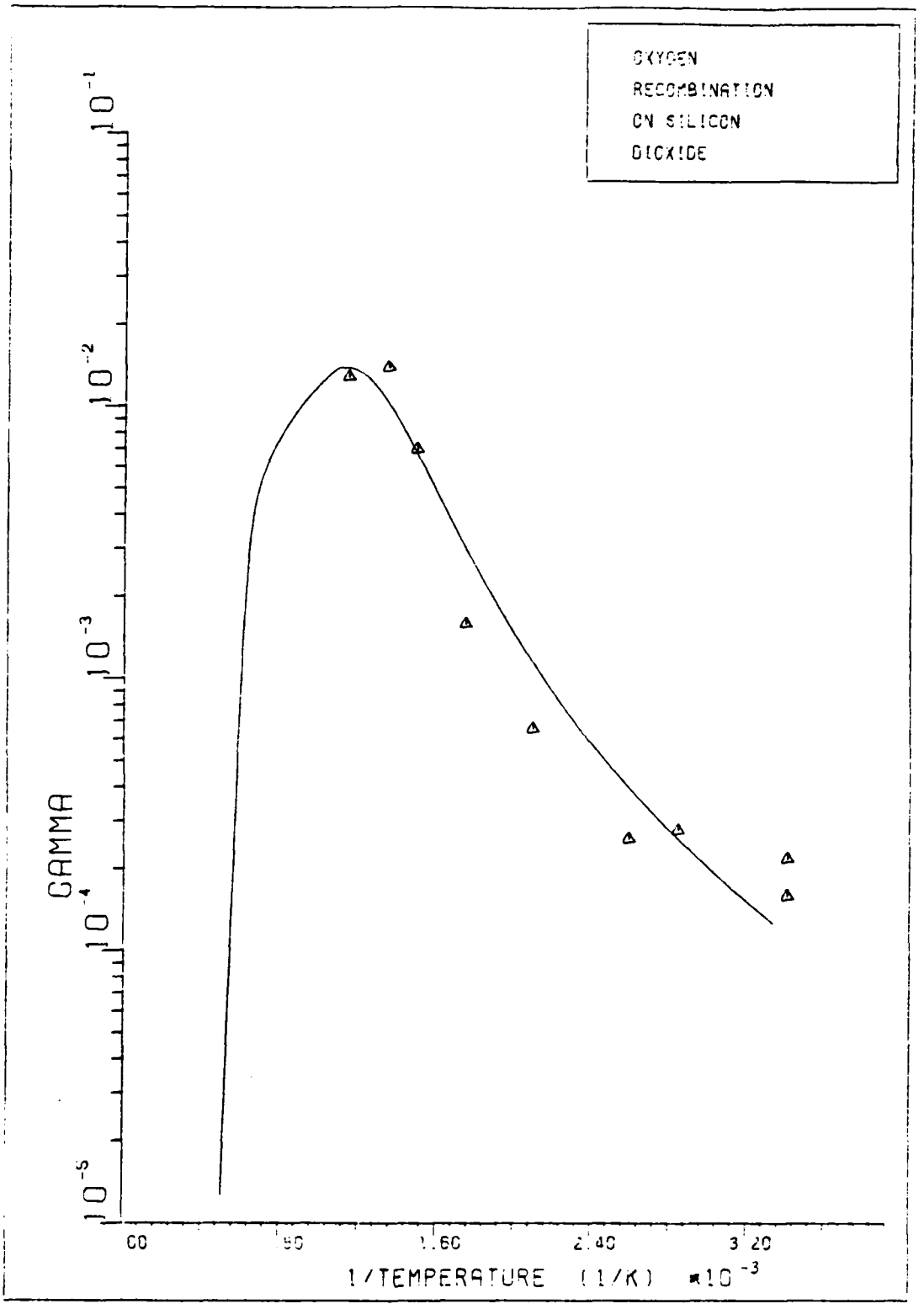

Figure 6. Recombination Coefficient vs. 1/Temperature for the Values of the Parameters given in Table II.

term in equation (52) dominates in this temperature range with the recombination process being controlled by the chemisorption rate through the initial sticking coefficient. Above 1600°K the thermal desorption rate term is the largest in the denominator of equation (52). At these temperatures the recombination process is second order, and the fractional surface concentration is very small. The oxygen atoms that are surface-matrix-bonded rapidly leave the surface again due to the high thermal desorption rate. There simply aren't many surface sites filled with a surface-matrix-bonded oxygen atom, which is a prerequisite for heterogeneous recombination. As a result, the recombination coefficient is very small and continues to decrease in value as the temperature increases.

TABLE II. Computational Parameters for Oxygen Atom Recombination on Silicon Dioxide Assuming Atomic Oxygen Chemisorption Only.

PARAMETER	VALUE
P, STERIC FACTOR	$0.0000224 \exp(0.00908\ T)$ (maximum value = 0.1)
E, ACTIVATION ENERGY	1 kcal/mole = 6.949×10^{-21} J/atom
S_o, INITIAL STICKING COEFFICIENT	$0.05 \exp(-0.002\ T)$
C_a, SURFACE SITES	5×10^{14} sites/cm^2
D, THERMAL DESORPTION ENERGY	81 kcal/mole = 5.629×10^{-19} J/atom

The fractional surface concentration is shown in Figure 7 as a function of the temperature. The adsorption rate, thermal desorption

rate, and the rate of recombination desorption are shown in Figure 8. The total rate of removal of chemisorbed (surface-matrix-bonded) atoms is the sum of the thermal desorption rate and the recombination desorption rate. At steady state conditions this total removal rate equals the adsorption rate.

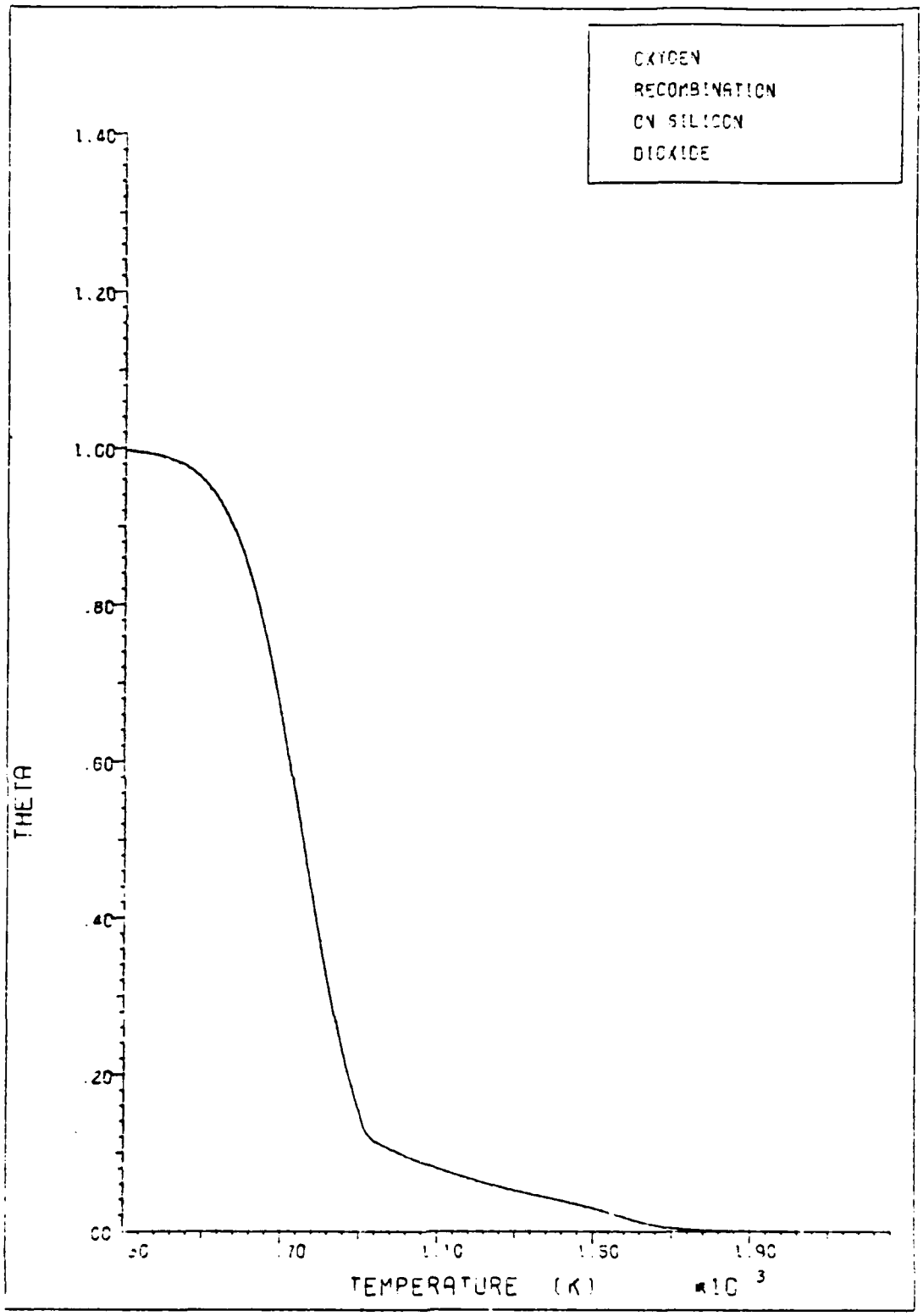

Figure 7. Fractional Surface Concentration for Atomic Oxygen vs. Temperature.

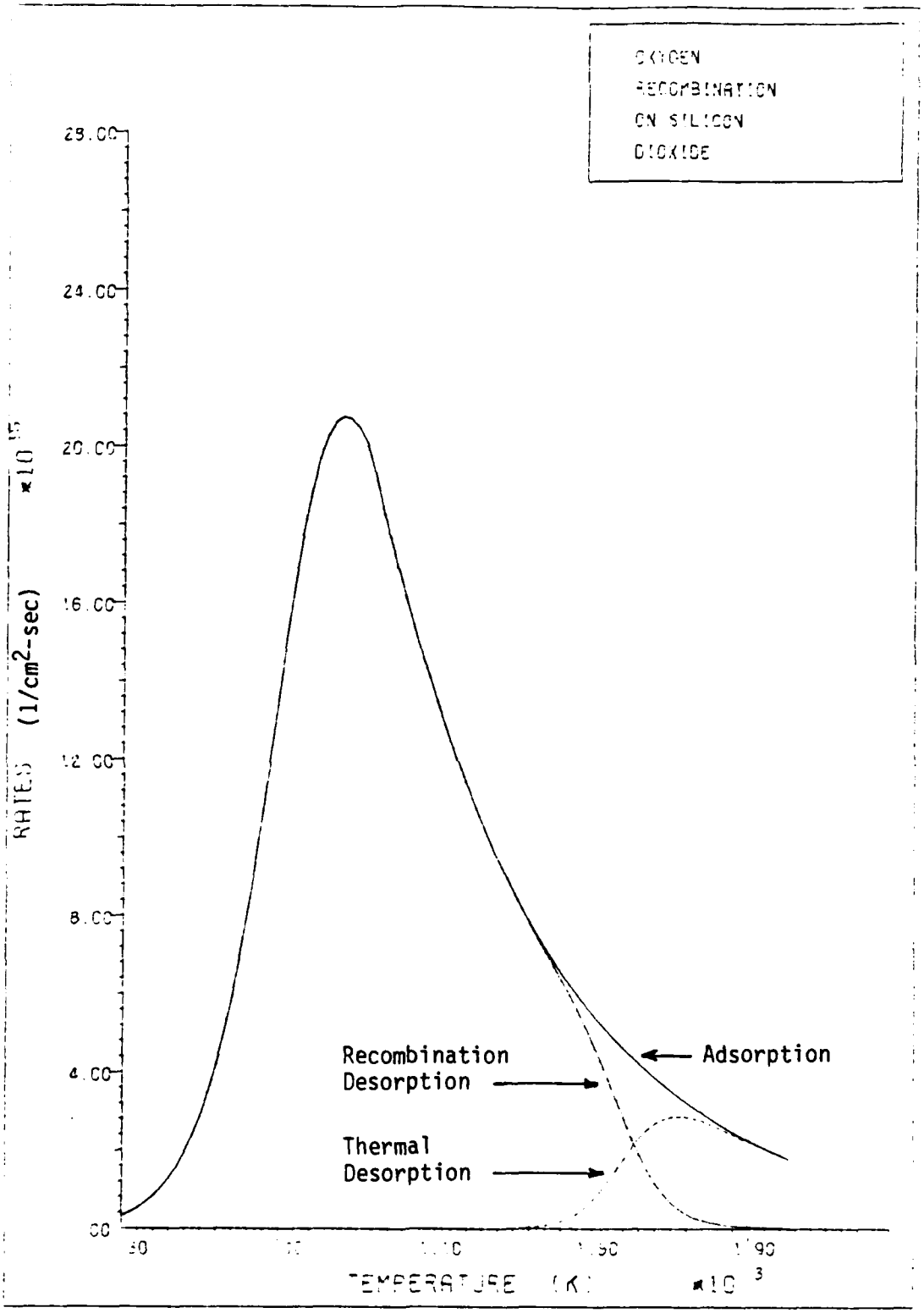

Figure 8. Adsorption, Thermal Desorption, and Recombination Desorption Rates vs. Temperature.

VI. Model Demonstration

In order to demonstrate the use of the present recombination model and to explore the rational limits which may be placed on the role of catalysis for an engineering problem, a set of boundary-layer calculations were made using numerical methods. As indicated in the introduction, that portion of the Space Shuttle reentry where oxygen is dissociated but nitrogen is not was chosen for an example problem. Such a portion of the Shuttle reentry is below 200,000 feet. According to Dunn and Kang (Ref 47), this allows the analysis of a one-foot nose radius body (of which the Shuttle is one) to be treated by conventional boundary-layer analysis. Above 200,000 feet an alternate method is required due to the thickening of the viscous region within the shock layer.

To suggest that the analysis described below exactly models the Space Shuttle problem is misleading, but a geometry somewhat akin to the Shuttle geometry was analyzed. This geometry was that of a 1.0 foot radius spherical Reinforced Carbon-Carbon (RCC) nose blended to a 40° half-angle cone. This cone is made of High-Temperature Reusable Surface Insulation (HRSI) tiles which are coated with silicon dioxide. Figure 9 is a schematic of the modeled geometry indicating the computational domain. This domain is from the X = 61. cm. location to approximately the x = 90. cm. location. This chapter contains an explanation of the numerical boundary-layer algorithm that was used and the results obtained.

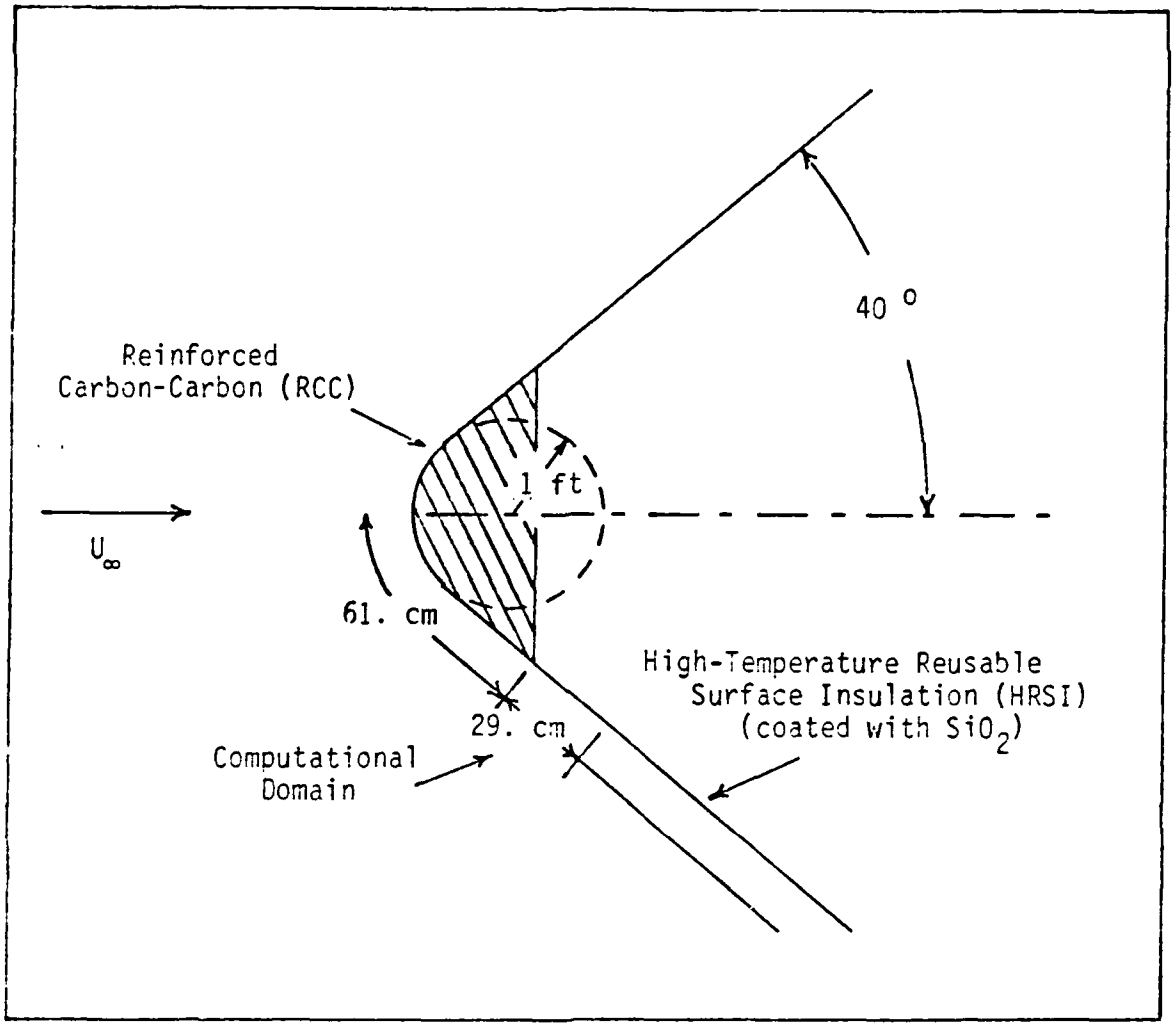

Figure 9. Schematic Showing Modeled Geometry Simulating Nose Region of Space Shuttle at 40° Angle of Attack.

Boundary-Layer Code

After the 61. cm. point, the boundary-layer was modeled using a two-dimensional, rectilinear computational space, but undergoing a pressure distribution for the axisymmetric cone (c.f., above and below). The boundary-layer code is a conventional two-dimensional boundary-layer method which has been described elsewhere (Ref 8), where it was validated for a high temperature, compressible, reacting flow (including catalytic walls) of fluorine atoms, molecules and diluent. The code was further validated in Reference 48 for low temperature, compressible air. The equations for continuity, momentum, species, and energy in boundary-layer form from Reference 8 are as follows:

$$\text{Continuity:} \quad \frac{\partial}{\partial x}(\rho u) + \frac{\partial}{\partial y}(\rho v) = 0 \tag{59}$$

$$\text{Momentum:} \quad \rho u \frac{\partial u}{\partial x} + \rho v \frac{\partial u}{\partial y} = - \frac{dp}{dx} + \frac{\partial}{\partial y}(\mu \frac{\partial u}{\partial y}) \tag{60}$$

$$\text{Species:} \quad \rho u \frac{\partial w_j}{\partial x} + \rho v \frac{\partial w_j}{\partial y} = \dot{m}_j''' + \frac{\partial}{\partial y}(\rho D_j \frac{\partial w_j}{\partial y}) \tag{61}$$

$$\text{Energy:} \quad \rho C_p (u \frac{\partial T}{\partial x} + v \frac{\partial T}{\partial y}) = u \frac{dp}{dx} + \mu (\frac{\partial u}{\partial y})^2 + \frac{\partial}{\partial y}(k \frac{\partial T}{\partial y}) + \sum_j \rho D_j \frac{\partial w_j}{\partial y} \frac{\partial h_j}{\partial y} - \sum_j h_j \dot{m}_j''' \tag{62}$$

where u is the x component of velocity, v is the y component of velocity, ρ is the mixture density, p is the pressure, μ is the mixture viscosity, w_j is the mass fraction of species j, $\dot{m}_j'''$ is the rate of production of species j per unit volume, D_j is the diffusivity of species j into the

mixture, C_p is the specific heat at constant pressure for the mixture, T is the temperature, h_j is the absolute enthalpy for species j, and k is the thermal conductivity for the mixture. The von Mises transformation was then used where ψ is the compressible stream function given by:

$$\frac{\partial \psi}{\partial y} = \rho u \tag{63}$$

$$\frac{\partial \psi}{\partial x} = -\rho v \tag{64}$$

The transformed equations are then given by the following:

$$\text{Momentum:} \quad \frac{\partial u}{\partial x} = -\frac{1}{\rho u}\frac{dp}{dx} + \frac{\partial}{\partial \psi}\left(\mu \rho u \frac{\partial u}{\partial \psi}\right) \tag{65}$$

$$\text{Species:} \quad \frac{\partial w_j}{\partial x} = \frac{1}{\rho u}\dot{m}_j''' + \frac{\partial}{\partial \psi}\left(D_j \rho^2 u \frac{\partial w_j}{\partial \psi}\right) \tag{66}$$

$$\text{Energy:} \quad \frac{\partial T}{\partial x} = \frac{1}{\rho C_p}\frac{dp}{dx} + \frac{\mu \rho u}{C_p}\left(\frac{\partial u}{\partial \psi}\right)^2 - \frac{1}{\rho u C_p}\sum_j \dot{m}_j''' h_j +$$

$$\frac{1}{C_p}\left(\sum_j D_j \rho^2 u \frac{\partial w_j}{\partial \psi}\frac{\partial h_j}{\partial \psi}\right) + \frac{1}{C_p}\frac{\partial}{\partial \psi}\left(k \rho u \frac{\partial T}{\partial \psi}\right) \tag{67}$$

An explicit finite difference method as given in Reference 8, was used to solve equations (65) - (67).

Thermodynamic and Transport Properties

The sensible enthalpy and specific heats for each of the five species were extracted from the JANAF data (Ref 49). The chemical enthalpy of formation from the JANAF data was added to the sensible enthalpy to obtain the absolute enthalpy. The specific heat for the mixture is

calculated as follows:

$$C_p = \sum_{j=1}^{N} x_j \, C_{p_j} \tag{68}$$

where x_j is the mole fraction of species j and C_{p_j} is the specific heat of species j. The mole fractions were calculated from:

$$x_j = M \frac{w_j}{M_j} \tag{69}$$

where M_j and M are the molecular weights of the individual species j and mixture, respectively, and w_j is the mass fraction of species j. The molecular weight M is calculated as follows:

$$\frac{1}{M} = \sum_{j=1}^{N} \frac{w_j}{M_j} \tag{70}$$

The mixture density was calculated by:

$$\rho = \frac{M \, p}{R \, T} \tag{71}$$

where p is the absolute pressure, T is the absolute temperature and R is the universal gas constant. The viscosity, thermal conductivity, bimolecular diffusivity, and the diffusivity of species i into the mixture were calculated as explained by Jumper, et. al., (Ref 8) and are summarized here. The viscosity was calculated as (Ref 50):

$$\mu_i = \frac{2.6693 \times 10^{-5} \sqrt{M_i T}}{\sigma_i^2 \, \Omega_\mu} \tag{72}$$

where Ω_μ is the reduced collision integral curve fit as a function of $k_B T/\varepsilon_i$. The values used for ε_i/k_B, the Lennard-Jones (6-12) characteristic energy of interaction divided by the Boltzmann constant, and σ_i, the

Lennard-Jones (6-12) characteristic diameter, came from Reference 51 and are given in Table III. The viscosity of the mixture was calculated using:

$$\mu_{mix} = \sum_{i=1}^{N} \frac{x_i \mu_i}{\sum_{j=1}^{N} x_j \phi_{ij}} \tag{73}$$

and

$$\phi_{ij} = \frac{1}{\sqrt{8}} \left[1 + \frac{M_i}{M_j}\right]^{-\frac{1}{2}} \left[1 + \left[\frac{\mu_i}{\mu_j}\right]^{\frac{1}{2}} \left[\frac{M_j}{M_i}\right]^{\frac{1}{4}}\right]^2 \tag{74}$$

The thermal conductivity was calculated using the following relationships from Reference 50.

$$k_i = \left(C_{p_i} + \frac{5}{4}\frac{R}{M_i}\right) \mu_i \tag{75}$$

$$k_{mix} = \sum_{i=1}^{N} \frac{x_i k_i}{\sum_{j=1}^{N} x_j \phi_{ij}} \tag{76}$$

The following relationship from Reference 50 was used to calculate the bimolecular diffusivity:

$$D_{ij} = \frac{0.0018583 \sqrt{T^3 \left(\frac{1}{M_i} + \frac{1}{M_j}\right)}}{p\, \sigma_{ij}^2\, \Omega_D} \tag{77}$$

where Ω_D was curve fit as a function of $k_B T/\epsilon_{ij}$ where

$$\epsilon_{ij} = (\epsilon_i \epsilon_j)^{\frac{1}{2}} \tag{78}$$

and

$$\sigma_{ij} = (\sigma_i + \sigma_j)/2 \tag{79}$$

The diffusivity of species i into the mixture was calculated with (Ref 50):

$$D_i = \frac{1 - x_i}{\sum_{\substack{j=1 \\ j \neq i}}^{N} \frac{x_j}{D_{ij}}} \tag{80}$$

TABLE III. Lennard-Jones (6-12) Data

Species	$\frac{\epsilon_i}{k_B}$ (K)	σ_i (Angstroms)
N	71.4	3.298
O	106.7	3.050
N_2	71.4	3.798
O_2	106.7	3.467
NO	116.7	3.492

Homogeneous Chemistry

The gas-phase (homogeneous) chemical reactions considered in this research are shown in Table IV. These are the same chemical reaction data used by Kang and Dunn, and Miner and Lewis for a five species gas (Ref 47, 52-53). Note: $T^{-1.5}$ was dropped from Kang and Dunn's equation

TABLE IV. Chemical Reactions and Rate Coefficients

No.	Reaction: Forward Direction	M	Forward Rate Coefficient, k_f (cm^3/mole·sec)	Backward Rate Coefficient, k_b (cm^3/mole·sec) or (cm^6/$mole^2$·sec)
1.	$O_2 + M \rightarrow 2\,O + M$	N	$3.6 \times 10^{18}\, T^{-1.0} \exp(-\frac{59{,}500}{T})$	$3.0 \times 10^{15}\, T^{-0.5}$
2.		O	$9.0 \times 10^{19}\, T^{-1.0} \exp(-\frac{59{,}500}{T})$	$7.5 \times 10^{16}\, T^{-0.5}$
3.		N_2	$7.2 \times 10^{18}\, T^{-1.0} \exp(-\frac{59{,}500}{T})$	$6.0 \times 10^{15}\, T^{-0.5}$
4.		O_2	$3.24 \times 10^{19}\, T^{-1.0} \exp(-\frac{59{,}500}{T})$	$2.7 \times 10^{16}\, T^{-0.5}$
5.		NO	$3.6 \times 10^{18}\, T^{-1.0} \exp(-\frac{59{,}500}{T})$	$3.0 \times 10^{15}\, T^{-0.5}$
6.	$N_2 + M \rightarrow 2\,N + M$	N	$4.085 \times 10^{22}\, T^{-1.5} \exp(-\frac{113{,}000}{T})$	$2.27 \times 10^{21}\, T^{-1.5}$
7.		O	$1.9 \times 10^{17}\, T^{-0.5} \exp(-\frac{113{,}000}{T})$	$1.1 \times 10^{16}\, T^{-0.5}$
8.		N_2	$4.7 \times 10^{17}\, T^{-0.5} \exp(-\frac{113{,}000}{T})$	$2.72 \times 10^{16}\, T^{-0.5}$
9.		O_2	$1.9 \times 10^{17}\, T^{-0.5} \exp(-\frac{113{,}000}{T})$	$1.1 \times 10^{16}\, T^{-0.5}$

No.	Reaction: Forward Direction	M	Forward Rate Coefficient, k_f (cm^3/mole·sec)	Backward Rate Coefficient, k_b (cm^3/mole·sec) or (cm^6/$mole^2$·sec)
10.		NO	$1.9 \times 10^{17} T^{-0.5} \exp(-\frac{113,000}{T})$	$1.1 \times 10^{16} T^{-0.5}$
11.	$NO + M \rightarrow N + O + M$	N	$7.8 \times 10^{20} T^{-1.5} \exp(-\frac{75,500}{T})$	$2.0 \times 10^{20} T^{-1.5}$
12.		O	$7.8 \times 10^{20} T^{-1.5} \exp(-\frac{75,500}{T})$	$2.0 \times 10^{20} T^{-1.5}$
13.		N_2	$3.9 \times 10^{20} T^{-1.5} \exp(-\frac{75,500}{T})$	$1.0 \times 10^{20} T^{-1.5}$
14.		O_2	$3.9 \times 10^{20} T^{-1.5} \exp(-\frac{75,500}{T})$	$1.0 \times 10^{20} T^{-1.5}$
15.		NO	$7.8 \times 10^{20} T^{-1.5} \exp(-\frac{75,500}{T})$	$2.0 \times 10^{20} T^{-1.5}$
16.	$NO + O \rightarrow O_2 + N$	--	$3.2 \times 10^{9} T \exp(-\frac{19,700}{T})$	$1.3 \times 10^{10} T^{1.0} \exp(-\frac{3580}{T})$
17.	$N_2 + O \rightarrow NO + N$	--	$7.0 \times 10^{13} \exp(-\frac{38,000}{T})$	1.56×10^{13}

6 in Table I of Reference 52. The VSLNQH code (c.f., below), used to obtain the initial conditions, uses chemical reaction data of a different form. The significance of this difference was not investigated.

These reactions were then used to compute the rate of creation/depletion in the following manner (Ref 22):

$$\begin{aligned}
\frac{d[N]}{dt} = {} & 2k_{f_6}[N_2][N] - 2k_{b_6}[N]^2[N] \\
& + 2k_{f_7}[N_2][O] - 2k_{b_7}[N]^2[O] \\
& + 2k_{f_8}[N_2][N_2] - 2k_{b_8}[N]^2[N_2] \\
& + 2k_{f_9}[N_2][O_2] - 2k_{b_9}[N]^2[O_2] \\
& + 2k_{f_{10}}[N_2][NO] - 2k_{b_{10}}[N]^2[NO] \\
& + k_{f_{11}}[NO][N] - k_{b_{11}}[N][O][N] \\
& + k_{f_{12}}[NO][O] - k_{b_{12}}[N][O][O] \\
& + k_{f_{13}}[NO][N_2] - k_{b_{13}}[N][O][N_2] \\
& + k_{f_{14}}[NO][O_2] - k_{b_{14}}[N][O][O_2] \\
& + k_{f_{15}}[NO][NO] - k_{b_{15}}[N][O][NO] \\
& + k_{f_{16}}[NO][O] - k_{b_{16}}[O_2][N] \\
& + k_{f_{17}}[N_2][O] - k_{b_{17}}[NO][N]
\end{aligned} \tag{81}$$

$$\frac{d[O]}{dt} = 2k_{f_1}[O_2][N] - 2k_{b_1}[O]^2[N]$$
$$+2k_{f_2}[O_2][O] - 2k_{b_2}[O]^2[O]$$
$$+2k_{f_3}[O_2][N_2] - 2k_{b_3}[O]^2[N_2]$$
$$+2k_{f_4}[O_2][O_2] - 2k_{b_4}[O]^2[O_2]$$
$$+2k_{f_5}[O_2][NO] - 2k_{b_5}[O]^2[NO]$$
$$+k_{f_{11}}[NO][N] - k_{b_{11}}[N][O][N]$$
$$+k_{f_{12}}[NO][O] - k_{b_{12}}[N][O][O]$$
$$+k_{f_{13}}[NO][N_2] - k_{b_{13}}[N][O][N_2]$$
$$+k_{f_{14}}[NO][O_2] - k_{b_{14}}[N][O][O_2]$$
$$+k_{f_{15}}[NO][NO] - k_{b_{15}}[N][O][NO]$$
$$-k_{f_{16}}[NO][O] + k_{b_{16}}[O_2][N]$$
$$-k_{f_{17}}[N_2][O] + k_{b_{17}}[NO][N] \qquad (82)$$

$$\frac{d[N_2]}{dt} = -k_{f_6}[N_2][N] + k_{b_6}[N]^2[N]$$
$$-k_{f_7}[N_2][O] + k_{b_7}[N]^2[O]$$
$$-k_{f_8}[N_2][N_2] + k_{b_8}[N]^2[N_2]$$
$$-k_{f_9}[N_2][O_2] + k_{b_9}[N]^2[O_2]$$
$$-k_{f_{10}}[N_2][NO] + k_{b_{10}}[N]^2[NO]$$
$$-k_{f_{17}}[N_2[O] + k_{b_{17}}[NO][N] \qquad (83)$$

$$\frac{d[O_2]}{dt} = -k_{f_1}[O_2][N] + k_{b_1}[O]^2[N]$$
$$-k_{f_2}[O_2][O] + k_{b_2}[O]^2[O]$$
$$-k_{f_3}[O_2][N_2] + k_{b_3}[O]^2[N_2]$$
$$-k_{f_4}[O_2][O_2] + k_{b_4}[O]^2[O_2]$$
$$-k_{f_5}[O_2][NO] + k_{b_5}[O]^2[NO]$$
$$+k_{f_{16}}[NO][O] - k_{b_{16}}[O_2][N] \qquad (84)$$

$$\frac{d[NO]}{dt} = -k_{f_{11}}[NO][N] + k_{b_{11}}[N][O][N]$$
$$-k_{f_{12}}[NO][O] + k_{b_{12}}[N][O][O]$$
$$-k_{f_{13}}[NO][N_2] + k_{b_{13}}[N][O][N_2]$$
$$-k_{f_{14}}[NO][O_2] + k_{b_{14}}[N][O][O_2]$$
$$-k_{f_{15}}[NO][NO] + k_{b_{15}}[N][O][NO]$$
$$-k_{f_{16}}[NO][O] + k_{b_{16}}[O_2][N]$$
$$+k_{f_{17}}[N_2][O] - k_{b_{17}}[NO][N] \qquad (85)$$

where the subscript on the forward rate constant k_f and backward rate constant k_b refers to the reaction in Table IV. $\frac{d[j]}{dt}$ is the rate of production of species j in moles/cm^3-sec, $\dot{m}_j'''$, that is found in both the species and energy equations. [j] is the molar concentration of species j in moles/cm^3 and is calculated as follows:

$$[j] = \frac{w_j \rho}{M_j} \tag{86}$$

Boundary Conditions Due to Recombination

At the wall, the rate of diffusion of atomic oxygen toward the wall must just equal the rate at which atomic oxygen disappears due to catalytic recombination forming molecular oxygen. Also, the rate at which molecular oxygen is formed determines the rate at which the molecular oxygen diffuses away from the wall (Ref 8). This results in the following boundary conditions:

$$w_0(1) = \frac{D_0 \, w_0(2)}{D_0 + \gamma \left(\frac{k_B T}{2\pi m_0}\right)^{\frac{1}{2}} \Delta y} \tag{87}$$

$$w_{0_2}(1) = w_{0_2}(2) + \frac{w_0(1)}{D_{0_2}} \quad \gamma \left(\frac{k_B T}{2\pi m_0}\right)^{\frac{1}{2}} \Delta y \tag{88}$$

where $w_0(1)$ and $w_0(2)$ are the mass fractions for atomic oxygen at the wall and at a distance Δy from the wall, respectively, and $w_{0_2}(1)$ and $w_{0_2}(2)$ are the mass fractions for molecular oxygen at the wall and at the first cell out from the wall.

As discussed by Jumper, et. al., (Ref 8), the heat transfer enhancement per unit area due to the recombination of oxygen atoms may be expressed as the following:

$$q_{recomb} = \rho \gamma w_0(1) \left(\frac{k_B T}{2\pi m_0}\right)^{\frac{1}{2}} (h_0 - h_{0_2}) \tag{89}$$

where the enthalpies, h_0 and h_{0_2}, are on a per mass basis.

The surface temperature was treated in two ways: the wall temperature could be specified or it could be calculated based on the radiation equilibrium assumption (Ref 7). Since the thermal conductivity of the Space Shuttle insulation tiles is very low, i.e., only a small amount of energy is conducted through the surface, the surface is at a temperature high enough so that the total heating is assumed equal to the energy that can be radiated away with an emissivity, ε of 0.85:

$$q_{total} = \varepsilon \sigma T^4 \tag{90}$$

where q is the total heating, σ is the Stefan-Boltzmann constant, and T is the surface temperature. When the second option was used, the surface temperature was determined by the total heating at the previous step.

Initial Conditions

The code written by Song and Lewis (Ref 54), VSLNQH: An Axisymmetric Viscous Shock-Layer Code for Nonequilibrium Finite-Rate Chemically Reacting Viscous Flows over Hyperboloid Geometries, was first used to obtain the initial conditions for the boundary-layer code. The VSLNQH code yielded mass fractions, temperature, and velocity profiles over the Reinforced Carbon-Carbon (RCC) nose cap to approximate a Shuttle flight condition of Mach 14.1 at an altitude of 188,000 feet assuming the RCC surface is at a uniform temperature of 1703°K (3065°R) and is noncatalytic. (This VSLNQH code can only treat noncatalytic or fully catalytic surfaces.) Table V and Figures 10-12 show the initial temperature, velocity, and mass fraction profiles, respectively, at the streamwise location of 61.0 cm. This corresponds to the RCC interface with the High-Temperature

TABLE V. Initial Conditions

Distance From Surface, y (cm)	Mass Fraction (gm/gm of mixture)					Temperature (°K)	Velocity (cm/sec)
	N	O	N_2	O_2	NO		
0.00000	0.000022	0.191825	0.75964	0.015284	0.033230	1702.78	00000.0
0.21129	0.000350	0.190908	0.75844	0.015591	0.034703	3191.58	86410.4
0.30592	0.000717	0.189528	0.75684	0.016087	0.036817	3580.02	112115.
0.36466	0.000986	0.188372	0.75554	0.016500	0.038592	3771.40	125300.
0.43215	0.001303	0.186799	0.75382	0.017081	0.040980	3953.37	138190.
0.50932	0.001641	0.184727	0.75168	0.017903	0.044037	4119.56	150347.
0.59703	0.001953	0.182074	0.74914	0.019064	0.047759	4263.63	161385.
0.69616	0.002186	0.178756	0.74626	0.020693	0.052090	4380.11	171071.
0.80752	0.002297	0.174686	0.74314	0.022925	0.056935	4465.66	179423.
0.93181	0.002273	0.169789	0.73986	0.025881	0.062181	4520.60	186721.
1.06963	0.002140	0.164033	0.73650	0.029624	0.067692	4549.77	193404.
1.22140	0.001947	0.157474	0.73314	0.034131	0.073289	4561.48	199877.
1.38734	0.001739	0.150269	0.72994	0.039316	0.078723	4564.51	206366.
1.56745	0.001542	0.142620	0.72707	0.045104	0.083652	4565.12	212904.
1.76149	0.001364	0.134713	0.72476	0.051507	0.087648	4566.37	219427.
1.96896	0.001203	0.126681	0.72323	0.058649	0.090226	4569.70	225846.
2.18910	0.001057	0.118617	0.72270	0.066705	0.090911	4576.39	232080.
2.66320	0.000803	0.102644	0.72509	0.086028	0.085429	4604.63	243710.
3.17351	0.000595	0.087116	0.73156	0.109120	0.071605	4655.75	253893.
3.98003	0.000364	0.065044	0.74419	0.145577	0.044823	4762.77	266177.
4.52719	0.000259	0.051486	0.75159	0.167520	0.029143	4839.54	272531.
5.06964	0.000181	0.039200	0.75718	0.186120	0.017321	4910.77	277680.
5.85845	0.000101	0.023617	0.76231	0.207487	0.006483	4997.21	283665.
6.60537	0.000046	0.011533	0.76466	0.222185	0.001579	5055.96	288137.
7.53115	0.000000	0.000000	0.76544	0.234560	0.000000	5100.48	292454.

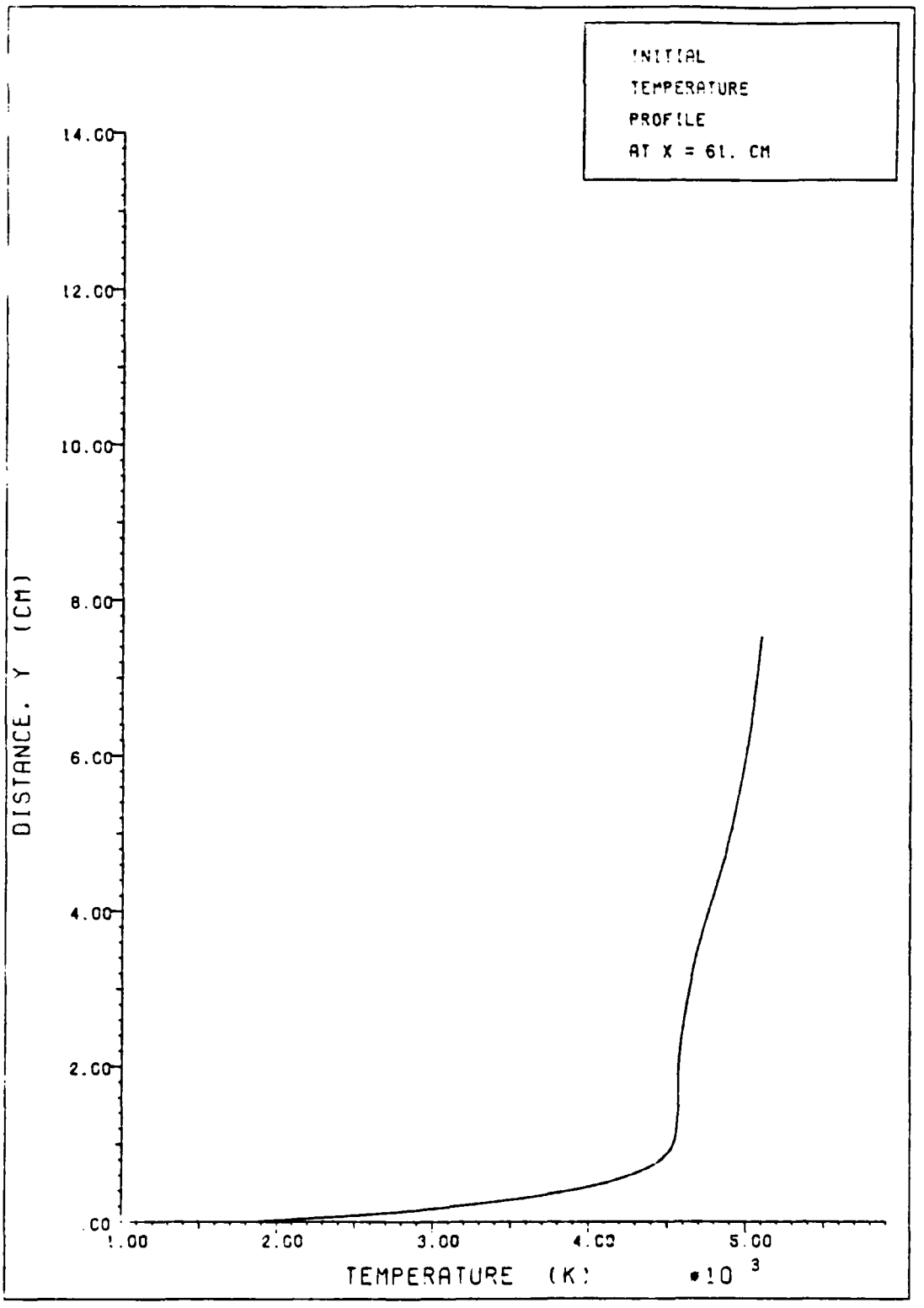

Figure 10. Initial Temperature Profile at x = 61.0 cm.

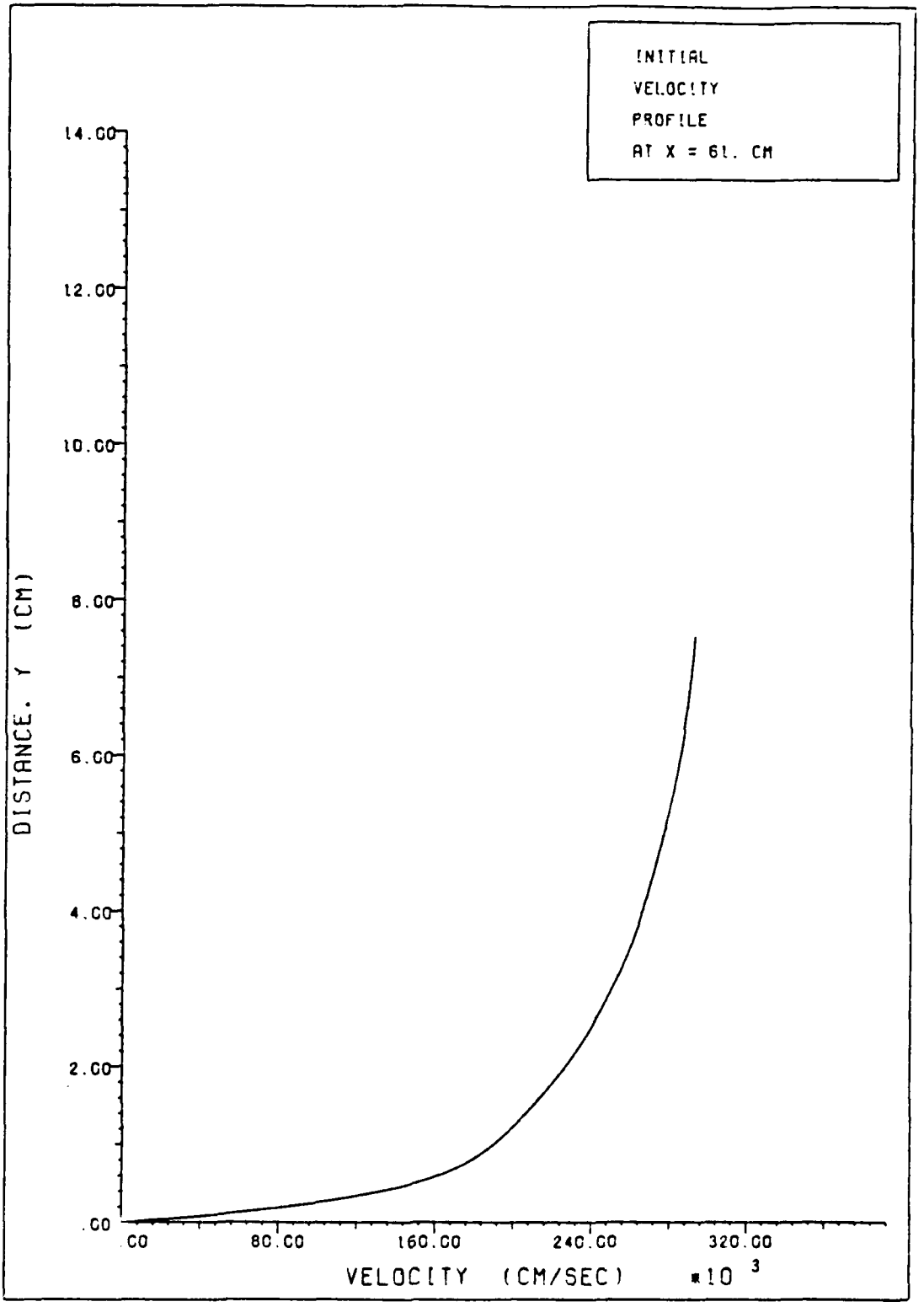

Figure 11. Initial Velocity Profile at x = 61.0 cm.

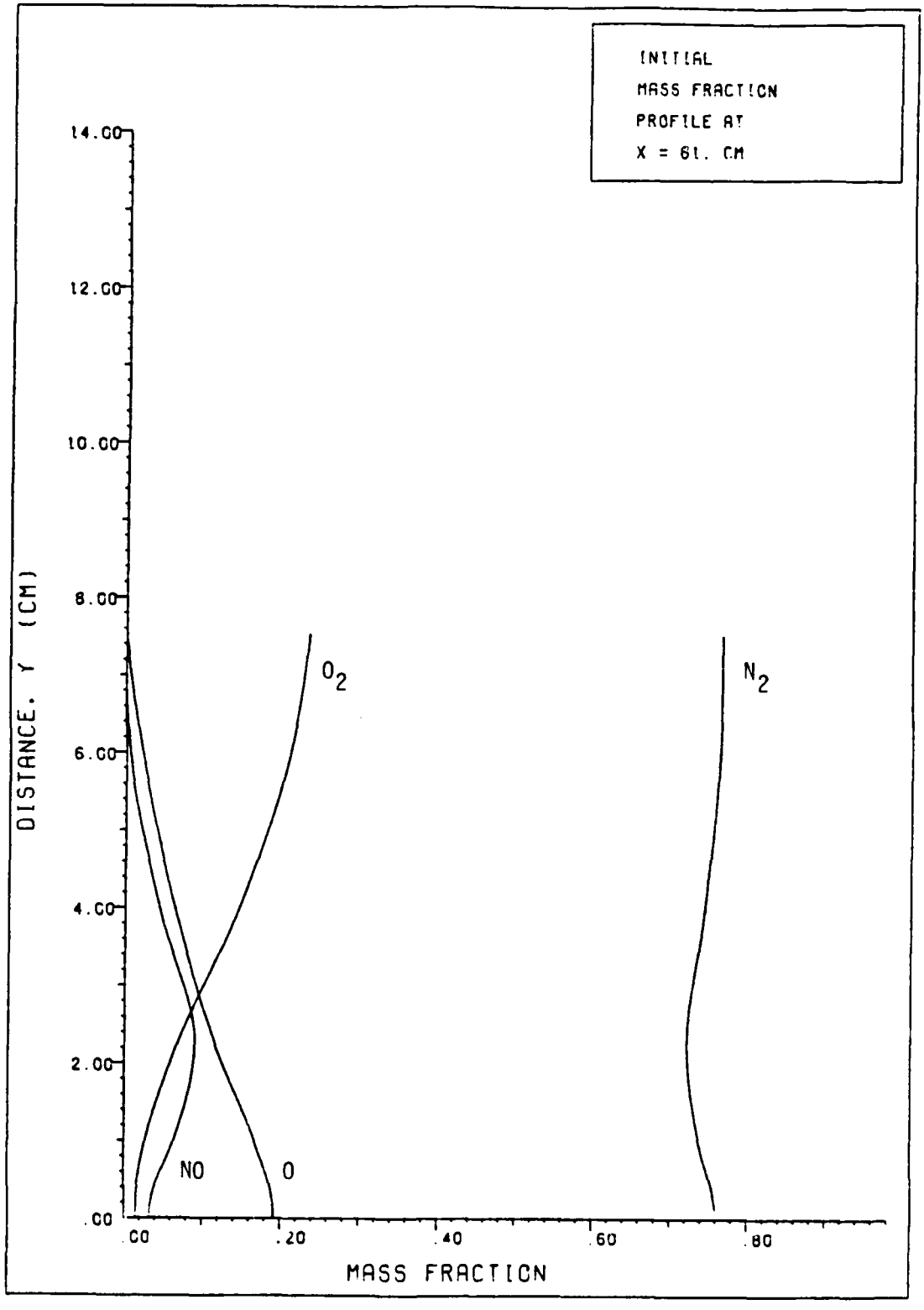

Figure 12. Initial Mass Fraction Profiles at x = 61.0 cm.

Reusable Surface Insulation (HRSI) tiles. These tiles are coated with predominately silicon dioxide. Figure 12 readily shows the high oxygen atom content (mass fraction of 19%) of the flow adjacent to the surface due to this flow having come through the near-normal portion of the bow shock and also not having been reduced by the noncatalytic assumption for the RCC surface. At this flight condition the nitrogen atom content along the surface is negligible (mass fraction of N = 0.0022% at x = 61.0 cm) and, as such, modeling this condition allowed for independent consideration of the oxygen atom recombination. The VSLNQH code is based upon the assumption that the Lewis number for each of the species is equal to 1.4:

$$Le_j = \frac{\rho C_p D_j}{k} \underset{=}{\text{assumed}} 1.4 \qquad (91)$$

That is, once the density, specific heat, and thermal conductivity for the air mixture is calculated, the diffusivity of each species j is calculated using $Le_j = 1.4$. The boundary-layer code used in this research does not make this assumption.

The VSLNQH code was also used to produce an initial pressure at the RCC/HRSI interface of 0.0424733 atm. and a pressure gradient of:

$$\frac{dp}{dx} = (3.74454 \times 10^{-6}) \times -(4.31620 \times 10^{-4}) \text{ atm/cm} \qquad (92)$$

valid over the next 27 cm.

Results and Discussion

The Song and Lewis VSLNQH code was run with the RCC surface assumed to be noncatalytic and at 1703°K. This code was further run to x = 89.

cm assuming a noncatalytic surface of fixed temperature. The surface temperature was set at 1500°K at 65.0 cm and 1353°K at 82.1 cm. Linear temperature distributions were assumed between these temperatures with the temperature remaining 1353°K downstream from 82.1 cm. The boundary-layer code was then run with the initial conditions from the VSLNQH code starting at the RCC/HRSI interface (x = 61.0 cm) with this same surface temperature distribution and with $\gamma = 0.00$. The results are shown in Figure 13. The results for the explicit boundary-layer code ($\gamma = 0$) are significantly higher than the VSLNQH code results (with $\gamma = 0$) initially, but at 89.0 cm the boundary-layer code results are 7% lower than the VSLNQH code results. In this nose region heat transfer predictions often differ by up to 40% (Ref 7). For comparison the results of the boundary-layer code with γ from the model and for the fully catalytic surface ($\gamma = 1.00$) are also shown in Figure 13, where all results are for the specified surface temperature distribution. This analysis also assumes that all of the energy released when recombination occurs is transferred to the surface.

Heating rates are shown in Figure 14 when radiation equilibrium is assumed on the HRSI tiles for three runs of the boundary-layer code. The corresponding surface temperatures are shown in Figure 15. The STS-2 flight test datum is shown on these two figures only for comparison and is <u>not</u> to be used to draw a conclusion relative to the catalycity of the surface.

A convergence check was performed by approximately halving $\Delta\psi$ and this check gave an error of 0.9% for the radiation equilibrium temperature at 80. cm.

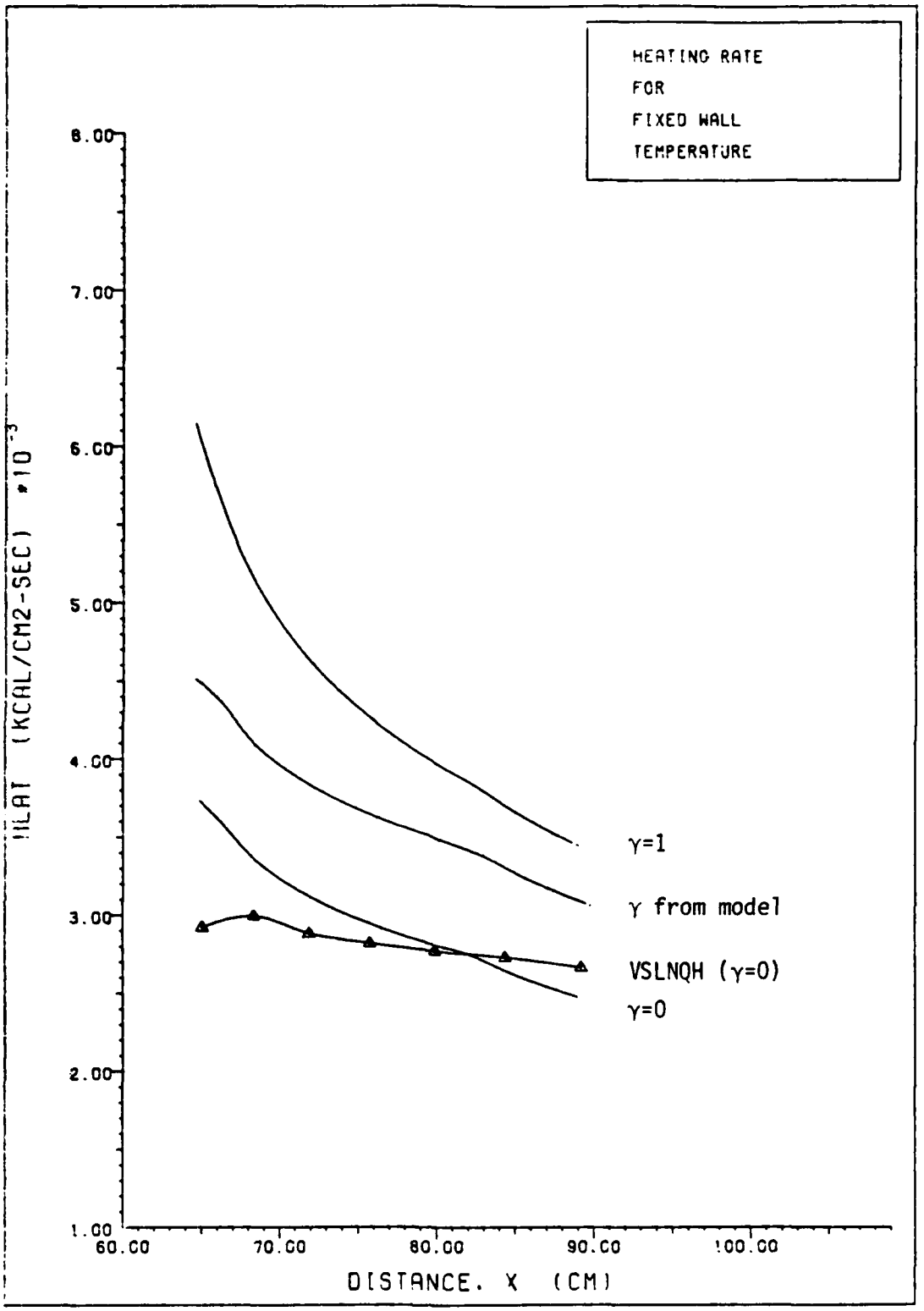

Figure 13. Heating Rate for Specified Surface Temperature Distribution.

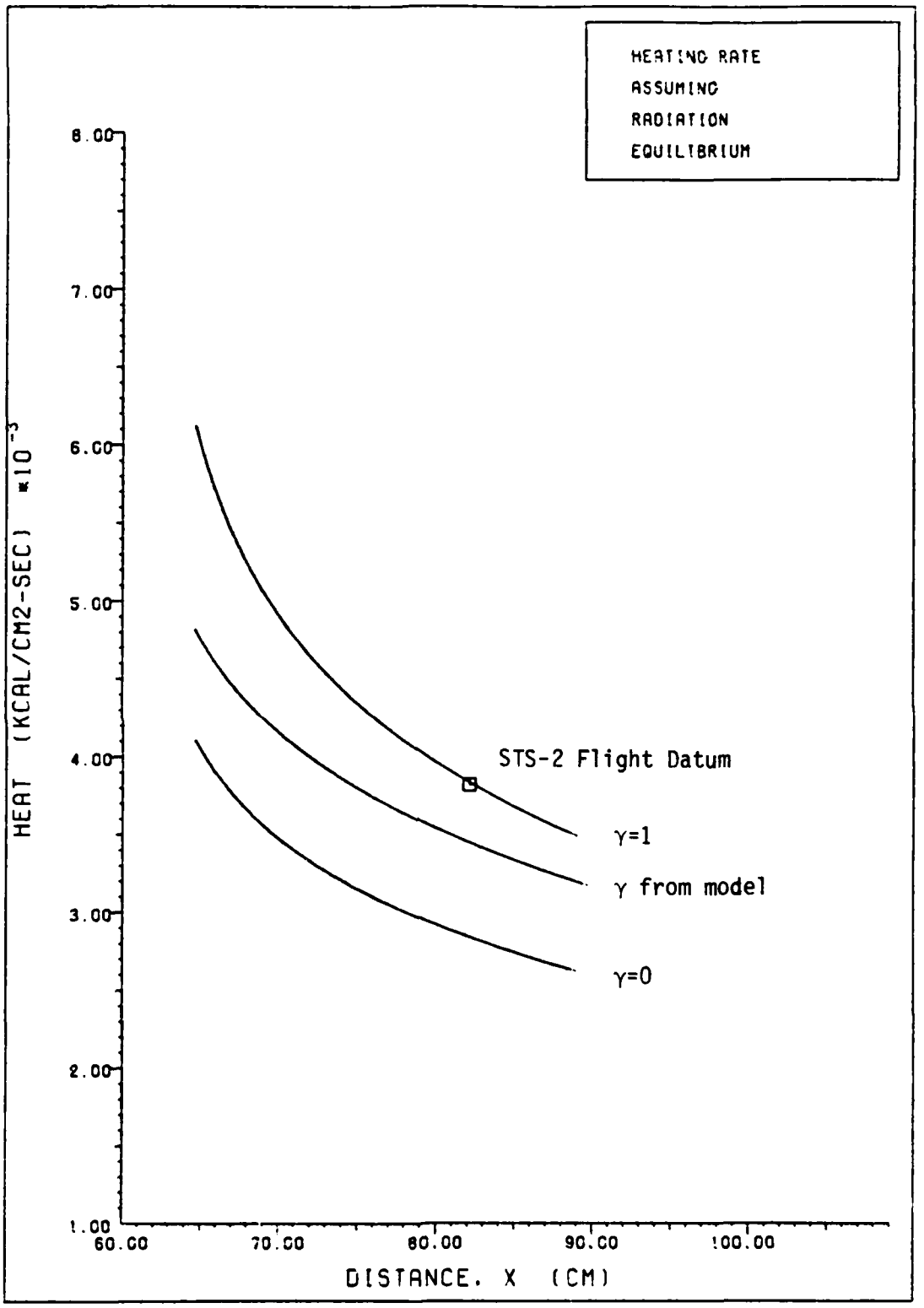

Figure 14. Heating Rate when Radiation Equilibrium is Assumed.

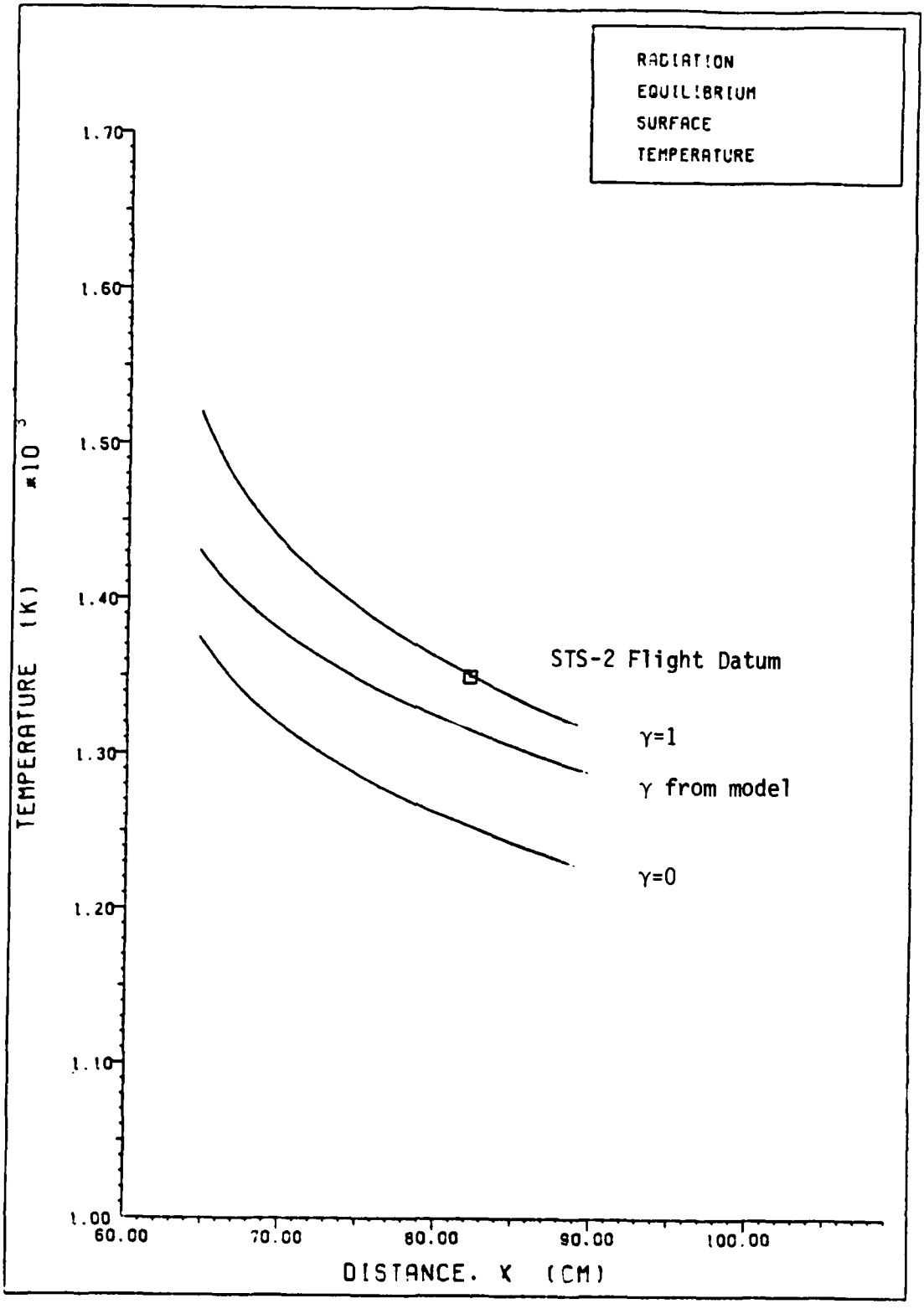

Figure 15. Radiation Equilibrium Surface Temperature.

A significant conclusion that can be drawn from Figure 14 is that the heating due to recombination of oxygen atoms can be large. In comparison with the heating for $\gamma = 0$, the SiO_2 surface experiences 21% more heating and a fully catalytic surface would experience 33% more at 89. cm when radiation equilibrium is assumed. Even though γ is relatively small, ranging from 5.5×10^{-3} at 65. cm (1431°K) to 7.2×10^{-3} at 89. cm (1289°K), the total heating of a silicon dioxide surface at 89.0 cm was only 9.1% below what would have been experienced by a fully catalytic surface at these simulated flight conditions. Or, put another way, the heating due only to recombining oxygen predicted by the model is approximately 63% of that which would be predicted for $\gamma = 1.0$, even though the γ's differ by nearly three orders of magnitude. This can be explained by noting that the reaction begins to become diffusion controlled (i.e., a limit to the rate at which oxygen atoms can diffuse to the surface) for the $\gamma = 1.0$ case.

The temperature profiles at $x = 89.$ cm are shown in Figure 16 for the three cases: $\gamma = 0$, γ from model, and $\gamma = 1$ when radiation equilibrium is assumed in each case. No significant difference exists.

The velocity profiles at $x = 89.$ cm for the same three cases, again with the radiation equilibrium assumption, are shown in Figure 17. There is no significant difference in these profiles either.

The initial mass fraction profile for the four species of significance, which is plotted in Figure 12, has $\frac{dw_i}{dy}$ gradients at the surface equal to zero for all the species since this profile was obtained from the VSLNQH code assuming a noncatalytic surface. The mass fraction profiles with γ from the model at the downstream location is shown in

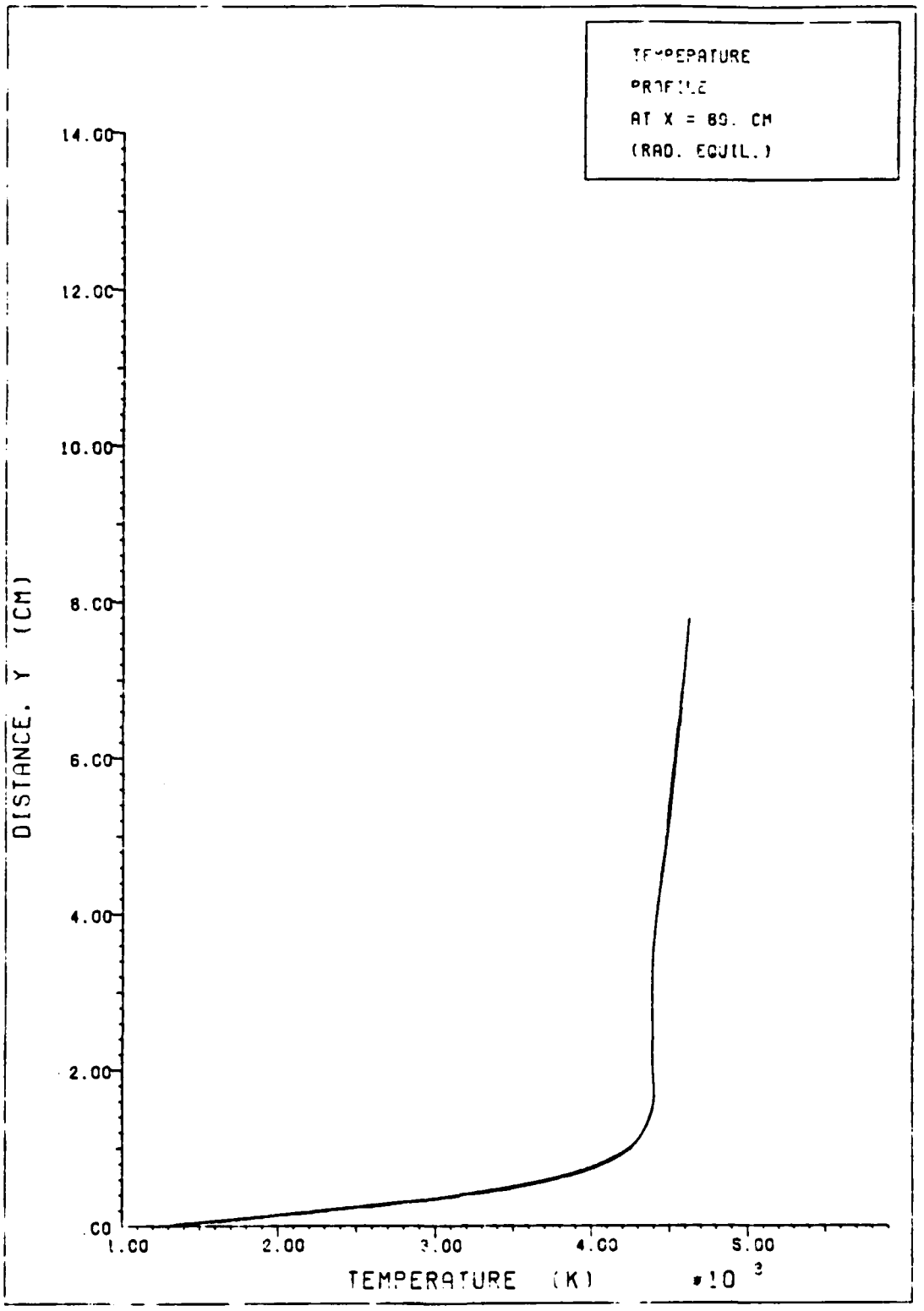

Figure 16. Temperature Profiles at x = 89. cm.

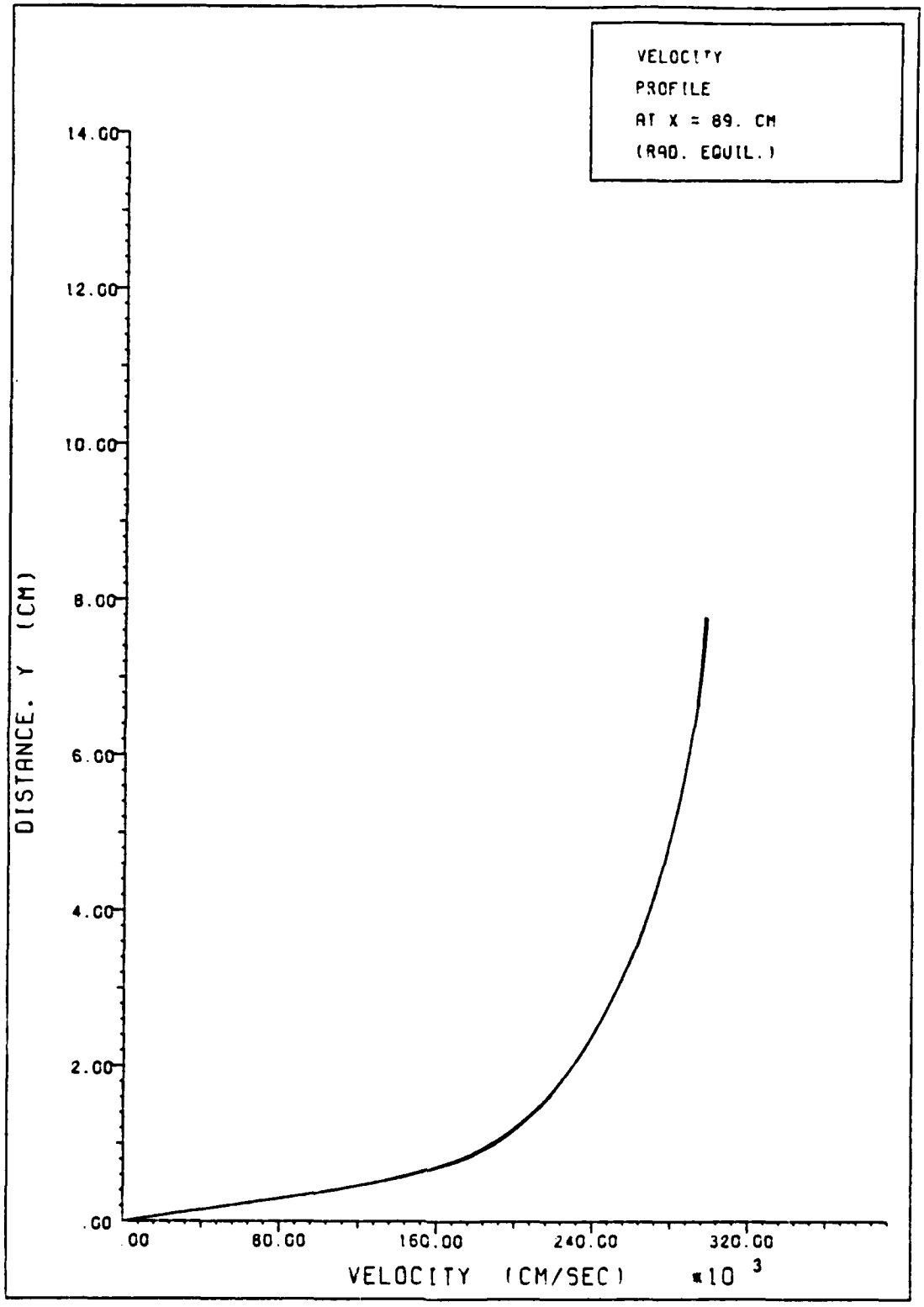

Figure 17. Velocity Profiles at x = 89. cm.

Figure 18 where the oxygen atom and molecule mass fractions are observed to have changed significantly. Note also the increase in the oxygen atom concentration out in the free stream due to the dissociation of oxygen molecules. Figure 19 shows the oxygen atom and molecule mass fractions for the three cases. The only significant difference in comparing the fully catalytic and noncatalytic mass fraction profiles 28 cm downstream is within the first centimeter from the surface. The atomic oxygen mass fraction is not zero (0.07% at x = 89. cm) at the wall even when the surface is modeled as fully catalytic, supporting the comments made by Jumper, et. al., (Ref 8).

The secondary objective of this research has been to demonstrate the use of the oxygen recombination model with proper treatment of surface boundary conditions. This demonstration has been dependent upon the initial conditions used from the VSLNQH code and the Kang and Dunn homogeneous chemical kinetics. Even though improved flow characterization and verification are required, this two-dimensional boundary-layer code has demonstrated how the oxygen recombination on silicon dioxide model can be used.

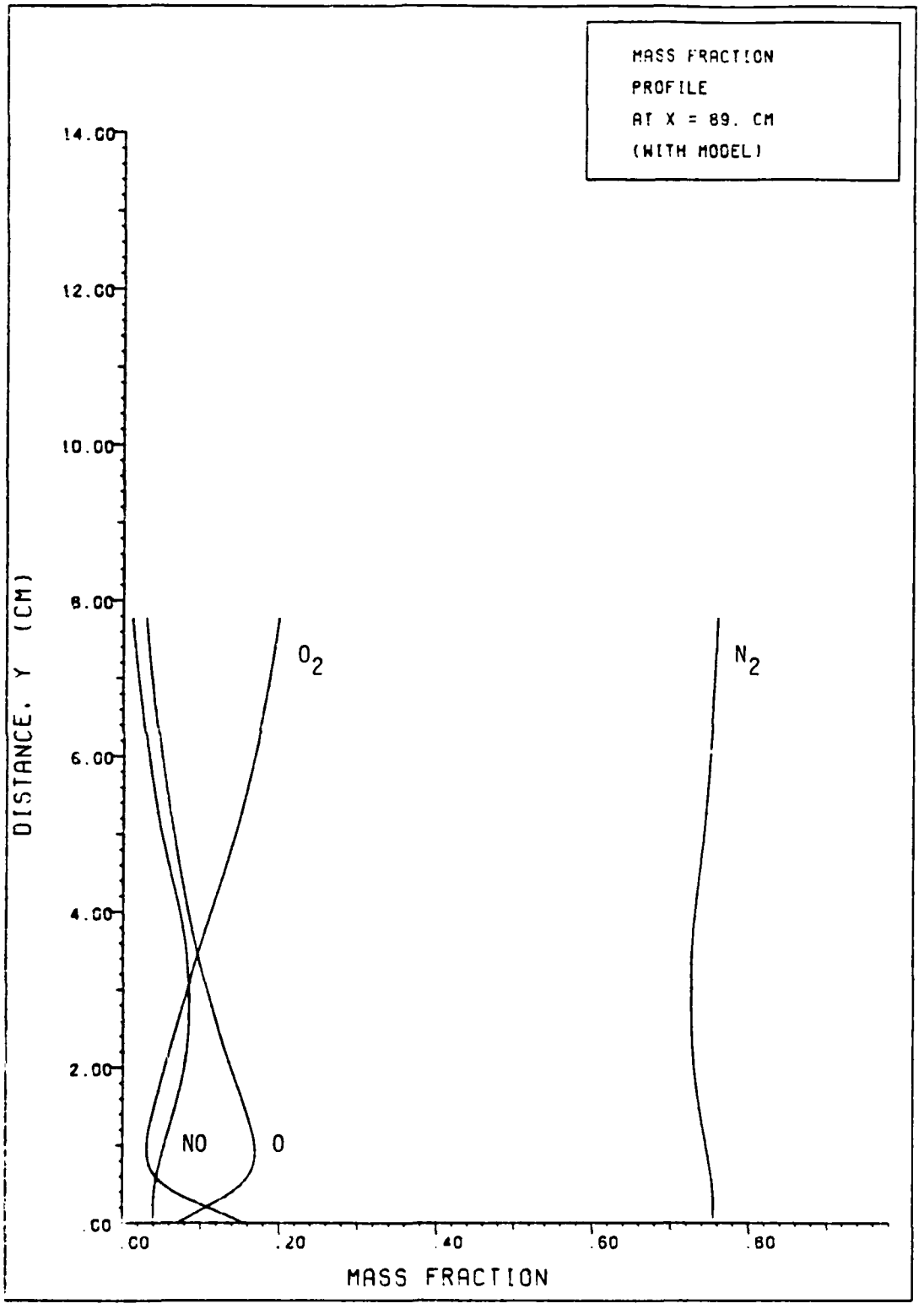

Figure 18. Mass Fraction Profiles at x = 89. cm.

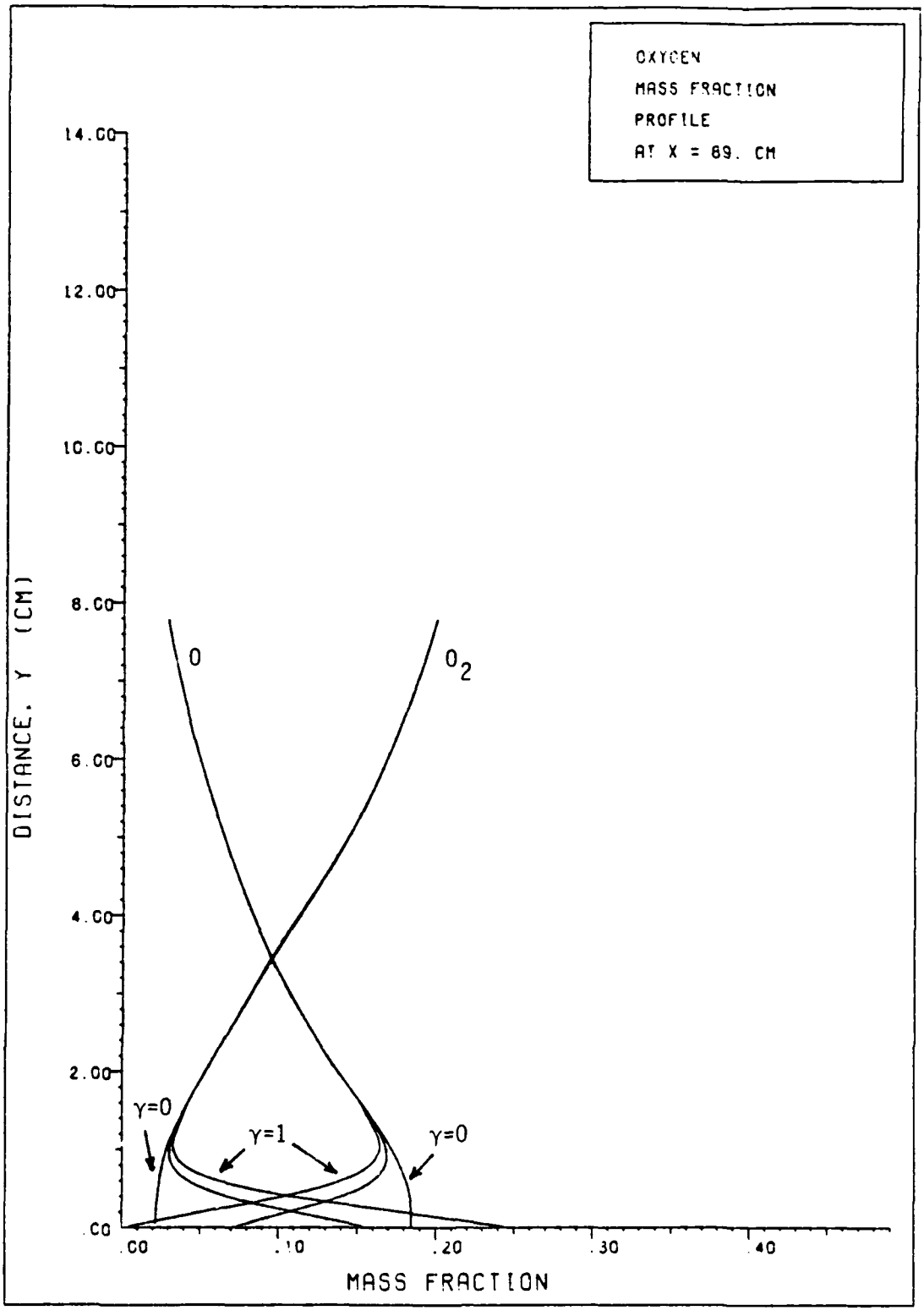

Figure 19. Mass Fraction Profiles for Atomic and Molecular Oxygen at x = 89. cm.

VII. Conclusions and Recommendations

This research dealt with the building of a detailed, steady-state, theoretical model for the recombination of atomic oxygen on a silicon dioxide surface. The Langmuir-Rideal heterogeneous recombination mechanism formed the basis for the model. The bonding of atomic oxygen to the surface and the thermal desorption of atomic oxygen from the surface were also included in the model. The hypothesis was made that the gas-phase oxygen atoms combine directly with the oxygen atoms that constitute the silicon dioxide surface, with other gas-phase oxygen atoms replacing the lost atoms that were bonded on the silicon dioxide surface. A set of two-dimensional, steady-state, laminar boundary-layer calculations was made using numerical methods to demonstrate the use of this model and to explore the rational limits which may be placed on the role of catalysis for oxygen recombination on a silicon dioxide surface.

The model agrees with the experimental data that is available in the literature, and provides an insight into the processes that control the recombination as a function of temperature. From 300°K to 740°K where Θ, the fractional surface concentration of atomic oxygen, is approximately unity due to rapid adsorption of atoms to the surface, the recombination process is first order with respect to the pressure of the oxygen atoms and is controlled by the recombination desorption rate. At more elevated temperatures (740°K to approximately 1600°K) where Θ is smaller, the recombination process is controlled by the chemisorption rate and remains first order. At high temperatures (above 1600°K) where

AD-A163 990 A MODEL FOR OXYGEN ATOM RECOMBINATION ON A SILICON DIOXIDE SURFACE(U) AIR FORCE INST OF TECH WRIGHT-PATTERSON AFB OH SCHOOL OF ENGINEERING 2/2

UNCLASSIFIED W A SEWARD DEC 85 AFIT/DS/AA/85-1 F/G 7/4 NL

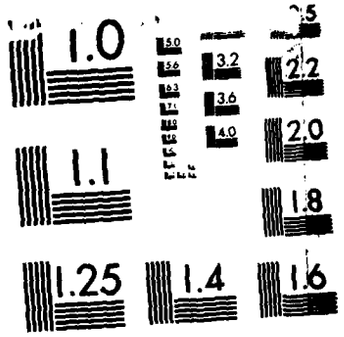

the thermal desorption of atomic oxygen is high, Θ is small, and the recombination process is second order and is dependent upon the chemisorption rate, the thermal desorption rate, and the recombination desorption rate. A maximum value for the recombination coefficient is 1.4×10^{-2} at 900°K which may have a significance in some applications.

A significant effect was found when realistic recombination rates predicted by the model were used in the boundary-layer code. Although the velocity profiles and temperature profiles where not appreciably changed, the mass fraction profiles show significant differences.

In terms of heat transfer, the model demonstrated the most significant influence. The total heat load on a reentry vehicle is highly dependent upon the catalycity of the surface. In comparison to conditions where the surface is fully catalytic and the total heating rate is 0.003494 kcal/cm^2-sec (x = 89. cm), a noncatalytic surface would experience a heating rate of 0.002626 kcal/cm^2-sec, with a silicon dioxide surface experiencing 0.003177 kcal/cm^2-sec, for the case where radiation equilibrium is assumed. At these conditions, though the silicon dioxide recombination rate predicted by the model is low, it would be a mistake to consider it noncatalytic; what can be said, however, is that the predicted catalycity of the silicon dioxide surface did reduce the overall heating by 9.1% below that which would be predicted by a fully-catalytic surface.

It has been established that the Langmuir Rideal mechanism is capable of describing heterogeneous oxygen recombination on silicon dioxide. The model is a realistic method, based on independent experimental data, for predicting the recombination rate which is required in flow programs for analyzing the reentry of vehicles into the earth's atmosphere.

Further experimental work is necessary to verify the very high temperature recombination coefficient results. Also, analytical and experimental work is required in the area of energy transfer to the surface as a result of the recombination on the surface, and how to properly treat the species in the gas stream that might leave the surface in an excited state.

Appendix A

Hydrogen Recombination on Silicon Dioxide Model

The heterogeneous recombination of hydrogen atoms on silicon dioxide surfaces has been extensively studied. It is well established that hydrogen atoms do chemisorb to silicon dioxide and that hydrogen molecules do not (Ref 55-56). More recently, Finlayson-Pitts (Ref 57) confirmed that hydrogen atoms chemisorb to silica forming stable bonds and furthermore that hydrogen molecules do not chemisorb to silica--neither as molecules nor dissociatively.

Figure 20 shows the recombination coefficient as a function of temperature from three independent sources. The data points shown by the stars of David are from Smith (Ref 58) as corrected by Wood and Wise (Ref 19). Wood and Wise determined that the order of the recombination process changes from first to second at a temperature greater than 500°K, and their data are shown as triangles on Figure 20. The data shown at temperatures greater than 500°K are the maximum values for the recombination coefficient due to their assumption that all of the energy liberated upon the recombination of atoms went into the surface. The third set of data is shown as squares and is in the temperature range where the recombination mechanism is first order (Ref 59). In contrast to the data for oxygen recombination on silicon dioxide, the data for hydrogen recombination from the three different groups of experimentalists differ by less than a factor of three. Unfortunately, only Wood and Wise performed their

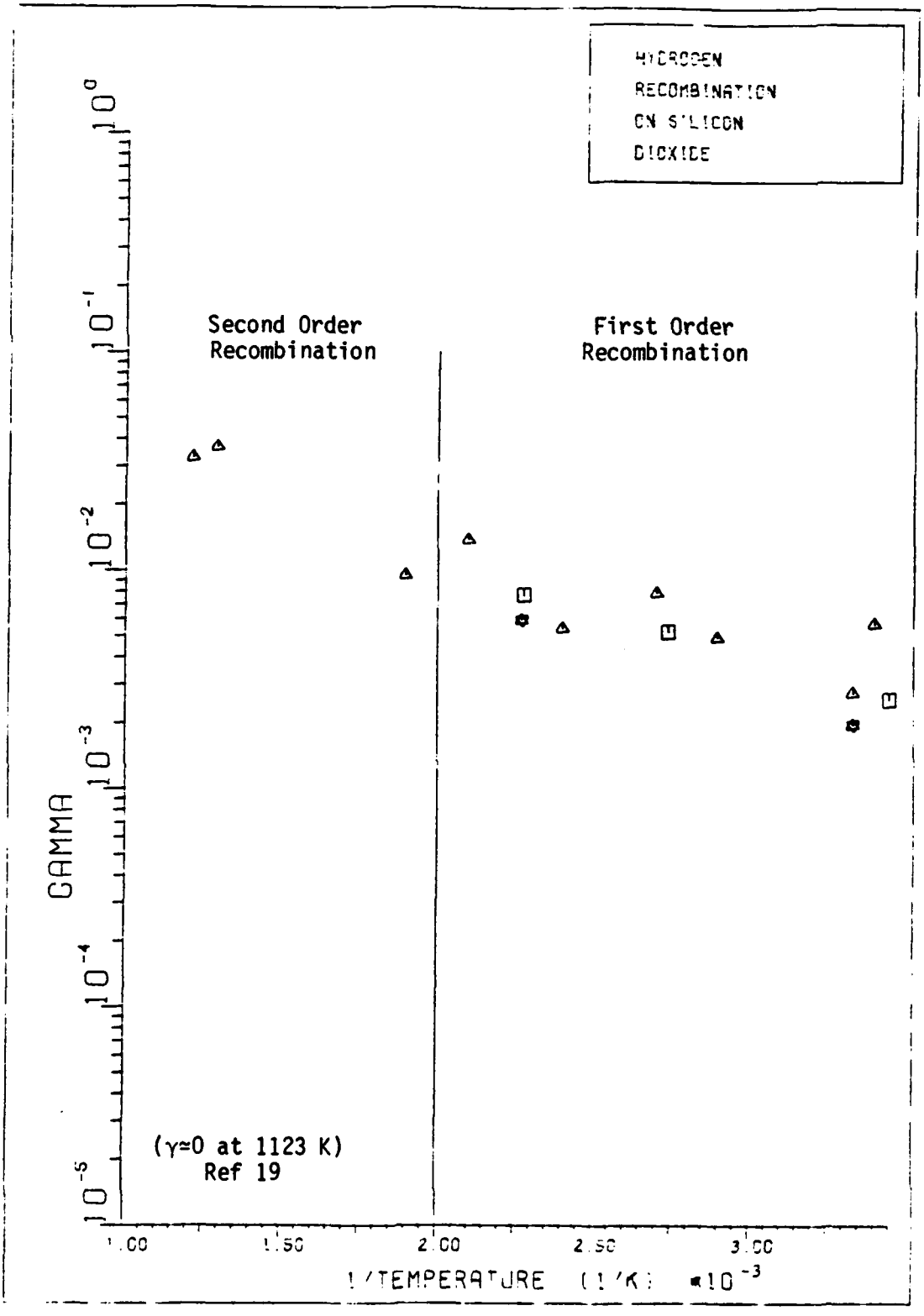

Figure 20. Hydrogen Recombination Coefficient Data vs. 1/Temperature.

experiments at elevated enough temperatures to find where the recombination kinetics changed from first to second order.

Wood and Wise (Ref 19) proposed that a Langmuir-Rideal mechanism dominates in the temperature range 300°K to 500°K, and that the recombination mechanism is the Langmuir-Hinshelwood (recombination of two adjacent, chemisorbed atoms) at the elevated temperatures where the recombination kinetics are second order. However, the Langmuir-Rideal recombination mechanism can be used to model the recombination process for hydrogen atoms on silicon dioxide above 300°K.

Analytical Form of Hydrogen Recombination Coefficient

The exact same components of the rate equation that were described in Chapter III are appropriate for hydrogen recombination as well. For steady state conditions, the recombination coefficient can be given by:

$$\gamma = \frac{2 P S_o \dot{N} \exp(-\frac{E}{k_B T})}{S_o \dot{N} + \delta + P \dot{N} \exp(-\frac{E}{k_B T})} \qquad (52)$$

For Θ, the fractional surface concentration, to be approximately unity at room temperature, the $S_o \dot{N}$ term in the denominator must dominate. The recombination coefficient is then given by:

$$\gamma \simeq 2 P \exp(-\frac{E}{k_B T}) \qquad (53)$$

and the recombination kinetics are first order. Since the empirical data from Wood and Wise show the kinetics going second order above 500°K, δ, the thermal desorption rate per unit area, must dominate the denominator

of equation (52) at these elevated temperatures. In order for this to be true, the energy required to thermally desorb an atom from the silicon dioxide surface must be significantly less than it is for oxygen. The $P \dot{N} \exp(-\frac{E}{k_B T})$ term will never dominate the denominator of equation (52).

Hydrogen Recombination Data

An Arrhenius plot of the recombination coefficient versus the reciprocal of the absolute temperature is linear for hydrogen recombination on silicon dioxide from room temperature to approximately 500°K. From this plot, the activation energy is 2.10 kcal/mole (1.46×10^{-20} J/atom) and the steric factor is 0.06.

Johnson (Ref 60) and Langmuir (Ref 61) found that the number of hydrogen atoms adsorbed per square centimeter of silicon dioxide surface is approximately 1.35×10^{15}.

The bond energy, D, of the chemisorbed hydrogen atoms onto silicon dioxide is reported by Wood and Wise (Ref 19) to be approximately 44 kcal/mole. They state that Hirschfelder's empirical rule (Ref 62) was used to make this estimate from the experimentally determined activation energy, E, of the recombination process. Hirschfelder's rule is the following:

$$E = 0.055\ D \tag{93}$$

If the above value of 2.1 kcal/mole is used for the activation energy, the chemisorption bond strength would be 38 kcal/mole from this rule.

Hickmott (Ref 32) performed thermal desorption studies of both physically adsorbed hydrogen atoms and chemisorbed hydrogen atoms in addition to hydrogen recombination tests. His results can be interpreted

such that his molecular flow due to chemisorbed atom recombination at 300°K is due to thermal desorption of chemisorbed hydrogen atoms followed by Langmuir-Rideal recombination of these thermally desorbed atoms with chemisorbed atoms. With this interpretation, the chemisorption bond strength would be approximately 25 kcal/mole.

Johnson (Ref 60) further found and Shuler and Laidler (Ref 63) and Laidler (Ref 16) explain that thermal desorption of atomic hydrogen becomes important at about 250°C.

In addition to measuring the recombination coefficient, Wood and Wise (Ref 19) report that the recombination process transitions from first to second order kinetics with respect to the pressure of the hydrogen atoms at a temperature of approximately 500°K.

Details of Hydrogen Recombination Model

The values for the parameters in the hydrogen recombination model are shown in Table VI. The initial sticking coefficient given in Table VI is not based independently on experimental data. Antonini (Ref 37) found that the initial sticking coefficient for oxygen molecules and for carbon dioxide molecules chemisorbing to fresh silicon dioxide decreases with increasing temperature. The same exponential form is used for oxygen atoms on silicon dioxide, but the pre-exponential factor was increased to get a better match with the recombination coefficient data shown in Figure 20. The final form is as follows:

$$S_o = 0.75 \exp(-0.002\ T) \qquad (94)$$

with the initial sticking coefficient decreasing from 0.4 at 300°K to 0.1 at 1000°K.

Table VI. Computational Parameters for Hydrogen Recombination on Silicon Dioxide

PARAMETER	VALUE
P, STERIC FACTOR	0.06
E, ACTIVATION ENERGY	2.10 kcal/mole = 1.46×10^{-20} J/atom
S_o, INITIAL STICKING COEFFICIENT	0.75 exp(-0.002 T)
C_a, SURFACE SITES	1.35×10^{15} sites/cm^2
D, THERMAL DESORPTION ENERGY	25 kcal/mole = 1.737×10^{-19} J/atom

Figure 21 gives the effect of changing the initial sticking coefficient with the desorption energy fixed at 25 kcal/mole (1.737×10^{-19} J/atom). The primary influence of the initial sticking coefficient is at the elevated temperatures. We observe from equation (52) that at the low temperatures where the $S_o \dot{N}$ term dominates the denominator, the initial sticking coefficient cancels out. As long as S_o is much greater than $P \exp\left(-\frac{E}{k_B T}\right)$ at the low temperatures, then gamma will be independent of the initial sticking coefficient. At an elevated temperature, an increase in S_o will increase gamma. Furthermore, increasing the initial sticking coefficient moves the maximum value of gamma to higher temperatures.

Figure 22 shows the influence of the hydrogen atom desorption energy on the value of the recombination coefficient with the other variables given by Table VI. The recombination coefficient is independent of the desorption energy at the low temperatures. However, at the elevated temperatures the desorption energy is very important. Not only is the

magnitude of the recombination coefficient affected but the thermal desorption term determines at which temperature the recombination kinetics transition from first order to second order. In order to satisfactorily match the data shown in Figure 20, 25 kcal/mole (1.737×10^{-19} J/atom) is used with the rest of the variables given in Table VI.

Figure 23 shows not only the empirical data given by Figure 20 but also shows the results of the model. The model's results match the empirical data very well. The maximum value of the recombination coefficient is 1.3×10^{-2} at 500°K. The recombination kinetics transition from first to second order with respect to the atomic hydrogen pressure at approximately 550°K. At 1120°K gamma is 1.1×10^{-7}. This value is in agreement with the value of approximately zero obtained by Wood and Wise at 1123°K.

Gelb and Kim Model for Hydrogen Recombination on Silicon Dioxide

Gelb and Kim (Ref 64) modeled hydrogen atom recombination on silicon dioxide using the Langmuir-Rideal mechanism. They used a value of 42 kcal/mole for the thermal desorption energy in accordance with the Hirschfelder relationship. As a consequence, they report a maximum value for the recombination coefficient at 833°K. From room temperature to 833°K the recombination kinetics would be first order, according to their model, with the recombination mechanism changing to second order above 833°K. Better agreement with empirical data is obtained if a value of 25 kcal/mole (1.737×10^{-19} J/atom) is used for the thermal desorption energy. Figure 24 shows the results of both their model and the model from this research; each with 25 kcal/mole used for the desorption energy.

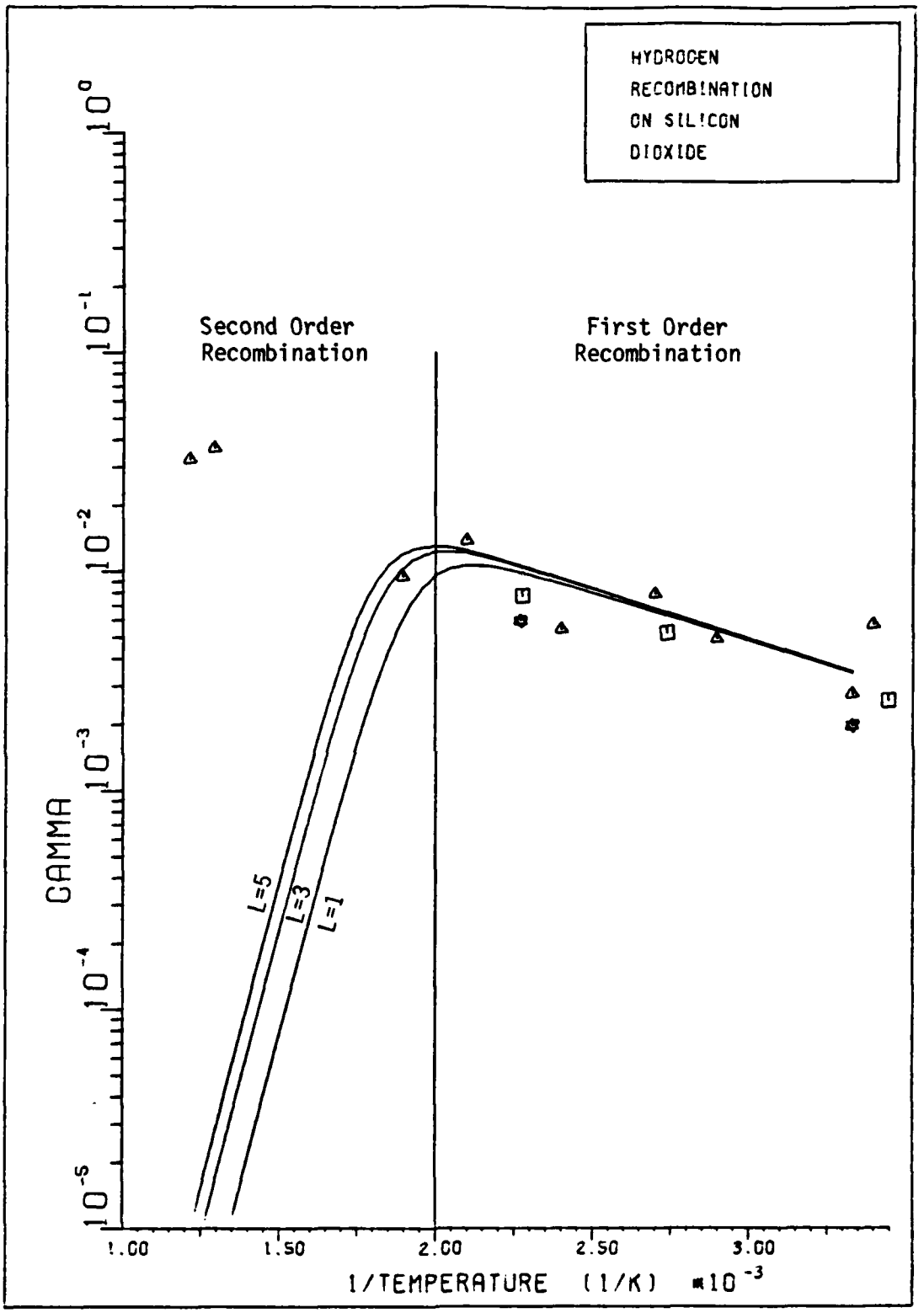

Figure 21. Hydrogen Recombination Coefficient vs. 1/Temperature for S_o = 0.15 L exp(-0.002 T) for L = 1, 3, 5.

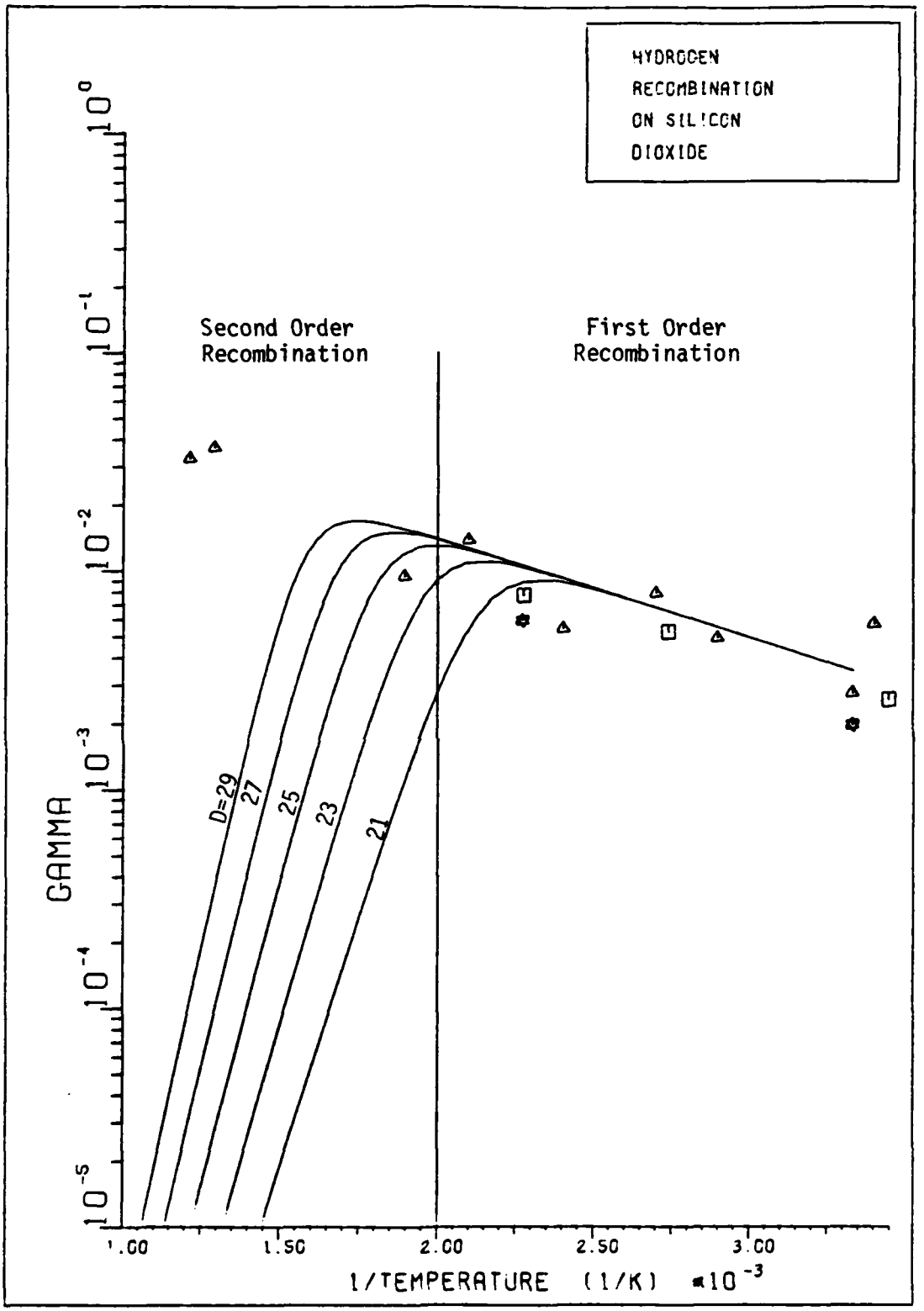

Figure 22. Hydrogen Recombination Coefficient vs. 1/Temperature for Bond Energy, D = 21, 23, 25, 27, 29 kcal/mole.

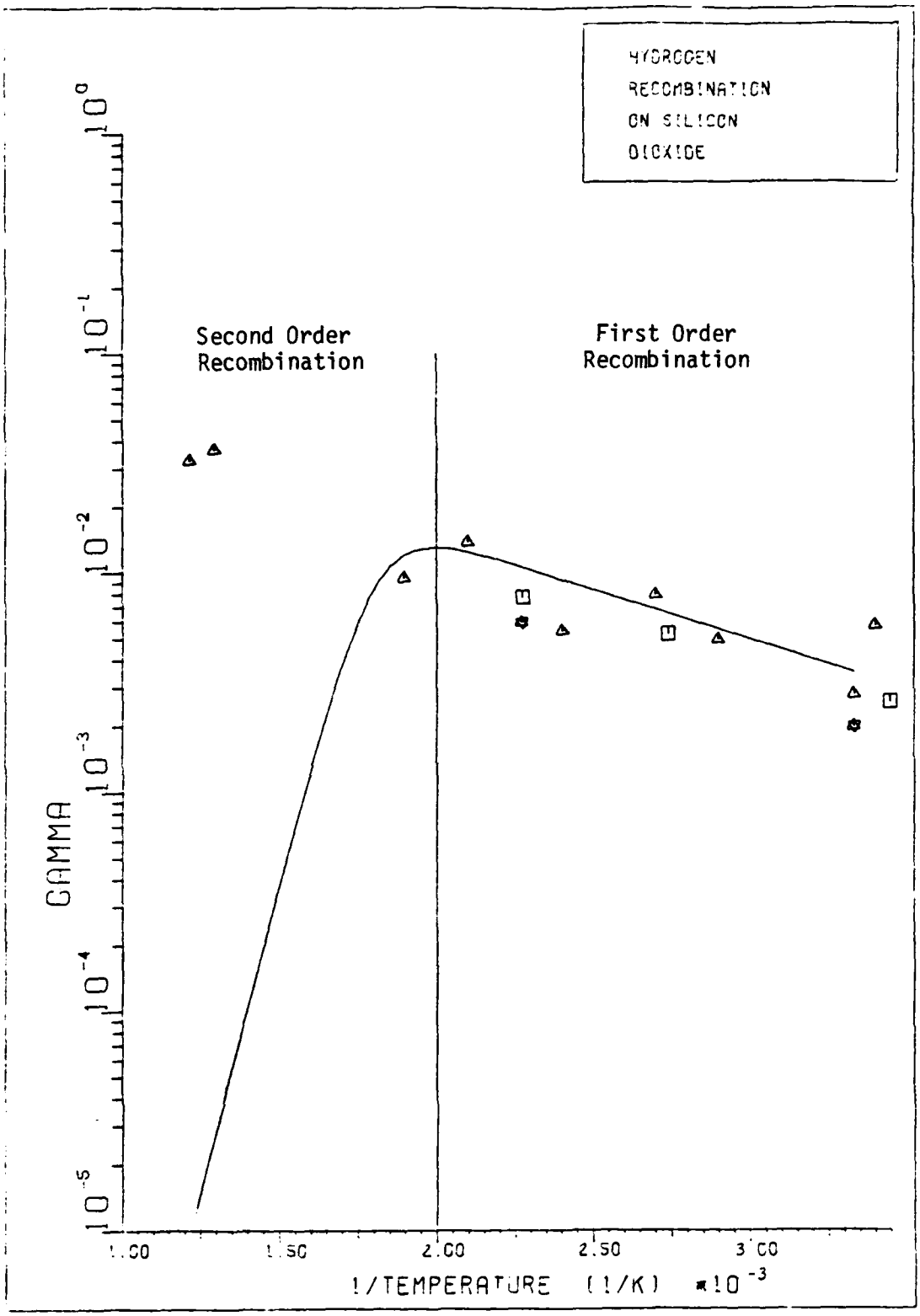

Figure 23. Hydrogen Recombination Coefficient vs. 1/Temperature for the Values of the Parameters Given in Table VI.

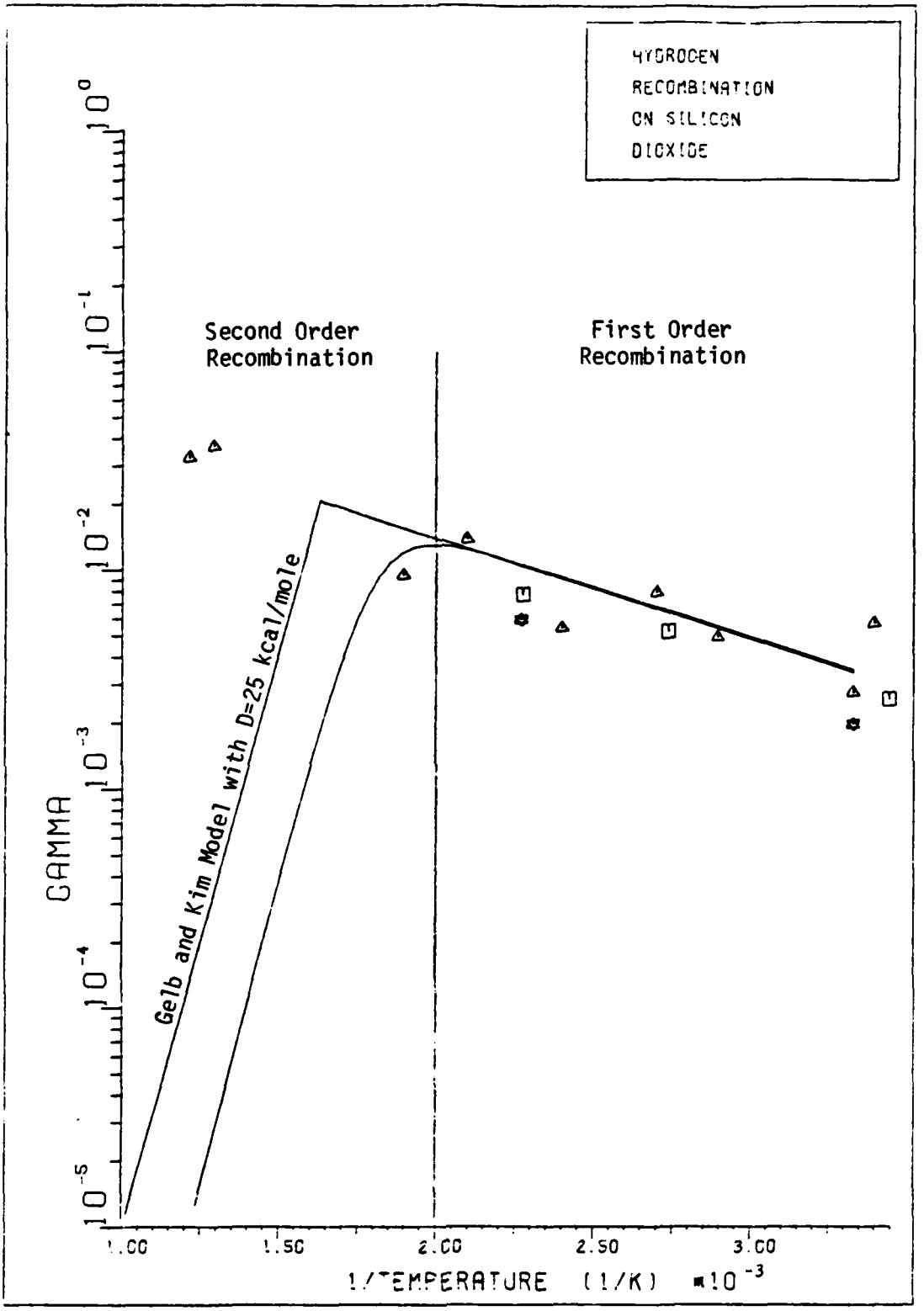

Figure 24. Hydrogen Recombination Coefficient vs. 1/Temperature for the Values of the Parameters Given in Table VI in Comparison with the Gelb and Kim Model with Bond Energy, D=25 kcal/mole.

Bibliography

1. Hodge, J. K., Y. K. Woo and P. T. Cappelano. "Parameter Estimation for Imbedded Thermocouples in Space Shuttle Wind Tunnel Test Articles with a Nonisothermal Wall." AIAA Paper 83-1533, New York: American Institute of Aeronautics and Astronautics, 1983.

2. Office of Advanced Manned Vehicles. Evaluation of the Space Shuttle Orbiter Second Orbital Flight. AFFTC-TR-82-1. Edwards AFB, California: Air Force Flight Test Center, February 1982.

3. McCarty, R. L. A Heat Transfer Investigation of Nonequilibrium Dissociated Air Over a Noncatalytic - Catalytic Discontinuity on a Ballistic Missile Decoy. MS Thesis, AFIT/GAE/AA/84D-14. School of Engineering, Air Force Institute of Technology (AU), Wright-Patterson AFB OH, December 1984.

4. Goulard, R. "On Catalytic Recombination Rates in Hypersonic Stagnation Heat Transfer," Jet Propulsion, 28: 737-745 (November 1958).

5. Pope, R. B. "Stagnation-Point Convective Heat Transfer in Frozen Boundary Layers," AIAA Journal, 6: 619-626 (April 1968).

6. Anderson, L. A. "Effect of Surface Catalytic Activity on Stagnation Heat-Transfer Rates," AIAA Journal, 11: 649-656 (May 1973).

7. Scott, C. D. "Effects of Nonequilibrium and Catalysis on Shuttle Heat Transfer." AIAA Paper 83-1485, New York: American Institute of Aeronautics and Astronautics, 1983.

8. Jumper, E. J., R. G. Wilkins and B. L. Preppernau. "Adaptation of a Wall-Catalytic Fluorine Recombination Model to Fluid-Dynamic Computations in an HF Laser Nozzle." AIAA Paper 85-1598, New York: American Institute of Aeronautics and Astronautics, 1985.

9. Breen, J., R. Cibrian, W. N. Delgass, N. G. Krishnan, P. C. Nordine and D. E. Rosner. "Catalysis Study for Space Shuttle Vehicle Thermal Protection Systems." NASA CR-134124, Washington: National Aeronautics and Space Administration, 1973.

10. Office of Advanced Manned Vehicles. Flight Test Results From the Entry and Landing of the Space Shuttle Orbiter for the First Twelve Orbital Flights. AFFTC-TR-85-11. Edwards AFB, California: Air Force Flight Test Center, June 1985.

11. Scott, C. D. "Catalytic Recombination of Nitrogen and Oxygen on High-Temperature Reusable Surface Insulation." AIAA Paper 80-1477, New York: American Institute of Aeronautics and Astronautics, 1980.

12. Laidler, K. J. Chemical Kinetics (Second Edition), Chapter 6. New York: McGraw-Hill Book Company, 1965.

13. Dickens, P. G. and M. B. Sutcliffe. "Recombination of Oxygen Atoms on Oxide Surfaces. Part 1 -- Activation Energies of Recombination," Transactions of the Faraday Society, 60: 1272-1285 (July 1964).

14. Jumper, E. J., C. J. Ultee, and E. A. Dorko. "A Model for Fluorine Atom Recombination on a Nickel Surface," Journal of Physical Chemistry, 84: 41-50 (1980).

15. Laidler, K. J. "Kinetic Laws in Surface Catalysis," Chapter 4, Catalysis, Volume I, edited by P. H. Emmett. New York: Reinhold, 1954.

16. Laidler, K. J. "The Absolute Rates of Surface Reactions," Chapter 5, Catalysis, Volume I, edited by P. H. Emmett. New York: Reinhold, 1954.

17. Greaves, J. C. and J. W. Linnett. "Recombination of Atoms at Surfaces. Part 6 -- Recombination of Oxygen Atoms on Silica From 20°C to 600°C," Transactions of the Faraday Society, 55: 1355-1361 (August 1959).

18. Hardy, W. A. and J. W. Linnett. "Mechanisms of Atom Recombination on Surfaces," Proceedings of the Eleventh Symposium (International) on Combustion. 167-179. The Combustion Institute, Pittsburgh, 1967.

19. Wood, B. J. and H. Wise. "The Kinetics of Hydrogen Atom Recombination on Pyrex Glass and Fused Quartz," Journal of Physical Chemistry, 66: 1049-1053 (June 1962).

20. Somorjai, G. A. Principles of Surface Chemistry. Englewood Cliffs, New Jersey: Prentice-Hall, 1972.

21. Hayward, D. O. and B. M. W. Trapnell. Chemisorption (Second Edition). London: Butterworths, 1964.

22. Vincenti, W. G. and C. H. Kruger, Jr. Introduction to Physical Gas Dynamics. Huntington, New York: Robert E. Krieger Publishing Co., 1967.

23. Glasstone, S., K. J. Laidler, and H. Eyring. The Theory of Rate Processes. New York: McGraw-Hill Book Company, 1941.

24. Hankey, W., R. Newmann and E. Flinn. Design Procedures for Computing Aerodynamics Heating at Hypersonic Speeds. WADC TR-59-610. Wright-Patterson AFB OH: Air Force Wright Aeronautical Laboratories, June 1960.

25. Kaufman, F. "Reactions of Oxygen Atoms," Progress in Reaction Kinetics, Volume I, edited by G. Porter. New York: Pergamon Press, 1961.

26. Linnett, J. W. and D. G. H. Marsden. "The Kinetics of the Recombination of Oxygen Atoms at a Glass Surface," Proceedings of the Royal Society of London, Series A, 234: 489-504 (March 1956).

27. Linnett, J. W. and D. G. H. Marsden. "The Recombination of Oxygen Atoms at Salt and Oxide Surfaces," Proceedings of the Royal Society of London, Series A, 234: 504-515 (March 1956).

28. Greaves, J. C. and J. W. Linnett. "Recombination of Atoms at Surfaces. Part 5 -- Oxygen Atoms at Oxide Surfaces," Transactions of the Faraday Society, 55: 1346-1354 (August 1959).

29. Harrison, W. A. "Is Silicon Dioxide Covalent or Ionic?" Proceedings of the International Topical Conference on the Physics of SiO_2 and its Interfaces, edited by S. T. Pantelides. 105-110. Pergamon Press, New York, 1978.

30. Wells, A. F. Structural Inorganic Chemistry (Third Edition). London: Oxford University Press, 1962.

31. Berkowitz, J. "Catalytic Oxygen Atom Recombination on Solid Surfaces," The Structure and Chemistry of Solid Surfaces, edited by G. A. Somorjai. 80-1 - 80-16. John Wiley & Sons, New York, 1969.

32. Hickmott, T. W. "Interaction of Atomic Hydrogen with Glass," Journal of Applied Physics, 31: 128-136 (January 1960).

33. Campbell, I. M. and B. A. Thrush. "The Association of Oxygen Atoms and Their Combination With Nitrogen Atoms," Proceedings of the Royal Society, Series A, 296: 222-232 (January 1967).

34. Rahman, M. L. and J. W. Linnett. "Recombination of Atoms at Surfaces. Part II - Nitrogen Atoms at Some Acid, Base and Salt Surfaces," Transactions of the Faraday Society, 67: 179-182 (January 1971).

35. Evenson, K. M. and D. S. Burch. "Atomic-Nitrogen Recombination," Journal of Chemical Physics, 45: 2450-2460 (October 1966).

36. Moore, W. J. Physical Chemistry (Third Edition). Englewood Cliffs, New Jersey: Prentice-Hall, 1962.

37. Antonini, J. F. "Ultra-High-Vacuum Adsorption Studies of CO_2 and O_2 on 'Fresh' and 'Passivated' Silica and Various Glass Surfaces," Proceedings of the Fourth International Vacuum Congress, Part One. 179-183. Institute of Physics and Physical Society, London, 1968.

38. Christmann, K., O. Schober, G. Ertl and M. Newmann. "Adsorption of Hydrogen on Nickel Single Crystal Surfaces," Journal of Chemical Physics, 60: 4528-4540 (June 1974).

39. Krongelb, S. and M. W. P. Strandberg. "Use of Paramagnetic-Resonance Techniques in the Study of Atomic Oxygen Recombinations," Journal of Chemical Physics, 31: 1196-1210 (November 1959).

40. Hochstrasser, G. and J. F. Antonini. "Surface States of Pristine Silica Surfaces," Surface Science, 32: 644-664 (1972).

41. Laidler, K. J. "The Mechanisms of Some Elementary Surface Reactions," The Journal of Physical & Colloid Chemistry, 53: 712-732 (1949).

42. Ehrlich, G. "Molecular Dissociation and Reconstitution on Solids," Journal of Chemical Physics, 31: 1111-1126 (October 1959).

43. Weston, R. E., Jr. and H. A. Schwarz. Chemical Kinetics. Englewood Cliffs, New Jersey: Prentice-Hall, 1972.

44. Adamson, A. W. A Textbook of Physical Chemistry (Second Edition), Chapter 14. New York: Academic Press, 1979.

45. Clarke, J. F. and M. McChesney. The Dynamics of Real Gases. Washington: Butterworths, 1964.

46. Lanning, F. C. "Silicon," The Encyclopedia of the Chemical Elements, edited by C. A. Hampel. New York: Reinhold Book Corporation, 1968.

47. Dunn, M. G. and S. W. Kang. "Theoretical and Experimental Studies of Reentry Plasmas." NASA CR-2232, Washington: National Aeronautics and Space Administration, 1973.

48. Ujcik, G. B. Predicting the Onset of Transition in the Presence of Heat Transfer. MS Thesis AFIT/GAE/AA/84D-23. School of Engineering, Air Force Institute of Technology (AU), Wright-Patterson AFB OH, December 1984.

49. National Bureau of Standards. JANAF Thermochemical Tables (Second Edition). NSRDS-NBS 37. Washington: Government Printing Office, June 1971.

50. Bird, R. B., W. E. Stewart, and E. N. Lightfoot. Transport Phenomena. New York: John Wiley & Sons, 1960.

51. Svehla, R. A. "Estimated Viscosities and Thermal Conductivities of Gases at High Temperatures." NASA TR-R-132, Washington: National Aeronautics and Space Administration, 1962.

52. Kang, S. W., M. G. Dunn and W. L. Jones. "Theoretical and Measured Electron-Density Distributions for the RAM Vehicle at High Altitudes." AIAA Paper 72-689, New York: American Institute of Aeronautics and Astronautics, 1972.

53. Miner, E. W. and C. H. Lewis. "Hypersonic Ionizing Air Viscous Shock-Layer Flows Over Nonanalytic Blunt Bodies." NASA CR-2550, Washington: National Aeronautics and Space Administration, May 1975.

54. Song, D. J. and C. H. Lewis. "VSLNQH: An Axisymmetric Viscous Shock-Layer Code for Nonequilibrium Finite-Rate Chemically Reacting Viscous Flows Over Hyperboloid Geometrics, Volumes I and II." Blacksburg, Virginia: VRA, Inc., August 1984.

55. Langmuir, I. "A Chemically Active Modification of Hydrogen," The Journal of the American Chemical Society, 34: 1310-1325 (July - December 1912).

56. Langmuir, I. "The Dissociation of Hydrogen into Atoms," The Journal of the American Chemical Society, 37: 417-458 (January - June 1915).

57. Finlayson-Pitts, B. J. "Interaction of Gas-Phase Deuterium Atoms with Silica Surfaces," Journal of Physical Chemistry, 86: 3499-3501 (1982).

58. Smith, W. V. "The Surface Recombination of H Atoms and OH Radicals," Journal of Chemical Physics, 11: 110-125 (March 1943).

59. Tsu, K. and M. Boudart. "Surface Diffusion and Recombination of Hydrogen Atoms on Glass," International Congress on Catalysis (2nd: 1960: Paris). Paper #23, 593-613. Editions Technip, Paris, 1961.

60. Johnson, M. C. "Pressure Measurements for Investigating the Mutual Behavior of Adsorbed Hydrogen Atoms," Transactions of the Faraday Society, 28: 162-165 (March 1932).

61. Langmuir, I. "Monolayers on Solids," Journal of the Chemical Society, Part I: 511-543 (1940).

62. Hirschfelder, J. O. "Semi-Empirical Calculations of Activation Energies," Journal of Chemical Physics, 9: 645-653 (August 1941).

63. Shuler, K. E. and K. J. Laidler. "The Kinetics of Heterogeneous Atom and Radical Reactions. I. The Recombination of Hydrogen Atoms on Surfaces," The Journal of Chemical Physics, 17: 1212-1217 (December 1949).

64. Gelb, A. and S. K. Kim. "Theory of Atomic Recombination on Surfaces," The Journal of Chemical Physics, 55: 4935-4939 (November 1971).

VITA

William Arthur Seward was born on 13 April 1948 in Rochester, New York. He graduated from high school in Lyndonville, New York, in 1966 and attended Cornell University from which he received the degree of Bachelor of Science in Mechanical Engineering in June 1971. Upon graduation, he received a commission in the USAF through the ROTC program. He was called to active duty in July 1971 and was stationed at Chanute Technical Training Center, Illinois where he completed the Aircraft Maintenance Officer Course in December 1971. He then served as a Squadron Aircraft Maintenance Officer in the 5th Organizational Maintenance Squadron, 5th Bomb Wing, Minot AFB, North Dakota, until entering the School of Engineering, Air Force Institute of Technology, in June 1974. He received the Master of Science degree in Aeronautical Engineering in December 1975 and then was assigned to the Aeronautical Systems Division at Wright-Patterson AFB, Ohio, as an Aircraft Propulsion Performance Engineer. In October 1978 he was assigned to the Air Force Academy as an instructor in the Department of Aeronautics. He returned to the Air Force Institute of Technology in July 1982 as a doctoral student in the Department of Aeronautics and Astronautics. He is currently the Technical Area Manager of the Advanced Plasma Research Group in the Power Division of the Aero Propulsion Laboratory.

Permanent Address: 13525 Roosevelt Highway
Waterport, New York 14571

UNCLASSIFIED

SECURITY CLASSIFICATION OF THIS PAGE

REPORT DOCUMENTATION PAGE

1a. REPORT SECURITY CLASSIFICATION Unclassified	1b. RESTRICTIVE MARKINGS
2a. SECURITY CLASSIFICATION AUTHORITY	3. DISTRIBUTION/AVAILABILITY OF REPORT Approved for public release; distribution unlimited.
2b. DECLASSIFICATION/DOWNGRADING SCHEDULE	
4. PERFORMING ORGANIZATION REPORT NUMBER(S) AFIT/DS/AA/85-1	5. MONITORING ORGANIZATION REPORT NUMBER(S)
6a. NAME OF PERFORMING ORGANIZATION School of Engineering Air Force Inst of Technology 6b. OFFICE SYMBOL (If applicable) AFIT/ENY	7a. NAME OF MONITORING ORGANIZATION
6c. ADDRESS (City, State and ZIP Code) Wright-Patterson AFB OH 45433	7b. ADDRESS (City, State and ZIP Code)
8a. NAME OF FUNDING/SPONSORING ORGANIZATION 8b. OFFICE SYMBOL (If applicable)	9. PROCUREMENT INSTRUMENT IDENTIFICATION NUMBER
8c. ADDRESS (City, State and ZIP Code)	10. SOURCE OF FUNDING NOS. PROGRAM ELEMENT NO. / PROJECT NO. / TASK NO. / WORK UNIT NO.
11. TITLE (Include Security Classification) A Model for Oxygen Atom Recombination on a Silicon Dioxide Surface (U)	
12. PERSONAL AUTHOR(S) William A. Seward, Major, USAF	
13a. TYPE OF REPORT PhD Dissertation 13b. TIME COVERED FROM _____ TO _____	14. DATE OF REPORT (Yr., Mo., Day) 1985 December 15. PAGE COUNT 115
16. SUPPLEMENTARY NOTATION	

17. COSATI CODES		
FIELD	GROUP	SUB. GR.
20	13	8
1	1	14

18. SUBJECT TERMS (Continue on reverse if necessary and identify by block number)
Heterogeneous Recombination, Space Shuttle Heating, Oxygen Recombination, Wall Recombination, Catalytic Oxygen Recombination

19. ABSTRACT (Continue on reverse if necessary and identify by block number)

Title: A MODEL FOR OXYGEN ATOM RECOMBINATION ON A SILICON DIOXIDE SURFACE

Chairman of Research Committee: Eric J. Jumper, Lt Col, USAF
Professor of Aerospace Engineering

See Reverse for Abstract

Approved for public release: IAW AFR 190-1.
7 JAN 86
LYNN E. WOLAVER
Dean for Research and Professional Development
Air Force Institute of Technology (AFIT)
Wright-Patterson AFB OH 45433

20. DISTRIBUTION/AVAILABILITY OF ABSTRACT UNCLASSIFIED/UNLIMITED ☒ SAME AS RPT. ☐ DTIC USERS ☐	21. ABSTRACT SECURITY CLASSIFICATION Unclassified
22a. NAME OF RESPONSIBLE INDIVIDUAL Eric J. Jumper, Lt Col, Professor	22b. TELEPHONE NUMBER (Include Area Code) (513) 255-2998 22c. OFFICE SYMBOL AFIT/ENY

DD FORM 1473, 83 APR EDITION OF 1 JAN 73 IS OBSOLETE.

UNCLASSIFIED

SECURITY CLASSIFICATION OF THIS PAGE

A steady state model for oxygen atom recombination for temperatures from 300°K to 2000°K on a silicon dioxide surface was developed based on the Langmuir-Rideal heterogeneous recombination mechanism. The bonding of atomic oxygen to the surface and the thermal desorption of atomic oxygen from the surface were also included in the model. The hypothesis was made that the gas-phase oxygen atoms combine directly with the oxygen atoms that constitute the silicon dioxide surface, with other gas-phase oxygen atoms replacing the lost atoms that were bonded on the silicon dioxide surface matrix. The model agrees with the experimental data that is available in the literature, and provides an insight into the processes that control the recombination as a function of temperature. A set of two-dimensional, steady-state, laminar boundary-layer calculations was made using explicit numerical methods to demonstrate the use of this model and to explore the rational limits which may be placed on the role of catalysis for oxygen recombination on a silicon dioxide surface like that of the Space Shuttle. The predicted catalycity of the silicon dioxide surface did reduce the overall heating below that which would be predicted by a fully catalytic surface.

END

FILMED

3 -86

DTIC